

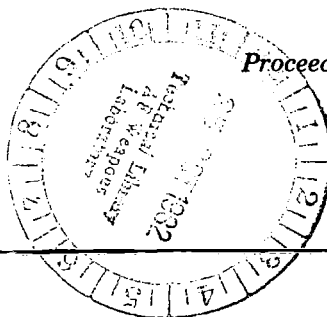
NASA Conference Publication 2242

NASA  
CP  
2242  
c.1

# Flight Effects of Fan Noise



LOAN COPY: RETURN TO  
AFWL TECHNICAL LIBRARY  
KIRTLAND AFB, N.M.



*Proceedings of a workshop held at  
Langley Research Center  
Hampton, Virginia  
January 26-27, 1982*

**NASA**



*NASA Conference Publication*

# Flight Effects of Fan Noise

David Chestnutt, *Editor*  
Langley Research Center  
Hampton, Virginia

Proceedings of a workshop held at  
Langley Research Center  
Hampton, Virginia  
January 26-27, 1982



National Aeronautics  
and Space Administration

Scientific and Technical  
Information Branch

1982



## PREFACE

This conference publication contains the highlights of a workshop on research on the simulation of in-flight fan noise and flight effects held at Langley Research Center, Hampton, Virginia, January 26-27, 1982. The workshop was cosponsored by the Langley Research Center Noise Control Branch and the Lewis Research Center Propulsion Systems Acoustics Branch. The purposes of the workshop were (1) to review the status of the overall program on the flight effects on fan noise, (2) to display for the first time flight-to-static noise comparisons for the Pratt & Whitney JT15D engine, and (3) to stimulate dialogue between certain industrial, university, and government groups to assess our ability to simulate in-flight fan noise.

The participants agreed that a major plateau had been reached in the static simulation of in-flight fan noise that will allow certain noise control concepts to be evaluated. However, there was a consensus that this plateau should be regarded as an interim step and that the technology should continue to be improved to permit better simulations in the future. Other recommendations concerning these improvements and indications of areas of needed research were addressed by the workshop presentations, which are summarized in this publication.

David Chestnutt, Langley Research Center  
Charles Feiler, Lewis Research Center



## CONTENTS

PREFACE . . . . .	iii
-------------------	-----

## INTRODUCTION

PROGRAM OVERVIEW . . . . .	3
David Chestnutt	
THE PROBLEM . . . . .	6
J. F. Groeneweg	

## SESSION I - ICD EXPERIENCE AND DESIGN CRITERIA

FUNDAMENTALS . . . . .	9
H. M. Nagib	
PRATT & WHITNEY AIRCRAFT (P&WA) EXPERIENCE. . . . .	10
A. A. Peracchio	
BOEING EXPERIENCE . . . . .	11
A. O. Andersson	
GENERAL ELECTRIC EXPERIENCE . . . . .	14
P. R. Gliebe	

## SESSION II - JT15D PROGRAM

MODIFICATIONS, INSTRUMENTATION, AND INLETS. . . . .	17
R. A. Golub	

## LERC ICD CONFIGURATION STUDIES - OUTDOOR ENGINE TEST STAND

FAR-FIELD NOISE . . . . .	19
J. G. McArdle	
BMT COMPARISONS . . . . .	20
L. J. Heidelberg	

## LERC ANECHOIC CHAMBER EXPERIMENTS

FAR-FIELD NOISE . . . . .	21
R. P. Woodward	
BMT RESULTS . . . . .	22
J. R. Balombin	

AMES 40 × 80 TUNNEL EXPERIMENTS

LARC RESULTS . . . . .	23
J. S. Preisser	
GENERAL ELECTRIC RESULTS . . . . .	24
R. G. Holm	
SESSION III - LARC FLIGHT RESULTS AND COMPARISONS	
CONVECTIVE AMPLIFICATION EFFECT . . . . .	27
R. Amiet	
FUNDAMENTAL BMT EXPERIMENTS . . . . .	28
W. F. O'Brien	
FLIGHT PROCEDURES, DATA COLLECTION, AND CALIBRATION . . . . .	31
A. W. Mueller	
AIRCRAFT FLYOVER DATA REDUCTION AND ANALYSIS . . . . .	32
Doreen Gridley	
BMT COMPARISONS . . . . .	34
J. A. Schoenster	
FAR-FIELD FLIGHT NOISE AND COMPARISONS WITH WIND TUNNEL AND STATIC RESULTS . . . . .	36
J. S. Preisser	
SUMMARY OF WORKSHOP RESULTS . . . . .	38
REFERENCES . . . . .	117
APPENDIX - BIBLIOGRAPHY . . . . .	118
ATTENDEES . . . . .	123

## INTRODUCTION



[illegible]

## PROGRAM OVERVIEW

David Chestnutt

It became evident by the mid-1970's that inflow turbulence gave rise to dominant interaction noise peculiar to engine static test stand installations. While this noise source was known much earlier, it was underestimated. This dominant noise was associated with the blade passage frequency and it was believed to be present only during static testing. Since there were few techniques to separate blade-passing-frequency components, it was very difficult to evaluate the effectiveness of various flight inlet noise control concepts. Interestingly, this difficulty didn't pose an immediate problem since inlet treatment tested statically seemed to perform even better in flight. Although this was a fortuitous result at the time, it overshadowed the obvious need to scientifically deal with the different dominant noise mechanisms encountered in flight. This became apparent with the advent of the more sophisticated inlet treatment concepts, including treatment optimization, that required the noise source to be accurately known for the most efficient noise suppression.

Another difficulty associated with this phenomenon was the presence of a strong blade-passing-frequency tone in an engine speed regime where the classic Tyler-Sofrin interaction theory indicated there should be none. This was particularly disturbing to designers who designed engines to take advantage of the cut-off phenomenon only to hear the tone during static tests. Even after the hypothesis of turbulence interacting with the fan during static testing was gaining acceptance there were instances of inlet and fan exhaust tones being observed during aircraft flyovers in engines that were cut off. The research results presented during this workshop served to offer an explanation for these heretofore anomalies.

In 1977 it was determined that NASA would formulate and conduct a program to resolve these serious problems. The program consisted of flight tests to provide criteria to evaluate various inflow control devices and to evaluate the adequacy of wind tunnel acoustic tests. Comparisons of these data were expected to determine the overall adequacy of flight noise simulation, to identify promising areas of noise reduction, and to allow more accurate noise prediction from static testing to the flight environment.

The NASA program is shown pictorially in Figure 1. It consists of LaRC flight testing using an OV-1B airplane carrying a Pratt & Whitney JT15D test engine under the right wing, wind tunnel testing with a JT15D engine at Ames Research Center, and JT15D engine static testing at the Lewis Research Center. In addition, there was testing of the JT15D fan only in the LeRC anechoic chamber. Grants with the Illinois Institute of Technology and Virginia Polytechnic Institute and State University, as well as contracts with the Pratt & Whitney Aircraft Company, the Boeing Company, and the General Electric Company, rounded out the NASA funded research effort. Figure 2 depicts these activities on a time scale that shows the program culminating in a substantial activity of data comparisons.

The broad objectives of the program were (1) to improve static test techniques to the point of adequately simulating flight, and (2) to improve static-to-flight noise predictions.

The program status was reported as follows. The wind tunnel tests at Ames Research Center have been completed. These tests consisted of operating the JT15D engine alone and in the presence of an OV-1 wing. All of the joint LaRC/Ames-conducted tests at Ames used a hardwall inlet and an Ames-designed fan exhaust muffler. In addition, there were Ames-sponsored JT15D tests conducted by the G.E. Company. The G.E./Ames tests employed several inlets including one softwall configuration. Both the LaRC and G.E. tests were run in the Ames 40 x 80 tunnel and on the Ames outdoor engine test stand. The Ames/G.E. outdoor tests were run with and without an inflow control device. The G.E. work for Ames has been completed and reported. LaRC has contracted with the G.E. Company to further analyze these data and to make comparisons with LaRC flight data. The JT15D static tests at LeRC are practically completed. A variety of inflow control devices were tested on the JT15D and reported. In addition, tests involving circular rods placed in front of the fan were conducted and partially reported. A purpose of these tests was to provide a dominant and well known source to help in the evaluation of the inflow control devices. The presentation by J. McArdle reports in much more detail on these studies at LeRC. Also, at LeRC, a series of tests was conducted in the anechoic chamber using a JT15D fan with and without an inflow control device (ICD). These results are presented by R. P. Woodward and J. Balombin. Their results were very preliminary and at present somewhat inconclusive. It appeared that anechoic chamber fan tests were going to be somewhat more difficult to conduct than outdoor engine test stand tests because of the indoor installation peculiarities and their influence on the inflow to the fan. The LaRC flight tests will conclude by September 1982 due to funding limitations. This workshop was concerned with flight data taken with the JT15D engine hardwall inlet only. These data were compared with similar hardwall inlet data from LeRC static tests and Ames wind tunnel tests. These comparisons were made in J. S. Preisser's and J. A. Schoenster's presentations. Flight tests were conducted in the fall of 1981 using a softwall inlet of LeRC design and LaRC fabrication. These data are being reduced and will be compared with similar LeRC data in the coming months. Also, jet noise data were measured last year and are being supplied in a data base form to the jet noise group at LeRC for further study. The remaining flight tests will be concerned with addressing questions raised by the flight to data comparisons, i.e., multiple pure tones (MPTs) and broadband levels lower in flight. In addition, the remaining flight tests will evaluate a softwall inlet of LaRC design and construction with circular rods in front of the JT15D fan to produce a dominant, well known noise source. It is currently planned to have a Flight Effects on Fan Noise Session in April 1983 at the AIAA Aeroacoustics Specialists Conference.

A capability for special flight operations, data measurement and automated data processing and analysis was developed for this program. A. W. Mueller and D. Gridley presented the details of this rather formidable accomplishment. The

magnitude and voluminous engineering detail required for the successful flights were presented in summary by R. A. Golub. In addition, Golub presented an outline of the complex on-board instrumentation system developed by LaRC, led by V. Knight. This system has proven to be exceptionally reliable and accurate for the task at hand.

In addition to the flight tests, LaRC was responsible for the overall program advocacy and coordination. One of the earlier contracts on the problem of ICD design was let by LaRC to P&WA and Boeing. This was a major effort that built on the P&WA JT9D and Boeing 747 experience. In addition, an extensive laboratory test series was conducted by P&WA along with an analytical study by Boeing. The results of this research were published and included an interim ICD design procedure (refs. 1 and 2). Dr. Peracchio of P&WA presented material from this research during the workshop.

J. Groeneweg spoke of some technical problems of static simulation of flight from an overall perspective by reiterating technical objectives and issues to be discussed and evaluated.

## THE PROBLEM

J. F. Groeneweg

Dr. John F. Groeneweg discussed the technical problems from the viewpoint of flight simulation using inflow control devices (ICDs). In Figure 3 the technical objectives of developing static experimental techniques and of verifying methods of projecting ground data to flight are listed. A table of ICDs is shown in Figure 4. This listing shows the various organizations that were using these devices on which we have information. The most pertinent design features were tabulated. Next, Groeneweg listed the technical themes/issues of the workshop. These are shown in Figure 5. Next, he discussed the effects of inlet flow on noise generation as a function of individual static test stand peculiarities and how these effects were typically eliminated during flight. The two main approaches to flight simulation in static facilities, forward velocity and inflow control, are illustrated in Figure 6 by results from tests in the LeRC  $9 \times 15$  anechoic wind tunnel and in the LeRC anechoic chamber with an ICD.

One of the most interesting results is shown in Figure 7. This illustrated the sensitivity of the blade passage tone to a seemingly small disturbance like an inlet probe wake both in a static situation and in a wind tunnel. The variability and magnitude of the SPL were significantly reduced when the fan was operated in a wind tunnel. However, also, when an inlet probe was inserted 40 probe diameters in front of the fan the SPL magnitude nearly returned to the static case. The variability did not return to its former static character. This illustrated the necessity of being exceptionally careful to eliminate even small upstream disturbances. It also alerted us to the possibility that an "approximately" clean inlet may not be sufficient for flight simulation.

Figure 8 is a block diagram depicting the sequence of events in fan noise generation by fluctuating blade forces in a duct. The JT15D experiments typically collected limited fluctuating pressure data on the blade surfaces, some inlet data, and far-field data. Figure 9 shows the predicted chordwise variation of rotor blade pressure generated by wakes of upstream rods. For reference, the locations and size of two blade mounted transducers were superimposed on the curves. If the pressure distribution was similar to that predicted from a cascade blade analysis (compressible, non-compact) of the 41-rod case there would be little chance of accurately describing the fluctuating pressure field with only two fixed transducers. However, the blade mounted transducers provided qualitative information regarding internal noise sources and gave a hint of where to look in the far-field to see what the internal sources may have produced.

## SESSION I

### ICD EXPERIENCE AND DESIGN CRITERIA



## FUNDAMENTALS

H. M. Nagib

Dr. Nagib discussed the situation in which ground tests can simulate flight conditions without forward velocity. He contended that upstream turbulence, including atmosphere turbulence, was not a major contributor to inlet turbulence. However, he listed the major contributors as follows:

- . Upstream isolated disturbances
- . Surface generated vorticity, including "ground" vortex
- . Inlet generated disturbances, including lip separation
- . Inflow control device (ICD) generated turbulence and disturbances

On the issue of using wind tunnel turbulence control technology for designing ICDs, he suggested that there was very little direct transfer. He noted that the current  $L/D = 8$  being used for many ICDs came from tunnel turbulence control technology but may not be the best.

Dr. Nagib had several recommendations for the program. These included: (1) re-examine the flight inlet geometry since there was an indication in his analysis that there may be a separation bubble present during static tests, and (2) reconsider inflow management techniques to concentrate on local velocity defects, concentrated mean vorticity, and disturbances caused by either the inlet or inflow control device, and use some form of controlled flow acceleration.

Dr. Nagib did not expect the simulation to be complete and recognized that certain compromises will be necessary in both the acoustic and fluid dynamic aspects of the problem.



## PRATT & WHITNEY AIRCRAFT (P&WA) EXPERIENCE

A. A. Peracchio

Dr. Peracchio presented an assessment of inflow control structure (ICS) effectiveness and design system development from the P&WA perspective. A photograph of the current P&WA ICS is shown in Figure 10 and the details of construction of this device are listed in Figure 11. A program that preceded the NASA OV-1B/JT15D program was the P&WA/Boeing Joint Noise Program in which a JT9D engine was tested statically using this inflow control structure and then flight tested using the same engine aboard a Boeing 747. Dr. Peracchio summarized in Figure 12 differences between static data obtained with and without an ICS and flight data, (the static data was projected to flight to allow direct comparison with the flight data). There was an observable improvement when an ICS was used with the JT9D, but no noticeable improvement on the noise variability. In Figure 13 he summarized schematically the ICS design system. The target of the design system is ICS designs that produce in-flight values of turbulence at the fan face. In addition, the output of the design was screen radius and covering material details. Figure 14 shows a comparison of an inflow control structure designed by the design system, and the existing P&WA ICS that was built before the design system was developed and used in the P&WA/Boeing Joint Noise Reduction Program. His conclusions, shown in Figure 15, pointed out that use of an ICS for static testing of the JT9D reduced the blade passage tone but not its first harmonic. These conclusions contained certain reservations. They were: (1) other engines may show different results and (2) elements in the projection of static data to flight require further assessment.

## BOEING EXPERIENCE

A. O. Andersson

Mr. Andersson spoke of the Boeing experience of flight simulation of fan noise in static tests. He categorized this experience as it related to (1) effects on the noise source, (2) effects on propagation, and (3) related measurement techniques. He focused on the aspects of flight simulation that require further attention.

Under "effects on source" Mr. Andersson listed five items of concern. These were:

- Nacelle deformation
- Ambient pressure and temperature
- Flow field outside of the boundary layer
- Boundary layer at the fan face
- Fan loading

The nacelle deformation under flight loads can have an effect on noise, e.g. through nacelle ovalization. If this is considered during static testing these deformations can be modelled.

The effect of ambient temperature and pressure was cited principally to remind us that the proper normalization by  $pc^2$  was often forgotten.

Effects of the flow field outside of the boundary layer have been examined as a function of the following:

- (1) Test stand related distortions including that of the inflow control device (ICD)
- (2) Atmospheric turbulence, the main reason for the ICD
- (3) Inlet angle of attack, which was a small effect at small angles
- (4) Inlet geometry (droop, bellmouth), which can be significant
- (5) Temperature distortions, which are small, based on limited model fan data

Mr. Andersson mentioned that Boeing routinely used ICDs in full scale and model scale tests for a number of years (since 1978). The full scale ICD was used with the JT9D and the model scale ICD was used with 12" and 15" dia. fans. He did not discuss design details nor performance of the ICDs since he thought that these aspects were thoroughly covered by others at the workshop.

The boundary layer at the fan face as an effect on the noise source was discussed next. Mr. Andersson said that there were two aspects of this effect. These included an increased boundary layer thickness during static tests and a circumferential distortion of the boundary layer due to angle-of-attack and mean flow distortion. He showed in Figure 16 the various bellmouth sizes used to study boundary layer thicknesses. Figure 17 shows the

effects of these bellmouth sizes on boundary layer thickness. In Figure 17 it is shown that the boundary layer thickness at the fan face in the static case was largely independent of the shape and size of the inlet lip. Calculations indicate a much smaller boundary layer thickness in flight, as shown in Figure 18. It was believed that boundary layer suction would be required to further reduce the thickness to that typically found in flight.

Dr. Andersson next discussed the effects on the noise source by fan loading. Figure 19 shows the nozzle area change required to simulate fan loading for various flight speeds as a function of fan nozzle pressure ratio. The corresponding changes in noise as a function of fan loading are shown in Figure 20. When several radial modes are present a change in fan loading will show up as a redistribution of the sound energy in the radiated field. This aspect of flight simulation should not be ignored.

In the area of effects on propagation the following aspects were discussed in detail:

- (1) Inlet shape geometry effects
- (2) Mean flow and boundary layer effects
- (3) ICD effects
- (4) Convective effects
- (5) 3-D character of the radiation pattern

Figure 21 shows striking effects of inlet shapes on far-field radiation. The noise source for all shapes tested was a vibrating plate which generated a 13,2 mode. As seen in the figure the noise differences were as much as 40 dB at some angles.

The effect of boundary layer on propagation as evidenced by far-field radiation patterns is shown in Figure 22. These results were obtained using a model fan with inlet rods in which the noise source was rod/blade interaction dominated. The curves are shown spaced by 10 dB for clarity. There was no apparent effect of the boundary layer on propagation.

The effect of a Boeing ICD is shown in Figure 23. The effect was relatively small, increasing with frequency but less than 2 dB at 14 kHz. The Boeing Co. found this effect important only in model scale. More important was the reflection associated with the ICD itself. Strong interference patterns or highly directional sources may have resulted. This effect is shown in Figure 24. These curves were also spaced 10 dB for clarity. Radical changes of the directivity were observed in the 0-30° range. To avoid this one must eliminate as much ICD structure as possible. The Boeing Co. has a "self-supporting" honeycomb dome for use in scale model tests. This structure virtually eliminated these directivity differences and this improvement is shown in Figure 25.

Convective effects were discussed as they occurred in the following areas:

- (1) Doppler frequency shifts
- (2) No change in source strength
- (3) Effects of propagation through external velocity gradients

There was no disagreement on item one. On item two, if the fan operated in the same flow field, in flight and statically, the source strength should be the same. However, on item three, in Mr. Andersson's opinion the apparent amplification was due exclusively to propagation through external velocity gradients at the lip and beyond. This was a change in directivity which might be mode dependent. It was, therefore, questionable that these gross effects can be modelled by a power of  $(1 - M \cos \theta)$ .

Finally, the three-dimensional effects on noise propagation were discussed. This 3-D character was observed (Figure 26) for a model fan with rods in front of the fan rotor in order to produce well-defined modes. Similar effects have been observed on a fan with inlet guide vanes. Mr. Andersson commented that the observed 3-D effect may not be as important for high bypass ratio engines. Further investigation appeared warranted.

In summary, Mr. Andersson stated that significant improvements in static simulation of flight sources were achieved with the use of ICDs. However, he believed that the following subjects need attention to further improve static simulation of flight fan noise.

Effects on source:

- inlet droop
- fan loading
- nacelle deformation
- remaining distortion interacting with the boundary layer

Effects on propagation:

- inlet geometry (probably the most important)
- mean flow gradients
- ICD attenuation or scatter
- 3-D character of fan noise

## GENERAL ELECTRIC EXPERIENCE

P. R. Gliebe

Mr. Gliebe discussed the use of ICDs from the G.E. perspective. His first figure, Figure 27, listed the purposes and objectives of testing with an ICD. Mr. Gliebe presented a summary of G.E. experience with ICDs which included a range of engines and fans, whereas the NASA tests were concerned entirely with the JT15D engine and the P&WA/Boeing tests were exclusively with a JT9D. The G.E. tests included the JT15D engine, another small engine, the Garrett QCGAT, and two large G.E. engines, the CF34 and the CF6-80A. Figure 28 shows various ICD/Vehicle/Facility combinations tested by the G.E. Co. The G.E. Co. found that there were several important considerations for design of small ICDs and these are presented in Figure 29. In addition, it was believed to be useful for better flight simulation to employ a reverse cone inlet during static noise tests. Typical results of G.E. testing are shown in Figure 30. These plots showed the advantage of using an ICD to study the effects of throttling on the 1/3 octave sound power level, PWL, as a function of rotor relative speed. Without an ICD no effect was observed whereas with an ICD a noise reduction was observed with reduced throttling. Most of this reduction was due to broadband noise reduction since the blade passing frequency was only 1-2 dB above the broadband noise level.

Mr. Gliebe continued his presentation by turning to the work done by G.E. for NASA Ames. Typical results from this work were shown using the JT15D engine in the 40 x 80 tunnel and outdoors, with and without an ICD. These results are plotted in Figures 31 and 32 and are fully reported in reference 3. This was followed by a discussion of the G.E./LeRC QCGAT engine test experience, which is reported in reference 4.

The G.E. CF34 engine test experience included the use of a full size (12 ft.) ICD of Boeing design which had a honeycomb L/D of 12. A 1/3 octave blade passing frequency power level is shown in Figure 33 as a function of fan speed. Similar results are shown for the CF6-80A engine in Figure 34. These data included results of a treated versus an untreated inlet. These results also revealed a sensitivity to location, i.e. terrain roughness produced turbulence level differences.

Mr. Gliebe concluded that the use of an ICD permitted evaluations of internal noise source changes which were not possible without an ICD. Also, G.E. Co. has found that the BPF tone reduction obtained by using an ICD depend on (1) operating line, (2) fan design, (3) treatment, and (4) facility environment.

SESSION II

JT15D PROGRAM



## MODIFICATIONS, INSTRUMENTATION, AND INLETS

R. A. Golub

Mr. Robert Golub discussed the engineering required to modify the engine and aircraft. Also discussed was the development of the instrumentation required to accomplish the flight research task. During these discussions an emphasis was placed on the commonality of the instrumentation and hardware used in each of the ground stator, wind tunnel and flight tests. Figure 35 shows a table of JT15D-1 design features. The only differences between the test engine and a production engine were the spacing between the core stator and rotor and the number of vanes in the core stator. The reason for this modification was to move the rotor-core stator acoustic interaction cut-on frequency beyond the operating range of the engine to facilitate the study of turbulence-rotor interaction. Only modified JT15D-1 engines were used in the various static, wind tunnel and flight tests.

Figure 36 shows the blade mounted transducers (BMTs) and supporting instrumentation. This instrumentation system was designed and fabricated by the P&WA under contracts to NASA LeRC and LaRC. The technology was developed and first used on a JT9D engine. The JT15D engine was a more demanding installation because of reduced space and higher g loadings on the transducers. After each transducer passed an initial exposure to the high g tests, they remained exceptionally reliable. Figure 37 shows a detailed sketch of the BMT locations used for comparison of data between the various test environments. Later in the workshop the recently discovered engine support strut potential field-rotor interaction noise source was discussed. The struts that generate this strong potential field are shown in Figure 38.

Figure 39 shows a photograph of the modified OV-1B aircraft carrying a modified JT15D engine which was used for the flight tests. The JT15D engine was installed under the right wing at the pylon mount station which normally would carry the right auxiliary fuel tank. This selected location minimized the engine acoustic installation effects, and made it possible to use the existing fuel system with minimal modifications. Also, the right wing was sufficiently strong to withstand the weight and thrusting loads of the JT15D engine without additional strengthening. Additionally, a complex on-board aircraft/JT15D engine instrumentation signal conditioning and recording system was developed for this program. The system provided for the recording of high frequency dynamic channels and provided multiplexing for the low frequency aircraft and engine state measurements.

Finally, comparisons were made of variations in the LeRC and LaRC engine operating line as a function of test environment. These are shown in Figure 40. The static tests operating line of the LeRC fan pressure ratio versus corrected weight flow was predictably higher since there was no attempt to simulate flight by adjusting the operating line during static tests. Interestingly, the operating line for the tunnel was unexpectedly lower than in



flight. This was a result of the way the fan exhaust area was obtained. An existing bypass duct muffler was used and mechanical tabs had to be inserted in the fan exhaust as the most expedient way to adjust the nozzle area equal to that of a typical flight fan exhaust. However, the tabs affected the nozzle discharge coefficient thereby altering the mass flow somewhat.

## LERC ICD CONFIGURATION STUDIES - OUTDOOR ENGINE TEST STAND

### FAR-FIELD NOISE

J. G. McArdle

Mr. Jack McArdle presented far-field noise results of two ICDs designated numbers 1 and 12, shown in Figure 41. ICD No. 1 was the first design while ICD no. 12 was the most recent. Early acoustic results using ICD no. 1 with the JT15D are shown in Figure 42.

One of the early discoveries in the program, illustrated in the data of Figure 42, was the presence of a strong strut-rotor interaction. This interaction of six struts with 28 rotor blades caused a circumferential mode of 22 to be generated. In order to validate the presence of this mode, a special instrumentation technique was used in the engine inlet and is shown in Figure 43. In addition, calculation of the theoretical far-field directivity pattern for the  $m = 22$  mode at the blade-passing-frequency (BPF) was made that matches the data quite well. Probability density functions of the data at 10, 20, and 30° showed a Gaussian shape typical for a multimodal noise source, while at 40° and up they showed a periodic shape typical of a single mode. With this evidence it was concluded that the  $m = 22$  mode was present and most likely dominant in the JT15D engine inlet at the speed tested.

Additional testing was done at LeRC with a series of ICD designs. The most recent design, ICD no. 12, was mated with a flight geometry inlet. This was the same inlet geometry and lip used for the flight tests. Acoustic results for this ICD/inlet configuration are shown in Figure 44. The BPF level was reduced considerably at all angles and the shape of the pattern was changed when the ICD was used. Also, it was observed that the broadband levels did not change from no ICD to the ICD number 12 configuration. Mr. McArdle presented other figures to further confirm these trends at different engine speeds and also observed the behavior of the  $2 \times \text{BPF}$  tone directivity.

Another experiment conducted at LeRC involved using 41 rods in front of the JT15D fan to produce the  $m = 13$  mode (caused by interaction between the 28 fan blades and the rod wakes) to further study the effects of the ICDs on sound transmission. These results are presented in Figures 45, 46, and 47. Other than in Figure 45, 6750 rpm, the ICD had little effect on the peak SPL. This tended to confirm the hypothesis that the rod/rotor generated mode of  $m = -13$  was so strong that it probably overshadowed any turbulence-rotor interaction affected by the ICD, so that the ICD had no deleterious effect on sound transmission from the inlet either in level or directivity.

## BMT COMPARISONS

L. J. Heidelberg

Mr. Heidelberg presented data shown in Figure 48 as typical BMT data prior to the use of inflow control devices (ICDs). This spectrum showed the presence of all harmonics of the shaft frequency. Use of ICD no. 12 revealed a drastically different spectrum, as shown in Figure 49, and allowed study of the effects of a lower-turbulence environment. Figure 50 shows a mean pressure plot of BMT B3 which clearly revealed a one cycle oscillation per revolution, six cycle oscillations per revolution and 66 cycle oscillations per revolution riding on the six oscillation signal. These corresponded to the six struts and the 66 stator vanes. The cause of the once-per-revolution oscillation was unknown. Mr. Heidelberg compared BMT results from ICD nos. 1, 5 and 12. He concluded that the differences were small and all ICDs compared were quite good based on BMT results. However, not all tones present in the various spectra were explainable. Heidelberg also showed BMT results of the effects of taping a portion of the outer surface of ICD no. 12 which revealed some effects from the tape in the high frequency region of the spectrum. In addition, there was some evidence that the tape width has an effect on the higher frequency peaks (42 and 48 distortion number). Also, Heidelberg showed BMT results from the LeRC 41 rod experiment. There was little change in the lower range of the spectrum (Figure 51) with the rods added. The broadband was somewhat higher throughout the spectral range. The most obvious difference was the 41 peak that corresponded to the 41 rods. There was a discussion of the unknown blade response to this 41 peak as opposed to the 6 peak. It was believed that the blade response was not linear between these two excitations so that conclusions about the disturbance strengths testing to the 6 and 41 peaks could not be drawn.

## LERC ANECHOIC CHAMBER EXPERIMENTS

### FAR-FIELD NOISE

R. P. Woodward

Mr. R. P. Woodward discussed the phase I portion of JT15D fan work done in the anechoic chamber. The phase II portion will be done in the near future. The phase I results were to be regarded as preliminary. A sketch of the anechoic chamber is shown in Figure 52. The far field results shown were for ICD no. 5, with and without boundary layer suction. A sketch of the fan installation is shown in Figure 53. In addition, a sketch showing the construction details of ICD number 5 is shown in Figure 54.

In order to test at the same operating line, performance data were gathered and are shown in Figure 55. (See ref. 5.) The bulk of the far-field data was taken with the fan on the standard operating line.

Sound power level spectra were compared which showed the difference between the baseline and with ICD no. 5 in Figure 56. Applying boundary layer suction further reduced the sound power levels across the entire spectrum as shown in Figure 57. Adding 41 rods in front of the fan produced the sound power spectrum shown in Figure 58. These results implied that since there was little effect on the tones and broadband noise when using ICD number 5, there was no noise attenuation due to the structure of the ICD. In addition, Woodward presented many figures which compared a baseline of no ICD to ICD number 5 and ICD no. 5 with boundary layer suction. These were plotted to show noise at the blade passage tone, its harmonic and multiple pure tones (MPTs). These were presented as Figures 59 through 66. Also, Woodward showed far-field noise results of the 41 inlet rod configuration in the form of sound power spectra (Figure 67). A series of directivity patterns, taken with a traversing microphone, concluded Woodward's presentation and are shown in Figures 68 through 71. These noise radiation patterns showed the effects of the same configurations discussed throughout the presentation. Since the data were preliminary, conclusions were not drawn.

## BMT RESULTS

J. R. Balombin

Mr. Joseph Balombin discussed the blade mounted transducer (BMT) results from measurements made in the LeRC anechoic chamber using the same JT15D fan and stator that Richard Woodward tested.

A typical power spectrum is presented in Figure 72 and indicates that all harmonics of the shaft rotational speed were present. This spectrum was taken with no ICD and was referred to as a baseline. Installation of ICD number 5 caused the spectrum to change radically as shown in Figure 73. Most notable was the large increase in broadband noise and a generally downward alteration of many of the blade harmonics.

In order to gain some appreciation of the origins of the BMT spectral components, Balombin did an analytical study of an idealized, pressure pulse pattern. Figure 74 is an evenly spaced pulse pattern which resulted in the spectrum of Figure 75. Variation of the pulse spacing (Figure 76) revealed a radical change in the spectrum (Figure 77). Further variation of the pressure pulse by increasing the pulse (Figure 78) revealed a spectrum not unlike an experimental spectrum (Figure 79).

Figure 80 presents the rms pressure at a BMT near the blade tip. The most significant changes occurred in the circumferential variations of the pressure level when the ICD was compared with the no-ICD or baseline case.

## AMES 40 x 80 TUNNEL EXPERIMENTS

### LARC RESULTS

J. S. Preisser

Mr. Jack Preisser presented results from the LaRC/Ames JT15D experiment in the 40 x 80 tunnel. The purpose of the experiment was viewed as (1) a preliminary test to the flight tests, and (2) a blade loading and far-field acoustic study of the JT15D in the wind tunnel. A primary concern dealt with possible interference effects of either the OV-1 wing or the propeller in the vicinity of the JT15D inlet. The experimental setup in the Ames tunnel is shown in Figure 81. In addition to the wind tunnel tests a series of outdoor static tests were conducted for comparison. Comparisons of blade-passing-frequency (BPF) directivity patterns were made, an example of which is shown in Figure 82. A major difference was observed between the static test and the wind tunnel tests, but only moderate differences were observed as the wind tunnel speed was increased. Additional study will be required to resolve these differences. Further testing at higher wind tunnel speeds revealed that there was little additional pattern alteration due to speed alone. This is illustrated in Figure 83 on a sound power basis. In addition, no appreciable effect of moderate variations in angle of attack was observed.

Comparisons were made of the fan blade mounted transducers (BMTs) under various test conditions and are shown in Figure 84. The major observable difference was the decrease in shaft harmonics across the spectrum as the tunnel speed was increased from 4 to 31 m/s. This was assumed to be caused by a dramatic decrease in the inflow turbulence as it was "blown away" by the higher tunnel speeds.

Finally, to determine the effect of the OV-1 wing on the acoustic spectra, Figure 85 was presented. At the lower speed of 4 m/s there was a significant change at the BPF when the wing was added. However, at the higher speed of 57 m/s, more representative of flight, there was no observable difference. Therefore, it was concluded that the wing should not produce any acoustic interference in flight.

Mr. Preisser presented his conclusions as follows:

- (1) There was a sound power reduction of 10 dB with simulated forward speed
- (2) Rotor-turbulence interaction clean-up was accomplished at 10 m/s
- (3) BMTs confirmed rotor-strut potential field interaction
- (4) No angle-of-attack effect was observed for small alpha
- (5) No installation effects due to the wing were observed at flight speeds in the forward arc

## GENERAL ELECTRIC RESULTS

R. G. Holm

Mr. Ray Holm of the G.E. Company discussed results of testing the JT15D engine in the  $40 \times 80$  tunnel under an Ames contract. The scope of the G.E./Ames program is shown in Figure 86. The program centered on the influence of inlet cant and certain inlet treatment effects. Results of the canted inlet test are shown in Figure 87. These results included both far-field acoustic data and static pressure distortion at about 5-7 cm in front of the fan face. Additional tests were made using the inlet configuration shown in Figures 88 and 89. Comparisons of static pressure distortions are shown in Figure 90. Corresponding narrowband spectra results are shown in Figure 91 for treated inlets. Far-field blade passing frequency (BPF) directivity patterns are compared in Figures 92 and 93 for various engine speed regimes.

In addition, Mr. Holm described testing of the JT15D engine by varying the fan operating line as shown in Figure 94. Corresponding BPF directivity patterns are compared in Figures 95 and 96.

Outdoor tests were conducted for comparison to the wind tunnel data. Farfield BPF directivity patterns are compared in Figure 97 and reveal much lower wind tunnel levels and a striking difference in the pattern shapes.

Turbulence spectra are presented in Figure 98 comparing axial components of turbulence about 8 cm upstream of the fan face. The comparisons were made with and without an ICD at a transonic tip speed. This figure showed a dramatic reduction in the relative power spectral density in the lower frequency regime when an ICD was added. Very revealing spectral difference plots are shown in Figure 99. They show typical tonal differences of 12 dB at various microphone locations for selected operating speeds.

Mr. Holm showed BMT results which compared the various inlet geometries in Figure 100. The BMT I was able to discern between the inlet geometries and showed a definite improvement when the canted inlet was compared to a curved inlet. This improvement is denoted by the diminished sinusoidal component in the BMT waveform.

### SESSION III

#### LARC FLIGHT RESULTS AND COMPARISONS





## CONVECTIVE AMPLIFICATION EFFECT

R. Amiet

Dr. Roy Amiet began his discussion by postulating that a fan noise source does not change in flight. All observed changes then would be due to external effects. He presented Figure 101 showing the common dipole correction. He next presented equations in Figure 102 on energy flow in a moving fluid. In the far field, these equations are much simplified, as shown in Figure 103. Dr. Amiet pointed out that power radiated by a dipole in a flow is quite different from power radiated by fixed dipole, as shown in Figure 104.

Assuming isotropic, irrotational flow, a hypothetical model was proposed which equated acoustic intensities on flight and static wavefronts as illustrated in Figure 105. This gave a static to flight correction which was different from the dipole assumption made earlier in that the power on the  $(1 - M \cos\theta_e)$  term was now 2 instead of 4. The angle correction for the two models was the same and the measurement angle for the static case was equal to the retarded angle for the flight case. Although this model satisfied overall acoustic energy conservation, it also gave an erroneous description of the path followed by the acoustic energy.

Thus, a final model was proposed, based on ray tracing principles. This satisfied overall acoustic energy conservation and also gave an accurate description of the path of energy flow. Acoustic intensities were equated on spheres centered on the actual source position as in Figure 106. The ray paths were assumed to be not bent appreciably by the flow. A further check of this assumption revealed that ray bending was slight up to a Mach number of 0.5. This model gave a forward flight correction in which the power on the  $(1 - M \cos\theta_e)$  factor was 2 for observers at an equal distance and measured angle from the static and flight sources.

Dr. Amiet presented the experimental status of this work in Figure 107. His conclusions on the convective amplification correction problem were as follows:

- Energy conserving solutions exist
- Solutions are based on different theoretical models
- Definitive wind tunnel experiment is required
- There is need to verify by comparison to flyover data

## FUNDAMENTAL BMT EXPERIMENTS

W. F. O'Brien

Dr. O'Brien began his presentation by stating that an important class of turbomachinery noise is produced by the interaction of the blades of a machine with flow perturbations within the machine. Such flow perturbations may be stationary in time and position, as would result from the potential field or wake of a strut or vane, or may be random in nature, as occurs with the ingestion of turbulent flow into a compressor. Disturbances originating from struts or vanes exist continually during operation of a machine, and will contribute to tone noise depending on the strength of the consequent flow response and pressure fluctuations. Perhaps the most widely studied interaction is that of inlet guide vanes, rotors and stators in a compressor or fan stage. Wakes from upstream inlet guide vanes will produce acoustic sources on rotor blades, as will the rotor wakes on stators (ref. 6). The upstream potential field of a downstream disturbance will also produce a significant rotor response, as measured by on-rotor, high-response transducers (ref. 7). If the resulting pressure disturbances are not at a frequency which will be cut off by the inlet duct, far-field measurements may detect the resulting tone noise.

Experiments designed to investigate the interaction effect of downstream vanes with upstream rotors have shown that the rotor pressure disturbance, and therefore the resultant acoustic source, decreased as stator vanes were moved downstream from the rotor trailing edge. Figure 108 shows some results. It has been found that vanes placed more than two rotor chord lengths downstream do not further reduce the measured tone noise from a compressor (ref. 8). Larger, less numerous downstream struts can also have acoustically significant effects. Results of experiments by Preisser et al. (ref. 9) in a small turbofan engine have shown blade pressure fluctuations correlating with the fan blade passage frequency with respect to six downstream support struts in the fan discharge duct. Other investigators (ref. 10) have observed the interaction of large downstream struts with upstream rotors in connection with aeromechanical concerns.

The present investigation was designed to provide insight into the fundamental aspects of fan rotor-downstream strut interaction. High response, miniature pressure transducers were embedded in the rotor blades of an experimental fan rig. Five downstream struts were placed in the discharge flow annulus of the single-stage machine. Rotor blade pressure measurements were reported and analyzed with the struts in place and removed. Significant interaction of the rotor blade surface pressures with the flow disturbance produced by the downstream struts was measured and compared with results without the struts in place.

The experiments described were conducted in a single-stage research compressor rig located in the Turbomachinery Laboratory of the Mechanical Engineering Department, Virginia Polytechnic Institute and State University, Blacksburg, Virginia. For the present investigation, a single-stage

configuration was selected, and a set of five struts was fabricated for installation downstream of the stator vanes. Figure 109 shows the arrangement and angle settings of the rotor blades, stator vanes and struts.

The strut location for the present series of experiments was as shown, approximately four rotor chord lengths downstream of the rotor blade trailing edge plane.

Measurement of on-rotor fluctuating pressure was provided by blade-mounted transducers. The transducers employed in the present investigation were KULITE Model LQ-125-10 with 10 psi full scale pressure. Six transducers were located on the pressure side of a rotor blade, in a line along the chord at the 50% span position. Locations were 10%, 25%, 40%, 55%, 70% and 85% of the chord of the rotor blade, measured from the leading edge. Signals from the transducers were amplified on-rotor by integrated-circuit operational amplifiers having a gain of approximately 800 before being transmitted from the rotor through a multi-channel slip ring. Power for the excitation of the transducers and operation of the amplifiers was also transmitted through the slip ring, and was regulated to desired levels by rotor-mounted integrated circuit series regulators. The signals from the on-rotor pressure measurement system were simultaneously recorded on an instrumentation recorder. A block diagram of the measurement system is shown in Figure 110. The on-rotor measurement system contained six channels of the electronics shown.

The compressor was operated at a rotational speed of 2860 rpm, corresponding to a rotor tip speed of 227 ft/sec (69.2 m/s). Test points were selected to represent design point and reduced aerodynamic loading of the compressor. Data obtained from on-rotor transducers Nos. 2 and 6 with downstream struts in place are shown in Figures 111 through 116. Spectrum analyses of each signal were shown following the presentation of the pressure data signal and the accompanying one-per-revolution signal. The transducer signals shown were averaged 200 times to remove random fluctuations. Each 0- to 2-kHz spectrum showed prominent peaks at the thirty-seventh harmonic of shaft speed, corresponding to the rotor blade interaction with the 37 downstream stators, and at the fifth harmonic of shaft speed, corresponding to the blade passage frequency with respect to the five downstream struts. The 0-500 Hz spectrum showed more detail of the strut influence. The fifth harmonic was present in the spectra for all three transducers, but the relative magnitude of the sixth harmonic was seen to increase for transducers closer to the leading edge of the rotor blade. The compressor rig had six support struts in the inlet duct, and this was thought to be the source of the increasing sixth harmonic content of the pressure signals from the forward transducers.

Data obtained from runs with the five downstream struts removed showed a significant reduction in the level of the fifth harmonic of the pressure signals, as shown in Figure 117 through 122. The compressor operating conditions and the aerodynamic loading of the rotor blades were the same for the runs with and without the struts in place.

The data showed a strong rotor-strut interaction in the tested configuration. The strength of the interaction was evident when spectra obtained with and without the struts in position were compared. Recalling that the struts were located at approximately four rotor blade axial chord distances downstream of the rotor, the level of the interaction was remarkable. Clearly, such rotor-strut interactions must be considered as a potential engine noise source.

From the data obtained, the following conclusions were drawn:

- 1) Downstream struts of symmetrical airfoil shape interacted significantly with a compressor rotor when placed four axial rotor blade chord lengths downstream. The interaction was large in magnitude, and was considered as a potential source of tone noise.
- 2) Upstream struts produced an interaction with the pressure side of the rotor blade. The interaction was strongest at the leading edge of the blade.
- 3) Downstream stators located approximately one axial rotor blade chord length downstream of the rotor produced a strong interaction with the rotor blade pressure field.
- 4) The interaction of various flow disturbances with the rotor blade pressure field appeared to vary along the chord of the rotor blade, based on the measurements made.

A more complete presentation of the data and results of the investigation as presented in the workshop is contained in reference 11.

## FLIGHT PROCEDURES, DATA COLLECTION, AND CALIBRATION

A. W. Mueller

Mr. Arnold Mueller presented extensive material which showed the integration of five data acquisition systems, all of which simultaneously recorded a synchronized time code signal.. These systems were (1) weather measurement, (2) aircraft performance, (3) JT15D engine performance, (4) acoustic measurement, and (5) flight path measurement. A photograph of the test aircraft in its normal test configuration with the right engine turned off is shown in Figure 123. The flight operations technique which consisted of the test director coordinating the simultaneous operations of all these systems is shown schematically in Figure 124. This figure shows that communications existed between the test director and personnel at the different data acquisition sites making it possible for the test director to be informed of any unusual events, such as wind gusts or malfunctioning instrumentation, which might compromise the tests. The operations and data acquisition at the weather site were discussed, and Figure 125 shows a typical profile of the results of the measured weather variables vs. altitude.

During the aircraft flight, the pilot and on-board JT15D engine operator performed duties essential to a successful test. These duties are listed in Figure 126. The flight profile of the aircraft was set up as indicated in the plan view of Figure 127. This permitted the JT15D engine to pass directly overhead of the microphone array. Typical rectangular position data (measured by a laser radar) are presented in Figure 128 for the time period when the aircraft flew over the microphone array. A conclusion drawn from this figure was that the aircraft position during a given flyover was well within acceptable limits for acoustic testing. This kind of accuracy was found to be repeatable throughout all of the flight testing.

The farfield JT15D acoustic data acquisition technique was verified by a special series of flight tests using an acoustic driver noise source. This noise source, attached to the OV-1B aircraft wing, was flight tested as indicated in Figure 129. The details of the tests, which included using an ensemble averaging technique and numerous correction procedures on the acoustic data, are discussed in reference 12.

## AIRCRAFT FLYOVER DATA REDUCTION AND ANALYSIS

Doreen Gridley

Ms. Gridley stated that the goal of data reduction and analysis of aircraft flyover data was twofold: first, to generate an automated system to handle the large amounts of data acquired in an accurate and efficient manner, and second, to obtain a data base management system capable of building and maintaining a data base containing all pertinent aircraft flyover data. To achieve these goals, acoustic, radar, weather, engine and aircraft performance data were all incorporated into the data reduction and analysis system.

Spectra and directivities for a variety of engine and aircraft configurations were the desired output of this system. Initially, these values were obtained by applying methods of time series analysis. However, due to the Doppler shift, the noise data were considered nonstationary and could not be handled by conventional time series analysis. The method employed to compensate for this problem was finding the Fast Fourier Transform (FFT) over a small increment of time over which the data was assumed to be locally stationary and then ensemble averaging the spectral results over several microphones. Narrowband sound pressure level data were calculated at many source-to-observer angles.

Figure 130 is a sample plot of an ensemble averaged spectrum at an angle of 80°. This plot was a result of a known point source (4000 Hertz) mounted on the aircraft in place of the JT15D engine. This experiment was used to verify the accuracy of the data reduction and analysis techniques employed as well as to investigate acoustic installation effects.

Average spectra were then corrected to 100 feet lossless conditions. The corrections applied included instrumentation corrections of pressure response, diffraction, and windscreen, as well as those due to the propagation effects—convective amplification, inverse square law, atmospheric absorption, ground impedance, and the Doppler shift. As an option, a background spectrum (also corrected) could be subtracted from any other spectrum.

Figure 131 is the corrected sound pressure level plot calculated from the values in Figure 130 and the corresponding radar and weather data. It was noted that a strong peak existed at 4000 Hertz and that the magnitude over all frequencies was quite different from that of Figure 130. The change in sound pressure level values was primarily due to the inverse square law and to atmospheric absorption corrections.

The directivity at the blade passing frequency was determined by retaining the peak sound pressure level values at that frequency over many source-to-observer angles. Figure 132 shows a directivity of flight-to-static data generated by this system and comparable static data. In this figure relatively good agreement was demonstrated.

Once spectra and directivities were generated, they were preserved on a data base along with many of the engine and aircraft performance data. Comparisons were then made by selecting specific tests or by placing restrictions on the performance parameters. Static and wind tunnel data corrected to the same conditions were also placed into the data base.

In conclusion, a data reduction system and method of analysis for aircraft flyover data were established which reduced nonstationary data so as to be representative of stationary data. Implementation of the methods described led to an excellent conversion of narrowband flight data to their static equivalent.



## BMT COMPARISONS

J. A. Schoenster

Mr. Schoenster stated that one of the recent methods developed to study the mechanism of fan noise generation was the measurement of fluctuating pressure on the surface of fan blades. In the JT15D program several transducers were mounted near the leading edge of a fan blade and data from these transducers were continuously recorded during testing. A precise measurement of the instrumented blade location relative to the circumference of the fan duct was also recorded. These measurements allowed pressure variations as a function of location around the circumference of the duct to be identified. It was the purpose of this presentation to show some comparisons of data from the flight test of the JT15D with that from static tests of the JT15D and from a static test of the JT15D with an ICD. The flight tests and static tests were conducted by the Langley Research Center while the ICD tests were conducted by the Lewis Research Center. Details of these tests were discussed in other workshop presentations.

The locations of the transducers on the blade are shown in Figure 133. BMTs I and M were situated similarly but were located on different blades and BMT M was mounted differently than the other transducers used in this study. Results from BMT H (Figure 134) were obtained during the static test of the engine. A similar space-time history plot from the same transducer obtained during flight is shown in Figure 135. The visible trends in the static data, particularly between 140° and 200°, did not exist in the flight data. It was believed that these pressure variations were unique to the ground tests and are not representative of flight. In addition, it was believed that these pressure fluctuations may result in noise, masking the engine flight noise.

A comparison of spectra from static tests to flight tests may be seen in Figures 136 and 137. The data in Figure 136 was obtained in the tunnel while the tunnel was off, and was therefore representative of the static test conditions. During flight it was seen that most of the engine harmonic frequencies disappear over the entire engine speed range. Peak responses remained at the fundamental engine rotation frequency, the second harmonic and the sixth harmonic, with a few other harmonics occasionally observable. The effect of forward speed in flight was to eliminate most of the engine harmonic peaks and "clean up" the spectral shape.

Measurements from a fluctuating pressure transducer located in the duct over a similar engine speed range are shown in Figure 138. At about 10,500 rpm a fan tone is cut on from the interaction of the six struts with the fan rotor and propagates out of the duct. A scan of the BMT spectra (Figure 120) in the same frequency range shows no noticeable effect on the BMT as a result of this cut-on mode.

The sixth harmonic seen in both the ground tests and flight was related to the six struts in the by-pass duct and appeared in all the tests of the JT15D. Plotting the amplitude of this signal (Figure 139) showed an orderly increase

in amplitude as a function of engine speed. This order appeared to disappear when the blade tip speed became supersonic, about 12,000 rpm. Because of some uncertainty in the calibration of the BMTs it was decided to match the level of the amplitude of the sixth harmonic from the spectral analysis between test conditions and observe the relationship of all the other parameters. Because of the availability of data and the relative linearity in this range an engine speed of 10,500 rpm was selected for the comparisons shown here.

A comparison of spectra in Figure 140 showed that the general shape over the frequency range was very similar for the three test conditions. One difference between the three spectra was that broadband noise between 500 Hz and 4000 Hz was somewhat higher with an ICD than in the tunnel. Also, the tunnel spectrum was slightly higher than the flight spectrum. The fundamental fan frequency was also slightly higher with the ICD. The differences above 10 kHz were caused by using different by-pass filters in each of the analyses.

The mean and standard deviation plots for all three conditions were almost identical. Shown in Figure 141 were data obtained during the flight test. The six cycles per revolution variation in the mean value and the lack of sensitivity of the standard deviation to circumferential location were very obvious. Also common to all conditions was the occurrence of maximum positive pressure in the vicinity of the bottom of the inlet (180°).

While somewhat more complex in shape, the enhanced spectra were also very similar for all three conditions. In general, the fundamental frequency, the second order (harmonic) and the sixth order were the dominant responses. In the tunnel tests and flight tests the 66th harmonic was also a major peak which corresponded to the 66 stator vanes. All other order responses were at least 10 dB below the maximum response from these three cases. The enhanced spectrum from flight is shown in Figure 142.

Preliminary evaluations of these data are shown in Figure 143. Analyses of these data will continue, so that additional evaluations and insights to the ground simulation methods may be obtained.

## FAR-FIELD FLIGHT NOISE AND COMPARISONS WITH WIND TUNNEL AND STATIC RESULTS

J. S. Preisser

Mr. Preisser listed the types of data corrections applied to the various data sets in order to make direct comparisons (Figure 144). All data was normalized to a stationary 30.48 m (100 ft.) radius with lossless atmospheric conditions. A signal-to-noise ratio of JT15D and OV-1B versus OV-1B aircraft-alone with a single engine operating was obtained and is shown as Figure 145. The figure revealed an excellent signal-to-noise ratio for the test at most frequencies. The only area of caution identified was around the first harmonic of the blade-passing frequency. A flyover series to verify data repeatability is shown as Figure 146. These data repeated within about  $\pm 3$  dB. It was noted that aircraft forward speed was varied from 230 to 323 fps and was found to be ineffective in changing the noise, as shown in Figure 147. The variation observed was well within the repeatability range of the data.

Figure 148 is presented to illustrate the points of comparison based on duct modes at various fan speeds and their corresponding cutoff ratios. The comparisons began with Figure 149, which shows spectra taken at  $50^\circ$  from the engine inlet. These spectra revealed the effects of an ICD plus striking similarities between tunnel and flight with a few exceptions. The spectrum shape of ICD number 12 was similar to the flight case except the levels were generally higher. The next comparison (Figure 150) of the same four configurations is of broadband far-field noise. These levels were obtained by choosing values at the base of the various BPFs. Very small differences were observed between the two static cases, with and without an ICD. However, when comparing these with either the wind tunnel or flight levels considerable differences were observed. It should be noted that these results were not corrected for any operating line differences. The fan pressure ratios were essentially matched, but there were some small differences in weight flow and the fan speed difference was up to about 200 rpm. The difference in blade incidence angle was less than  $1^\circ$ . Figure 151 compares the no-ICD configuration, the ICD number 12 configuration, and the flight configuration. These comparisons were of the BPF noise radiation patterns at a fan speed near 10800 rpm. Excellent agreement was found between the ICD number 12 pattern and the flight pattern. A similar comparison was made (Figure 152) between the flight and wind tunnel BPF directivity patterns at a fan speed near 12000 rpm. The levels matched quite well but there were pattern differences that remained unexplained.

The remaining comparisons dealt with the MPT behavior in the various test environments. Figure 153 shows that there was little change in the spectra when the ICD was added. However, the flight spectrum showed dramatic differences both in level and character. In particular, there were large increases in the BPF and 2 BPF tones. The corresponding BPF radiation patterns are shown in Figure 154. This showed a sharp increase above all other test environments in the flight BPF beyond  $50^\circ$ . Figure 155 is a plot of sound power in the first 27 MPT peaks from  $0^\circ$  to  $90^\circ$  for each test environment. This showed a markedly lower level at all angles of the MPTs in flight compared with ground based tests. Some of this difference may be ascribed to engine operating line differences between ground

tests and flight. However, operating line differences are estimated to be less than half of the noise differences shown in this figure.

Mr. Preisser concluded his presentation by making the following observations: (1) the flight BPF directivity was repeatable, (2) there was no additional forward speed effects observed at increased speeds, (3) there were high broadband noise levels observed with an ICD, (4) there was good ICD/tunnel/flight agreement of BPF directivity at subsonic tip speeds, (5) there were high BPF noise levels observed at supersonic tip speeds in flight, and (6) there was low MPT power observed in flight.

## SUMMARY OF WORKSHOP RESULTS

The final afternoon of the workshop was devoted to discussions of the results presented over the preceding day and a half. It was concluded that the evolution of inflow control devices (ICDs) has "sufficiently" reduced the inflow related noise to permit many aspects of the fan internal sources to be correctly observed. It was understood that care had to be taken to minimize ICD related effects, such as flow disturbances associated with ICD rib structure and acoustic reflections. It was concluded that the current ICDs may not exactly simulate flight and an ICD user should be aware of these differences in his analysis of inlet noise data. There were some reservations in that these conclusions were based on data from only two engines, namely the JT15D and the JT9D, and there is a remote possibility that there may exist an engine that may respond differently, acoustically, to the current ICD type design practice.

It was agreed that blade mounted transducers (BMTs) had proven their worth. Certain information gained from these devices could not have been obtained any other way. However, due to their cost, it appeared that their use for the foreseeable future would be limited to research studies or to use as a diagnostic tool for special engine problems.

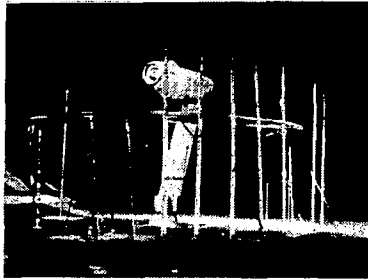
In the area of inlet treatment the G.E. experience between static ICD and wind tunnel tests revealed that good agreement was elusive. Apparently an ICD must be better for testing inlet treatment performance than for simply matching inlet hardwall data between static and flight or wind tunnel tests. This was believed to be due to the lower noise levels being examined with treatment which would require that the inflow turbulence induced noise be reduced lower than for hardwall inlet testing.

The agreement at subsonic tip speeds between static ICD and flight acoustic BPF data was regarded as exceptional. This agreement was not only due to the new precision data collection and analysis techniques, but obviously to the good flight simulation provided by the LeRC ICD number 12. However, some discrepancies remained, such as differences in the sound pressure levels in the 20°-40° range of the BPF radiation patterns. These differences are thought to be due to the large flight corrections necessary in this range. This area will need further study to resolve these questions.

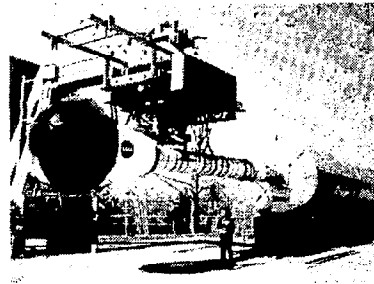
Two other significant differences were observed between static and flight that also require further study. These were in the areas of broadband noise and the multiple-pure-tone (MPT) noise. Although no appreciable differences were observed in broadband noise when various ICDs were tested, there were significantly lower broadband noise levels observed in flight. Similarly, the MPT noise observed in flight was significantly lower than that observed during the static tests. This effect included an apparent shifting of acoustic energy from the MPTs into the BPF tone. An explanation for some of this difference may be due to the slight geometric differences in the manufacture and wear of the two fan rotors. Future flight testing will examine this possibility. However, it was suspected that this was a real flight effect phenomenon which must be more thoroughly studied since it will significantly affect fan noise prediction.



(a) Langley OV-1B flight test.



(b) Ames 40 x 80 tunnel.



(c) Lewis static test stand.

Figure 1.- Forward speed effects on turbofan noise (JT15D engine).

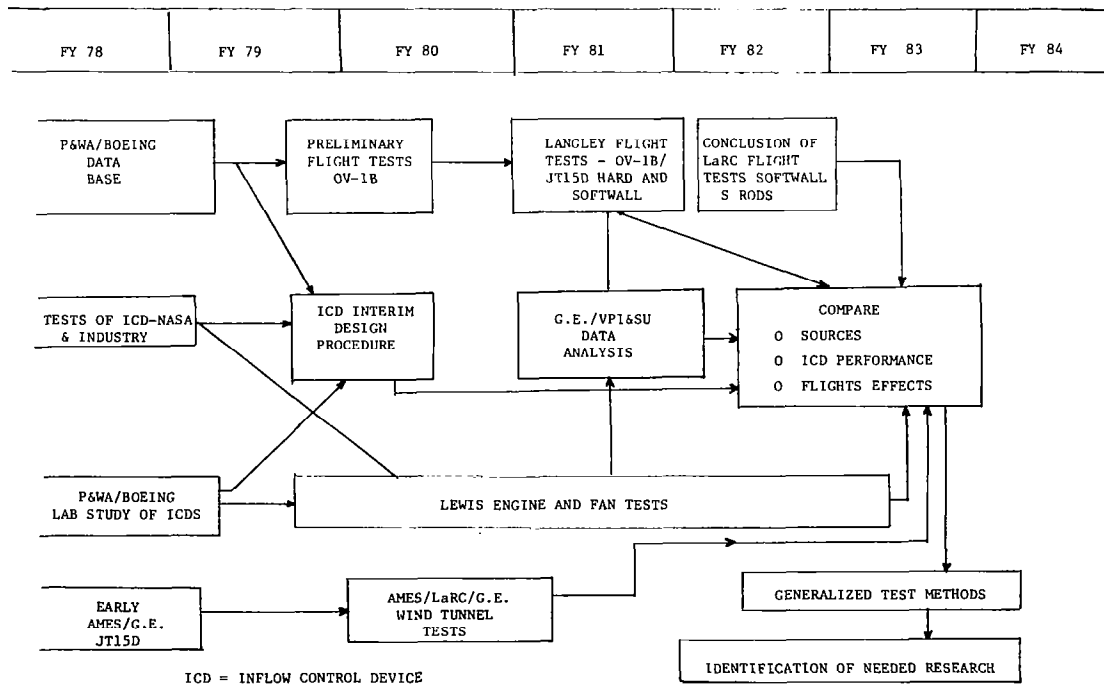


Figure 2.- Flight effects on fan noise program.

1. DEVELOP STATIC EXPERIMENTAL TECHNIQUES THAT REVEAL IN-FLIGHT GENERATION MECHANISMS & DIRECTIVITY

TECHNIQUES:      - INFLOW CONTROL DEVICES  
                       - ANECHOIC WIND TUNNELS

2. VERIFY METHODS OF PROJECTING GROUND DATA TO FLIGHT

ADJUST FOR:      - CONVECTIVE AMPLIFICATION  
                       - ATMOSPHERIC ATTENUATION  
                       - GROUND REFLECTION  
                       - SPHERICAL SPREADING  
                       - DOPPLER SHIFT

Figure 3.- Technical objectives.

ORGANIZATION	FACILITY/ SOURCE	D <sub>ICD,M</sub>	$\frac{D_{ICD}}{D_{FAN}}$	CONSTRUCTION	
				HONEYCOMB L/D	SCREEN OR PERFORATED PLATE % OPEN AREA
BOEING	OUTDOOR/ JT9D	7.3	3	12	46 UPSTREAM
GENERAL ELECTRIC	OUTDOOR ANECHOIC CHAMBER/ ROTOR 11	7.3	3+	SIMILAR TO BOEING	
		2.0	4	8	52 SPACED DOWNSTREAM
NASA LEWIS	OUTDOOR/ JT15D	0.8-2	1.7-4	4 TO 8	40-50 DOWNSTREAM
	ANECHOIC CHAMBER/QF-1 QF-13, JT15D	1.0-2	2.0-4	8	"
PRATT & WHITNEY	OUTDOOR/ JT9D	7.3	3	8	51 UPSTREAM

Figure 4.- Inflow control devices.

- o NATURE OF INFLOW DISTURBANCES TO BE CONTROLLED  
ATMOSPHERIC TURBULENCE, WAKES, VORTICES
- o NATURE OF RESIDUAL IN-FLIGHT SOURCE MECHANISMS  
ROTOR-STATOR, ROTOR-STRUT, ROTOR - B.L.
- o BEHAVIOR OF SPECTRAL COMPONENTS  
BPF (CUTOFF), 2 x BPF, MPT, BROADBAND
- o SENSITIVITY OF TONE GENERATION TO INFLOW DISTURBANCES
- o DIAGNOSTIC TOOLS APPLIED  
INFLOW SAMPLING: BLADE PRESSURES  
CONTROLLED SOURCE: ROD WAKE-ROTOR INTERACTION

Figure 5.- Technical themes/issues.

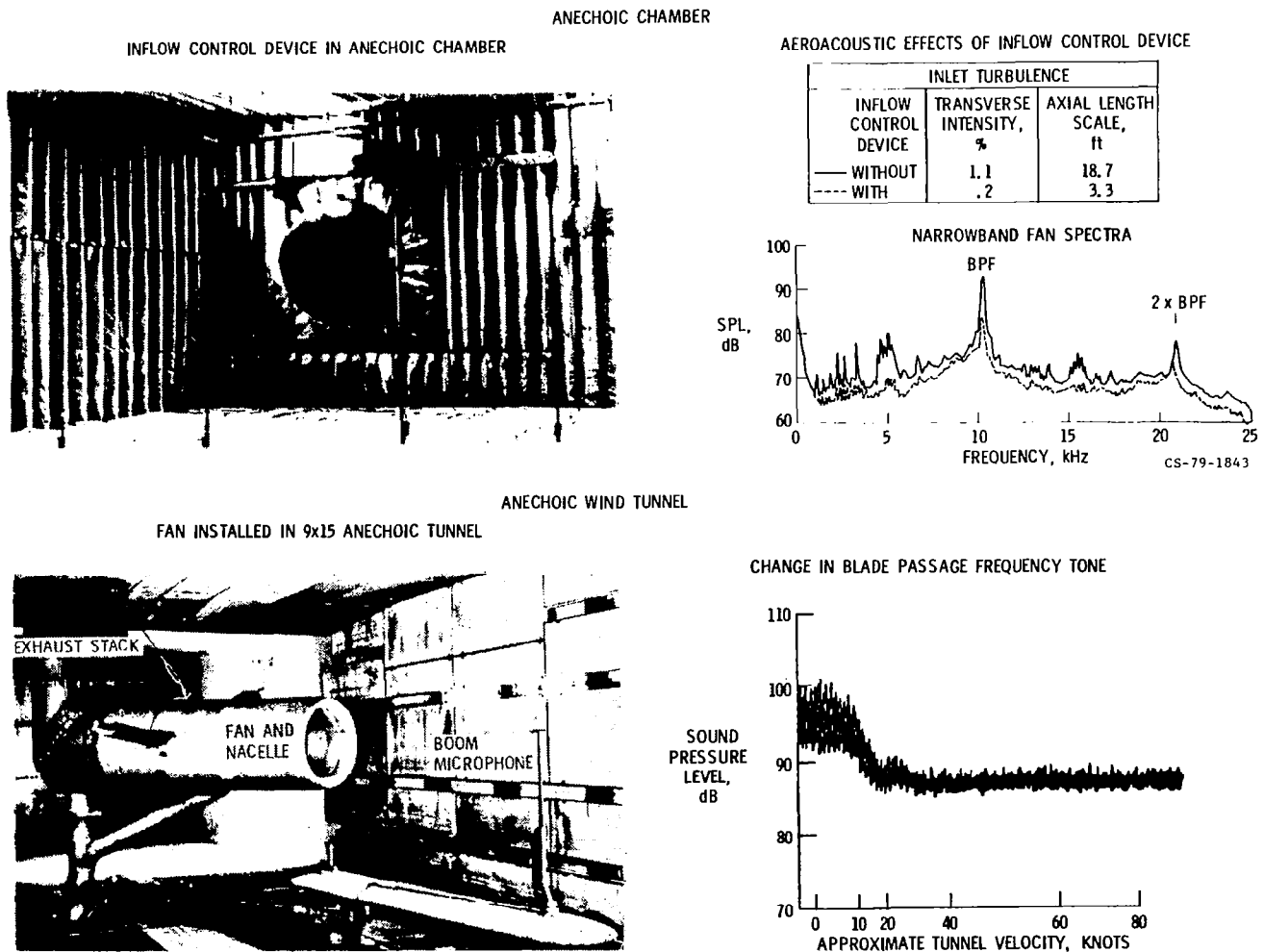


Figure 6.- Flight simulation in static fan test facilities.



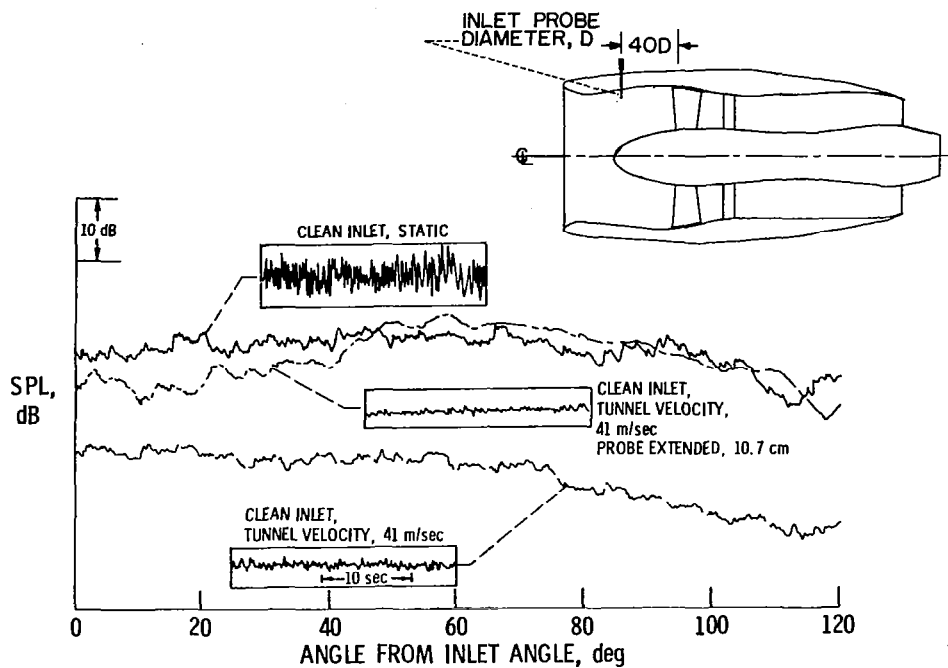


Figure 7.- Sensitivity of blade passage tone to inlet probe wake.

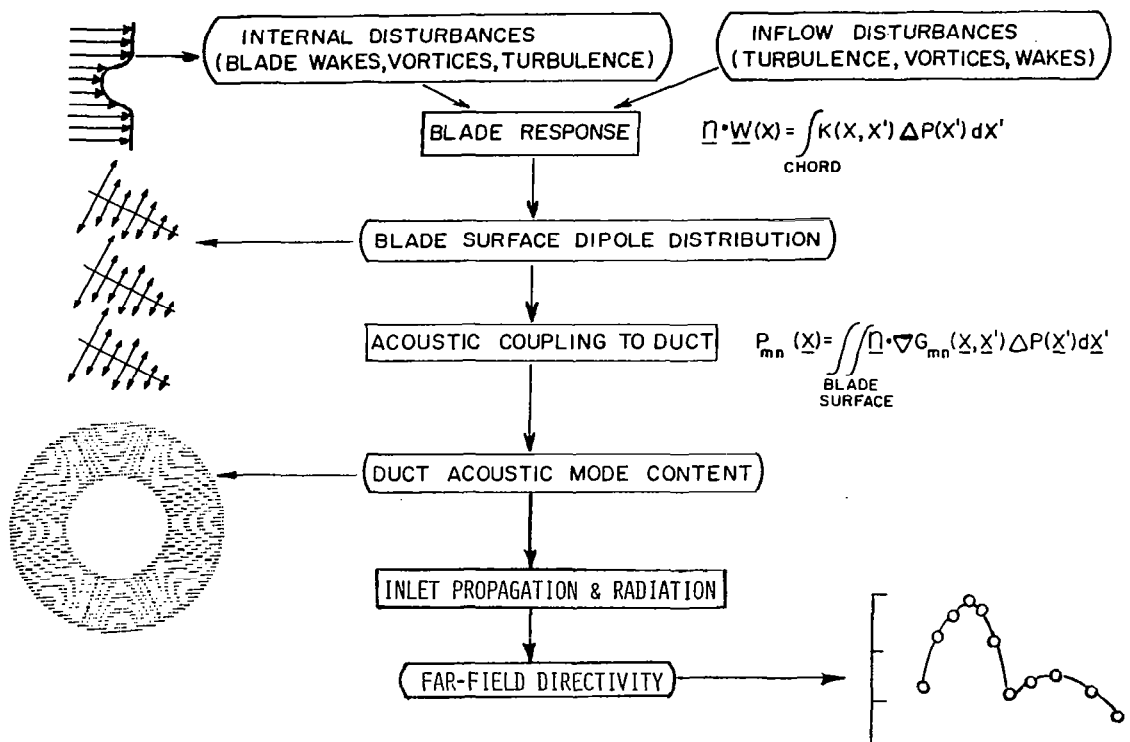


Figure 8.- Fan noise generation by fluctuating blade forces.

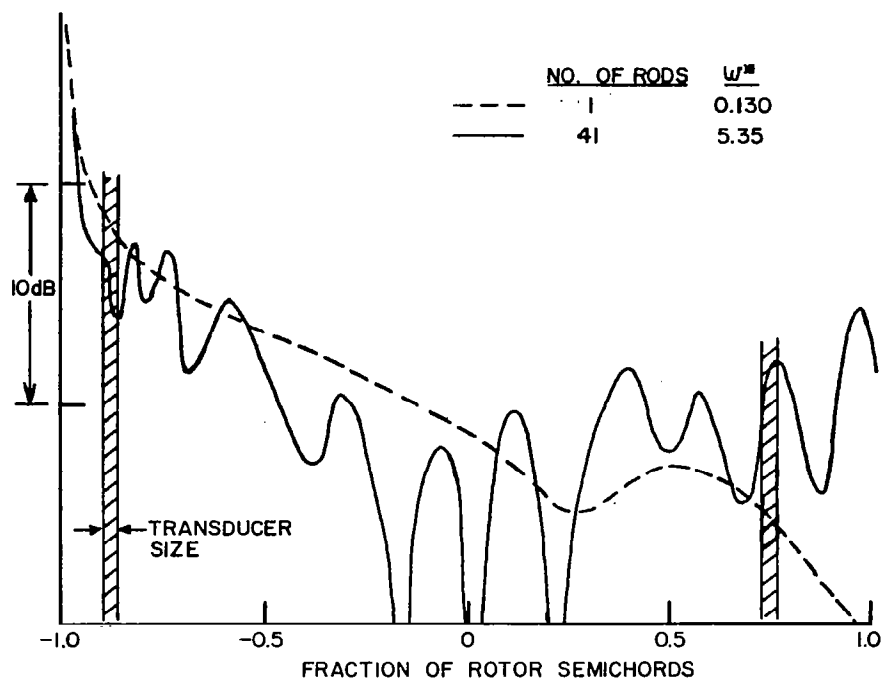


Figure 9.- Chordwise variation of fundamental rotor blade pressure generated by wakes of upstream rods.

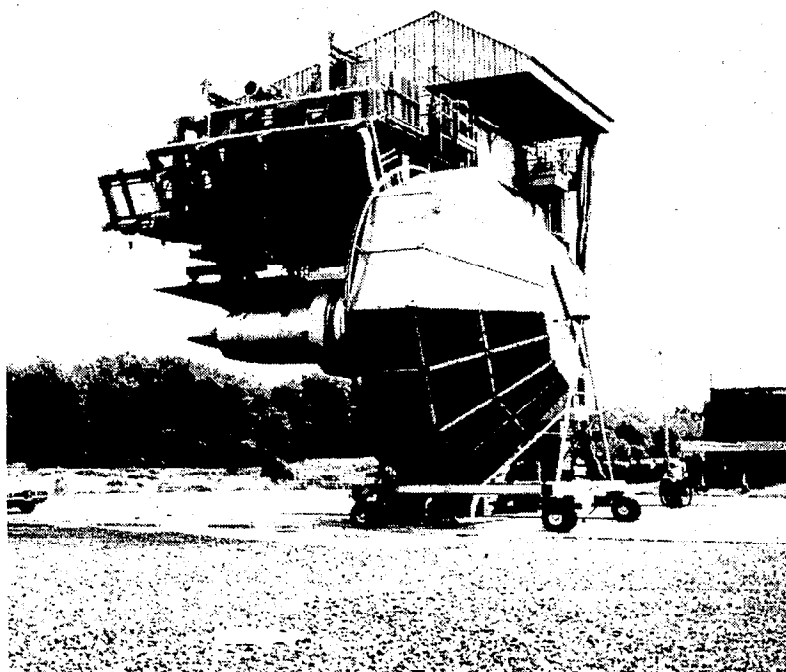


Figure 10.- JT9D engine with Pratt & Whitney Aircraft inflow control structure.

o CONSTRUCTION -

PERFORATED PLATE/HONEYCOMB

o SPECIFICATIONS

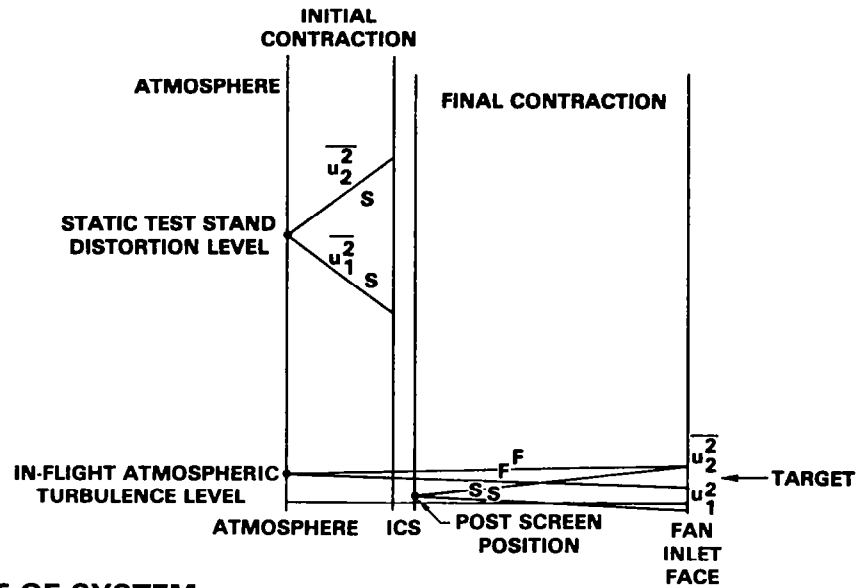
RADIUS	3.66M	(12')
HONEYCOMB CELL SIZE	0.0095M	(.37")
HONEYCOMB THICKNESS	0.0762M	(3.00")
PERFORATED PLATE HOLE SIZE	0.0048M	(.189")
PERFORATED PLATE THICKNESS	0.0031M	(.122")
PERFORATED PLATE OPEN AREA RATIO	51%	(51%)

Figure 11.- Details of Pratt & Whitney Aircraft inflow control structure.

	NO ICS	WITH ICS
FLIGHT CONDITION	$(BPF_{ma} - BPF_{PI})_a$ dB	$(BPF_{ma} - BPF_{PI})_a$ dB
APPROACH 30° FLAP	- 3 ± 1.7	1.2 ± 1.6 dB
APPROACH 25° FLAP	- 4.5 ± 1.4	- 0.1 ± 1.4
TAKEOFF	- 3.2 ± 1.5	- 1.8 ± 2.3
CUTBACK	- 5.0 ± 2.7	- 2.6 ± 2.3
AVERAGE OVER ALL ANGLES AND POWER SETTINGS	- 3.9 ± 2.04	- 0.8 ± 2.4

Figure 12.- Summary of effect of inflow control structure on static and flight data comparisons.

• **SCHEMATIC OF SYSTEM ELEMENTS**



- **OUTPUT OF SYSTEM**
  - **SCREEN RADIUS**
  - **COVERING MATERIAL DETAILS**

Figure 13.- Inflow control structure design system.

	<u>PRESENT DESIGN</u>	<u>P&amp;WA</u>
<b>NOMINAL RADIUS</b>	3.47m	3.66m
<b>DETAIL DIMENSION (HONEYCOMB)</b>	0.0067m	0.0095m
<b>DETAIL DIMENSION (PERFORATED PLATE OR GAUZE)</b>	0.003m	0.0048m
<b>THICKNESS (HONEYCOMB)</b>	0.0117m	0.0762m
<b>THICKNESS (PERFORATED PLATE OR GAUZE)</b>	0.0009m	0.0031m
<b>OPEN AREA RATIO (PERFORATED PLATE OR GAUZE)</b>	54%	51%

Figure 14.- Comparison of inflow control structure system design to P&WA design.

- **ICS REDUCES BLADE PASSAGE BUT NOT TWICE  
BLADE PASSAGE FREQUENCY TONE NOISE LEVELS**
  - **ICS IMPROVES AGREEMENT BETWEEN STATIC  
AND FLIGHT**
  - **ICS EFFECTIVENESS DEMONSTRATED FOR JT9D-7  
ENGINE**
- {OTHER ENGINES WITH DIFFERENT ACOUSTIC CHARACTERISTICS  
MAY SHOW DIFFERENT RESULTS}
- **ELEMENTS IN THE PROJECTION OF STATIC DATA  
TO FLIGHT REQUIRE FURTHER ASSESSMENT**

Figure 15.- Conclusions.

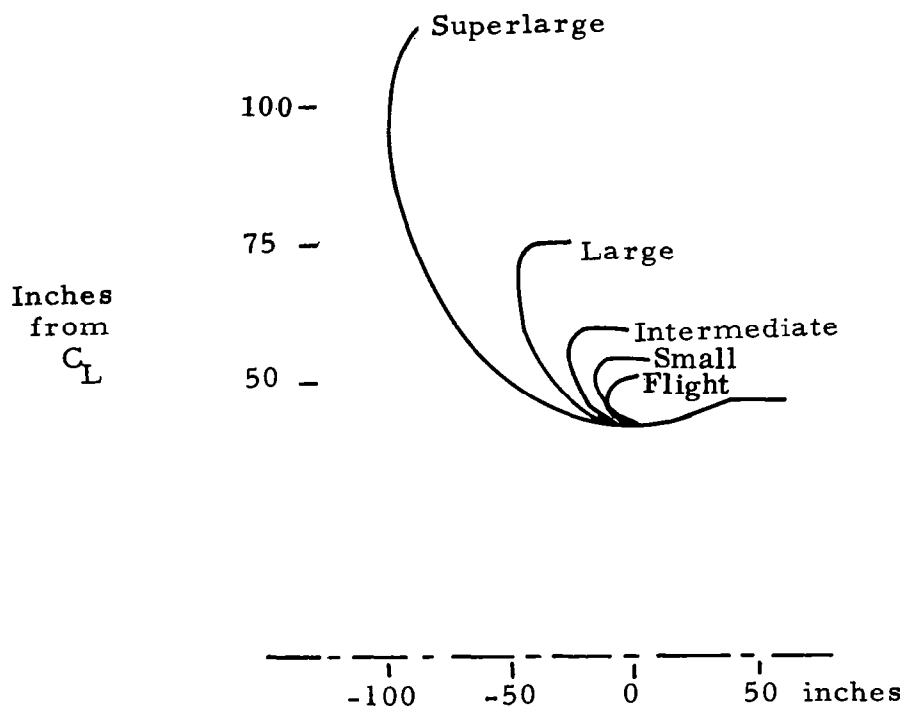


Figure 16.- Bellmouth sizes.

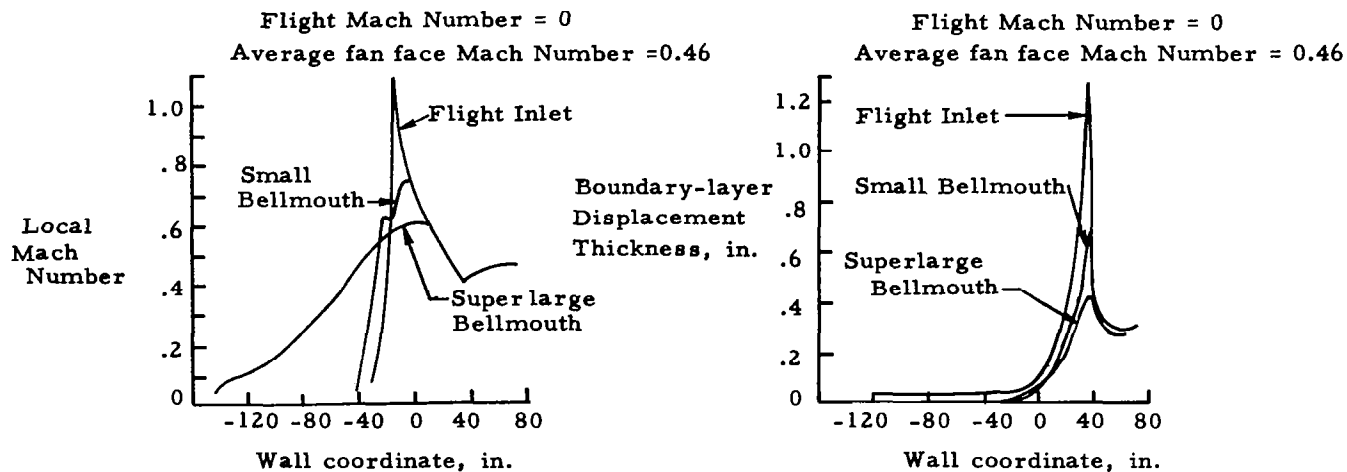


Figure 17.- Effect of bellmouth on boundary layer thickness.

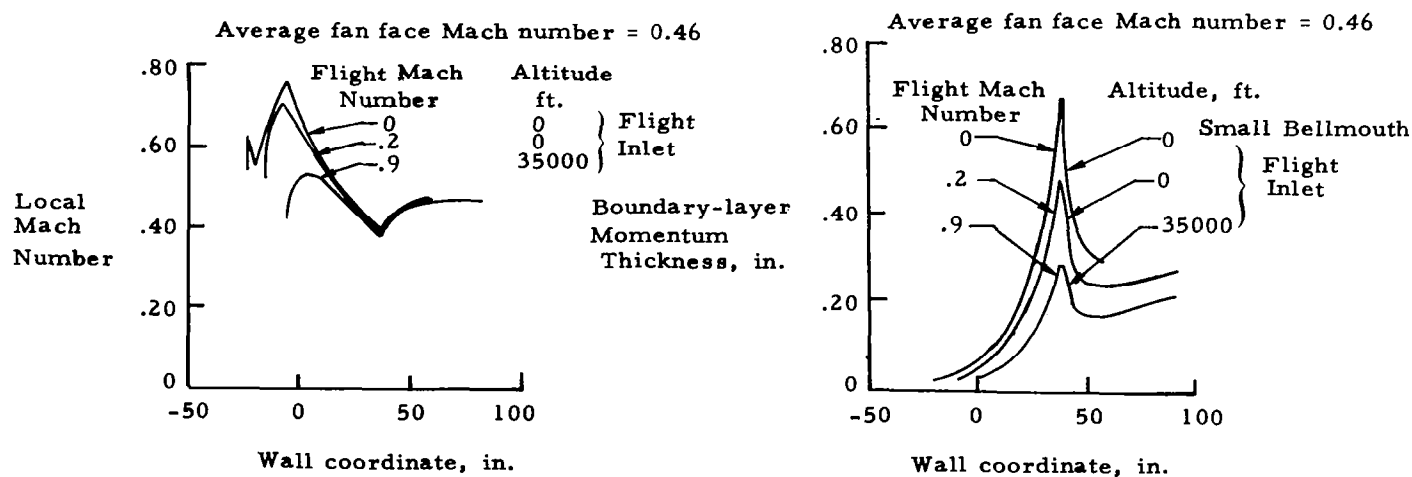


Figure 18.- Effect of flight on boundary layer thickness.

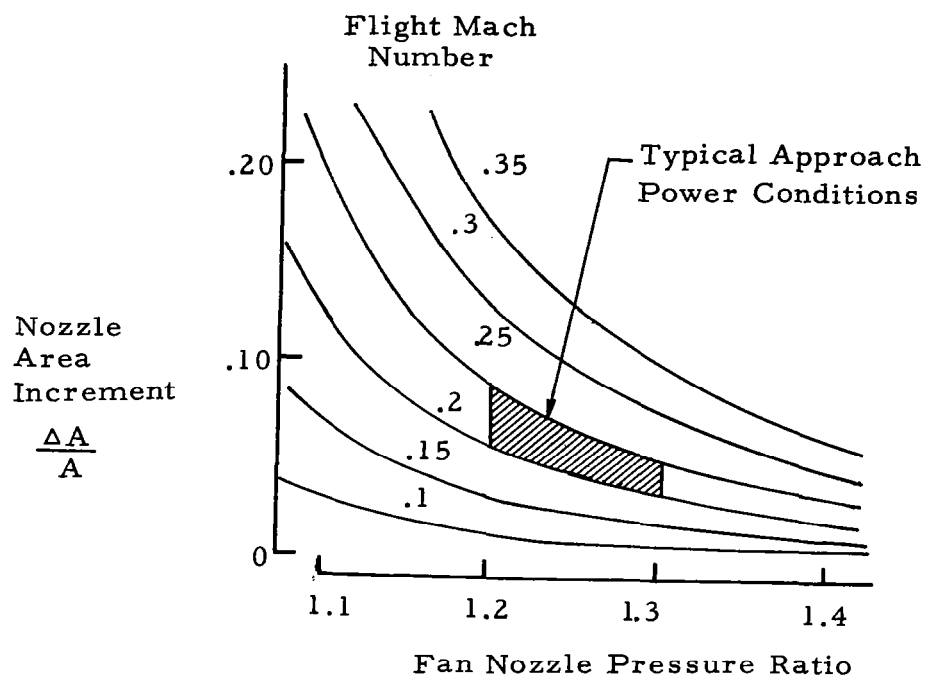


Figure 19.- Nozzle area change required for fan loading simulation.

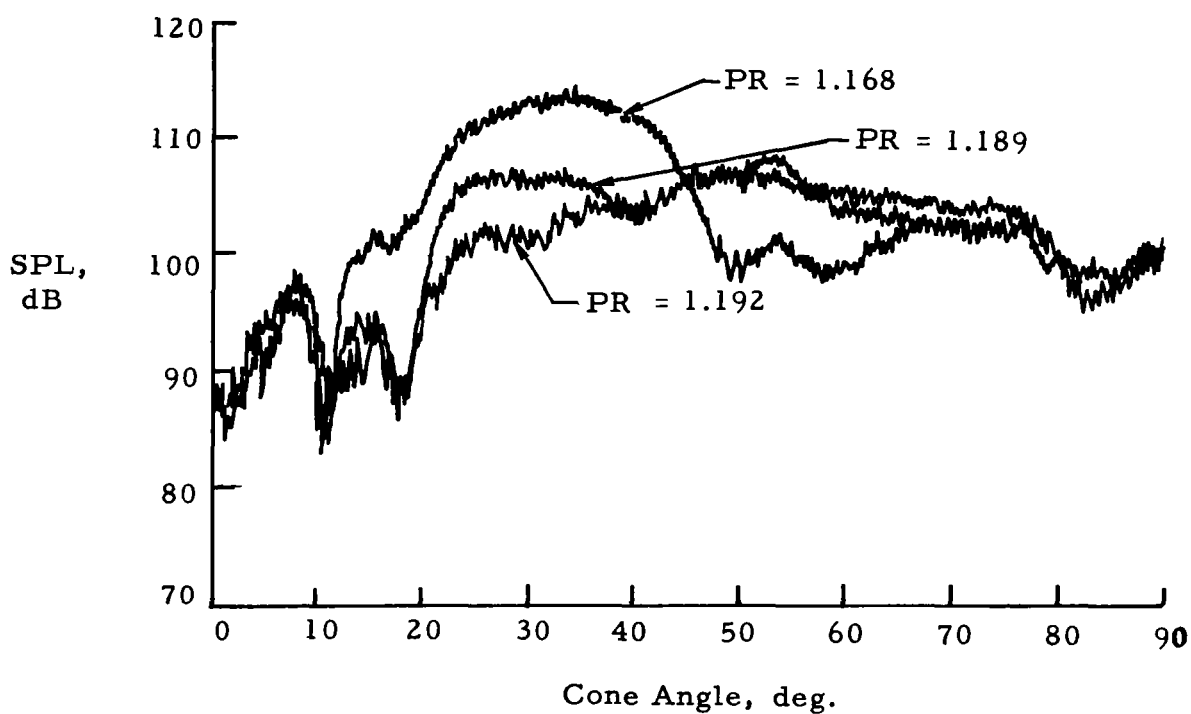


Figure 20.- Effect of fan loading.

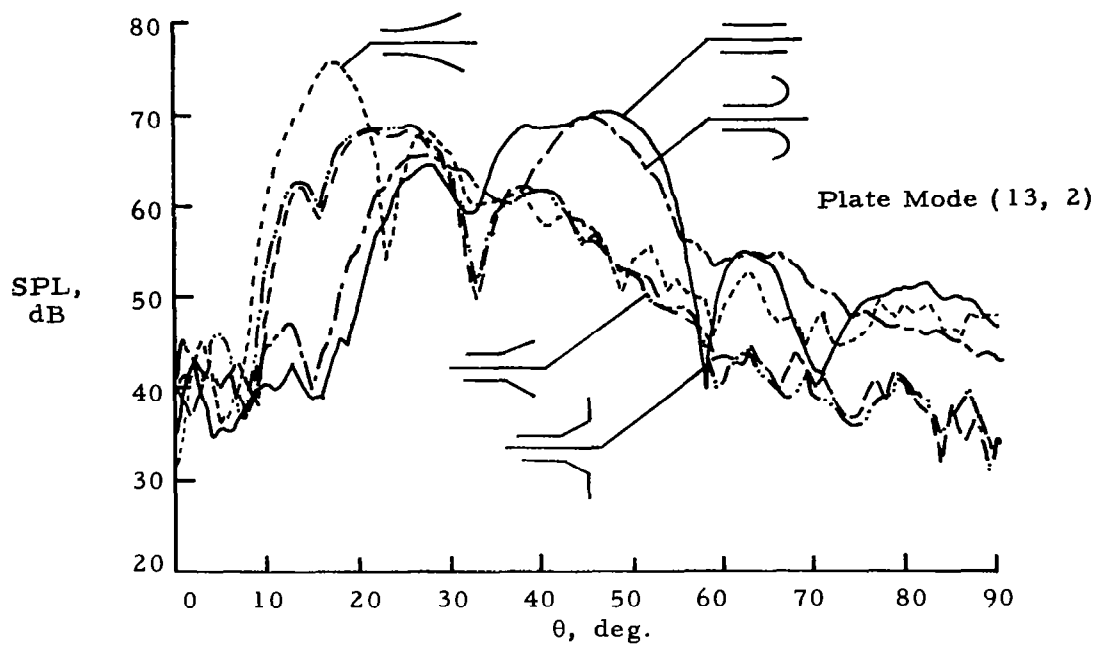


Figure 21.- Effect of inlet shape on radiation.

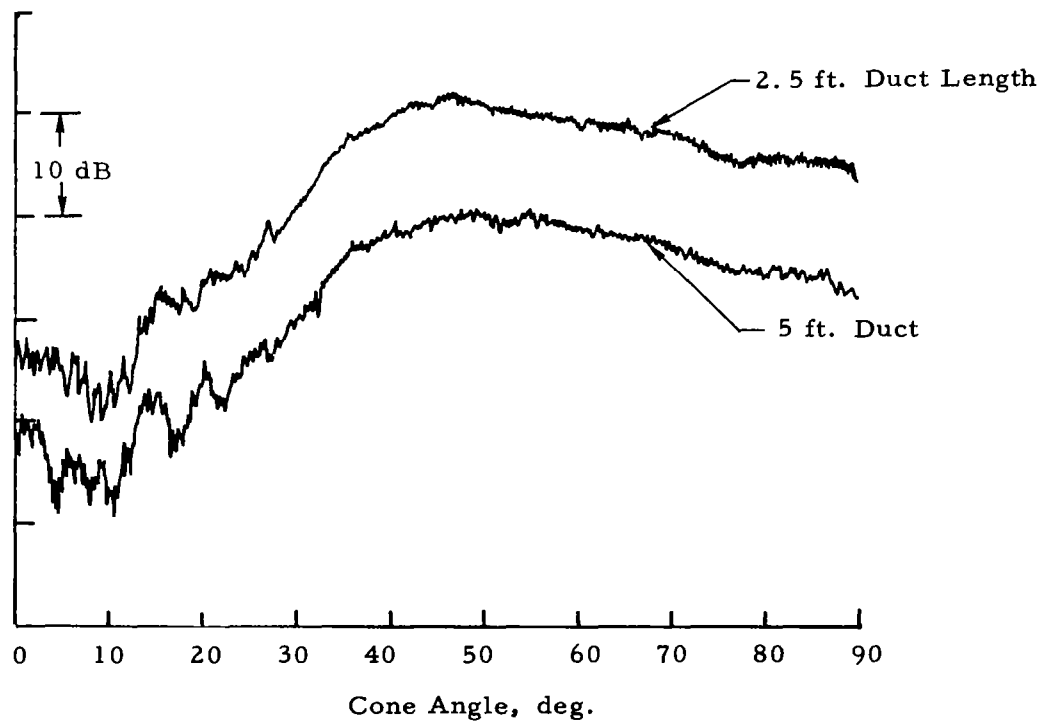


Figure 22.- Effect of boundary layer on propagation.



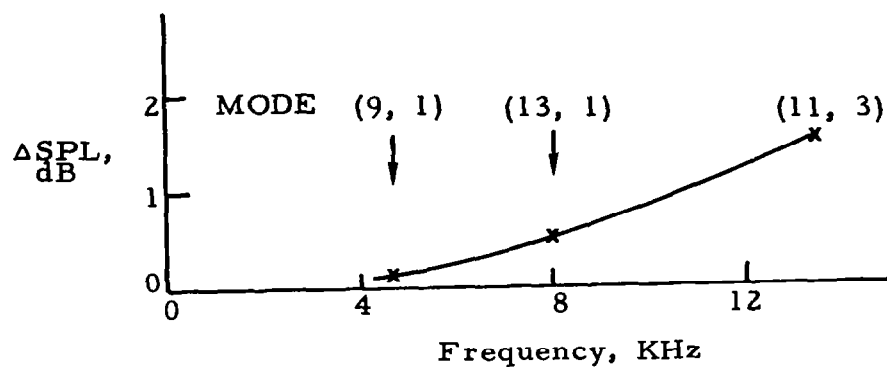


Figure 23.- Sound attenuation by ICD.

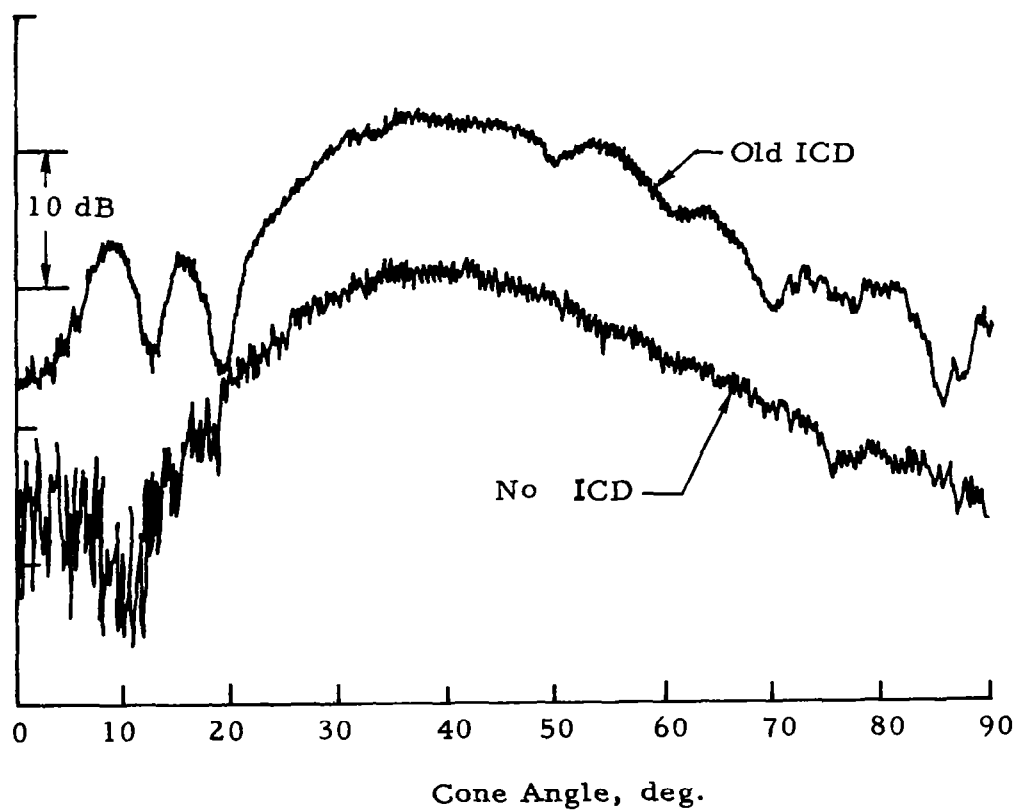


Figure 24.- Effect of ICD on propagation; old ICD structure versus no ICD.

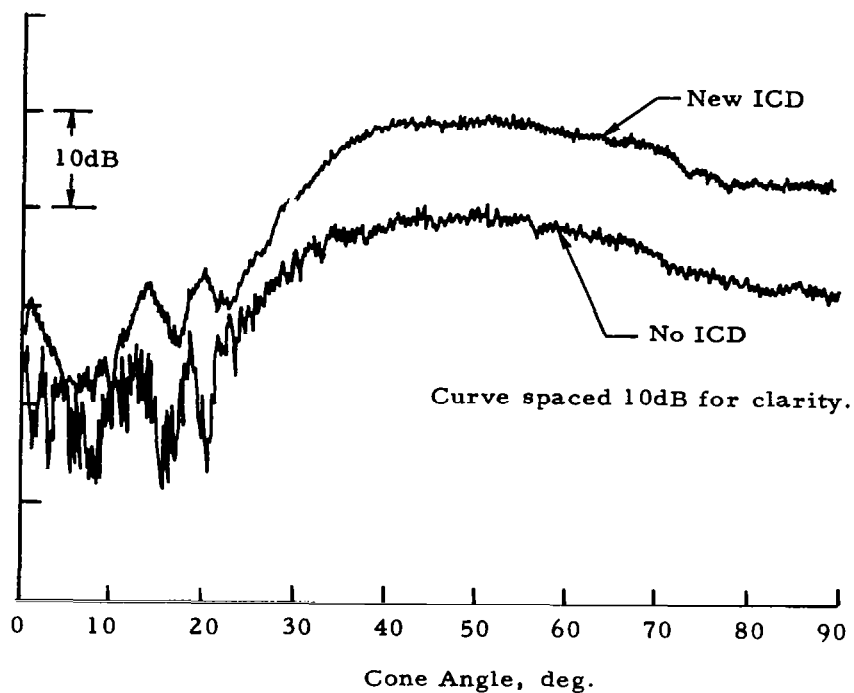


Figure 25.- Effect of ICD on propagation.

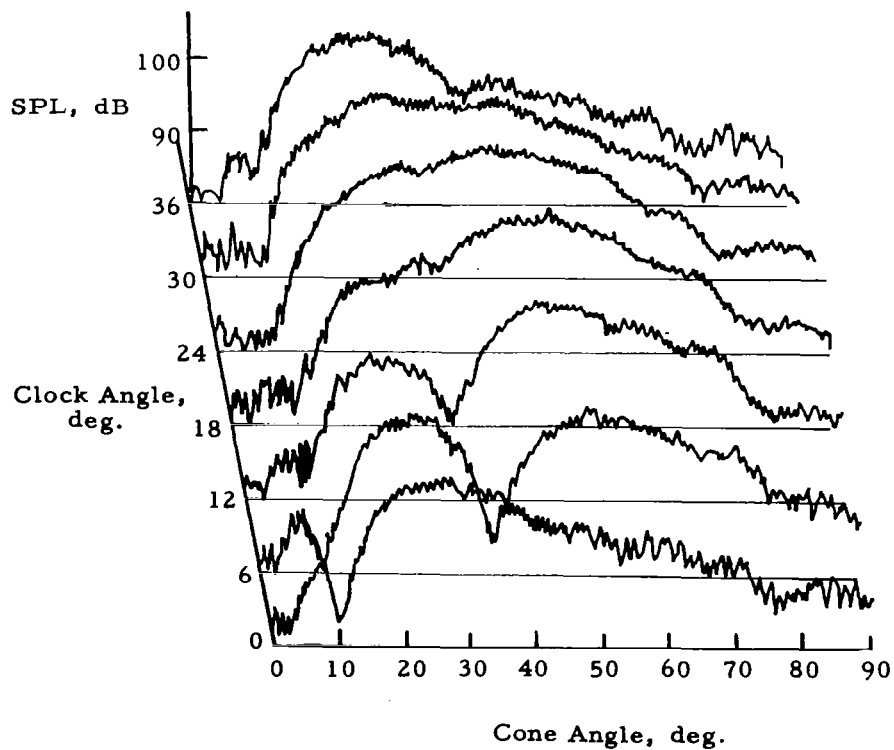


Figure 26.- 3-D character of fan noise.

- SIMULATE INLET FLOW "QUALITY" EXPERIENCED IN FLIGHT
- MEASURE ENGINE "TRUE" SOURCE NOISE PRESENT IN FLIGHT
- NO ADDITIONAL NOISE SOURCES ADDED
- NO ALTERATION / ATTENUATION OF ENGINE NOISE RADIATION PATTERNS

Figure 27.- Purpose and objectives of testing with an ICD.

CONFIG.	ICD	VEHICLE	$\frac{D_{ICD}}{D_{Fan}}$	FACILITY
1	SMALL	ROTOR 11 FAN	4.13	G.E. ANECHOIC CHAMBER
2	SMALL	JT15D ENGINE	3.93	NASA - AMES OTS
3	SMALL	QCGAT ENGINE	2.69	NASA - LEWIS OTS
4	FULL-SIZE	CF34 ENGINE	6.55	EDWARDS FTC OTS
5	FULL-SIZE	CF6-80A ENG.	3.33	EDWARDS FTC OTS

Figure 28.- ICD/vehicle/facility combinations.

- HONEYCOMB LAYER TO DAMPEN TRANSVERSE TURBULENCE  
VELOCITY - 1/2 % GOAL

$$\text{HONEYCOMB } l/d = 8.0$$

- INNER CONTROL SCREEN TO DAMPEN AXIAL TURBULENCE  
COMPONENT - 1/2 % GOAL

- OVERALL SIZE SELECTED TO ACHIEVE HONEYCOMB  
ENTRANCE VELOCITIES OF  $\approx 20 - 25$  FPS

$$D_{\text{ICD}} / D_{\text{FAN}} = 4.125$$

Figure 29.- Small ICD design considerations.

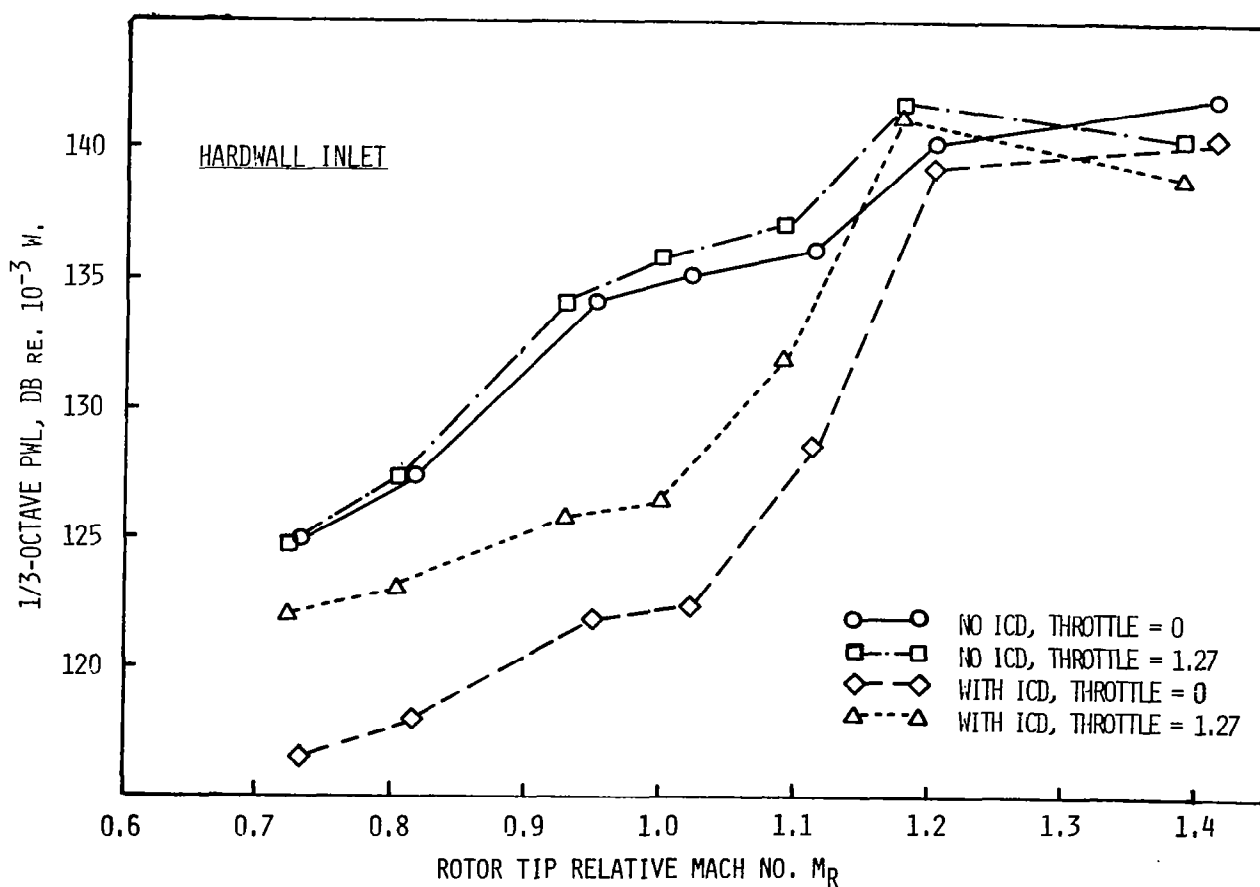


Figure 30.- Blade passing frequency noise with and without ICDs.

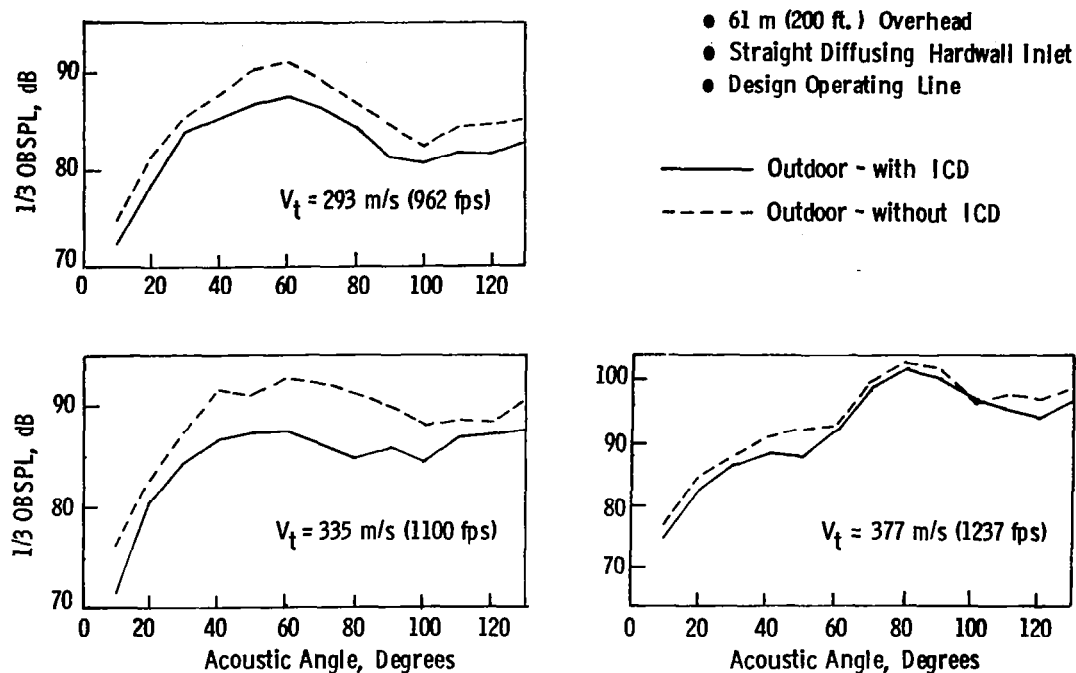


Figure 31.- Scale BPF 1/3-octave-band SPL for subsonic, transonic, and supersonic fan tip speeds.

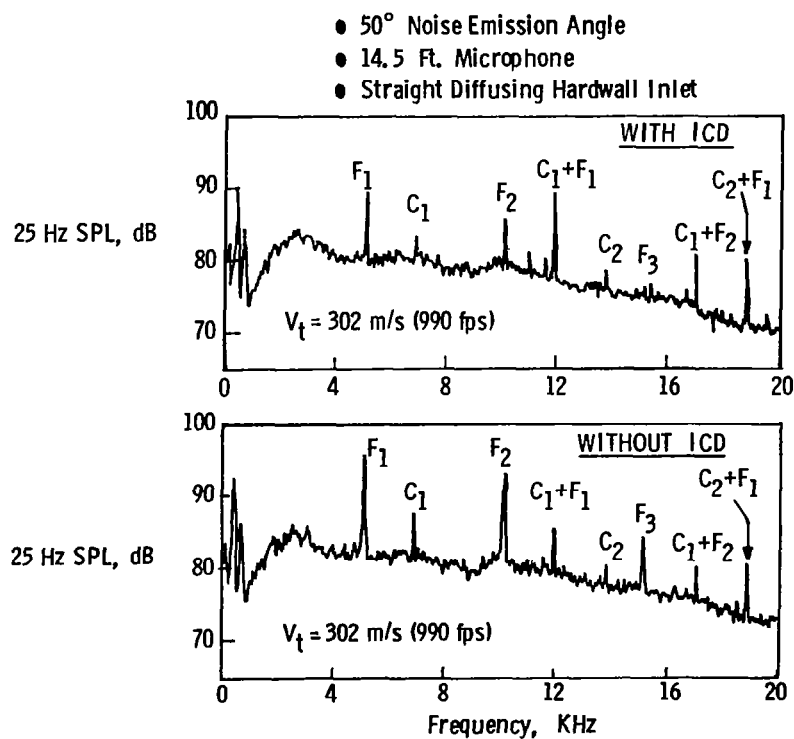


Figure 32.- Comparison of narrowband spectra.

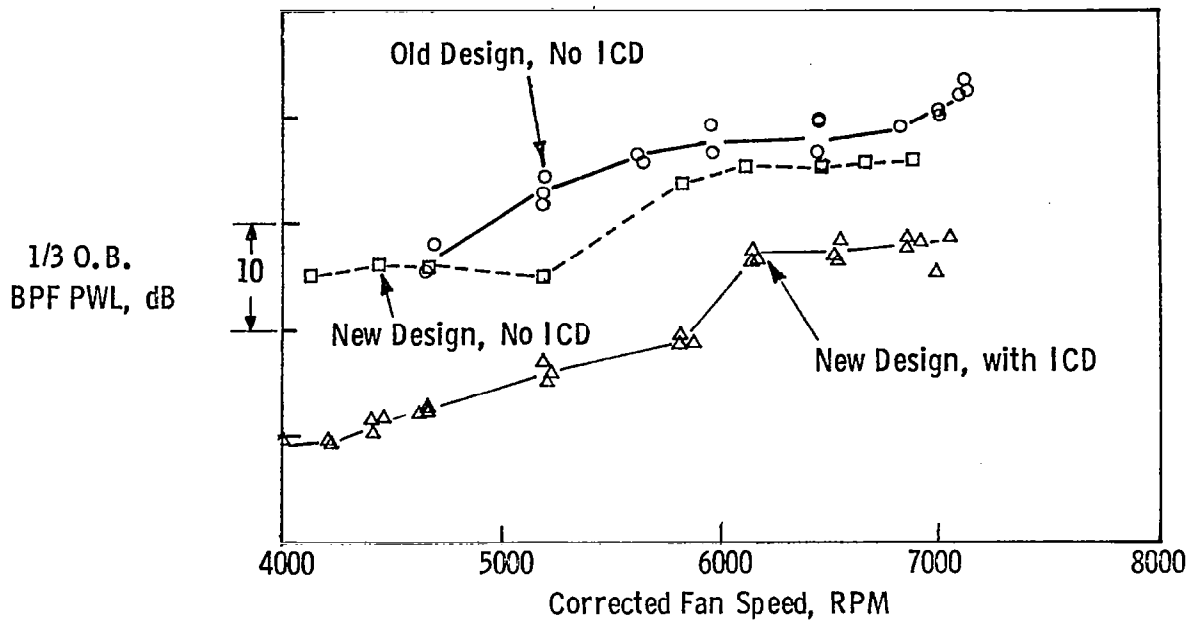


Figure 33.- CF-34 noise tests, 1/3-octave PWL versus corrected fan speed.

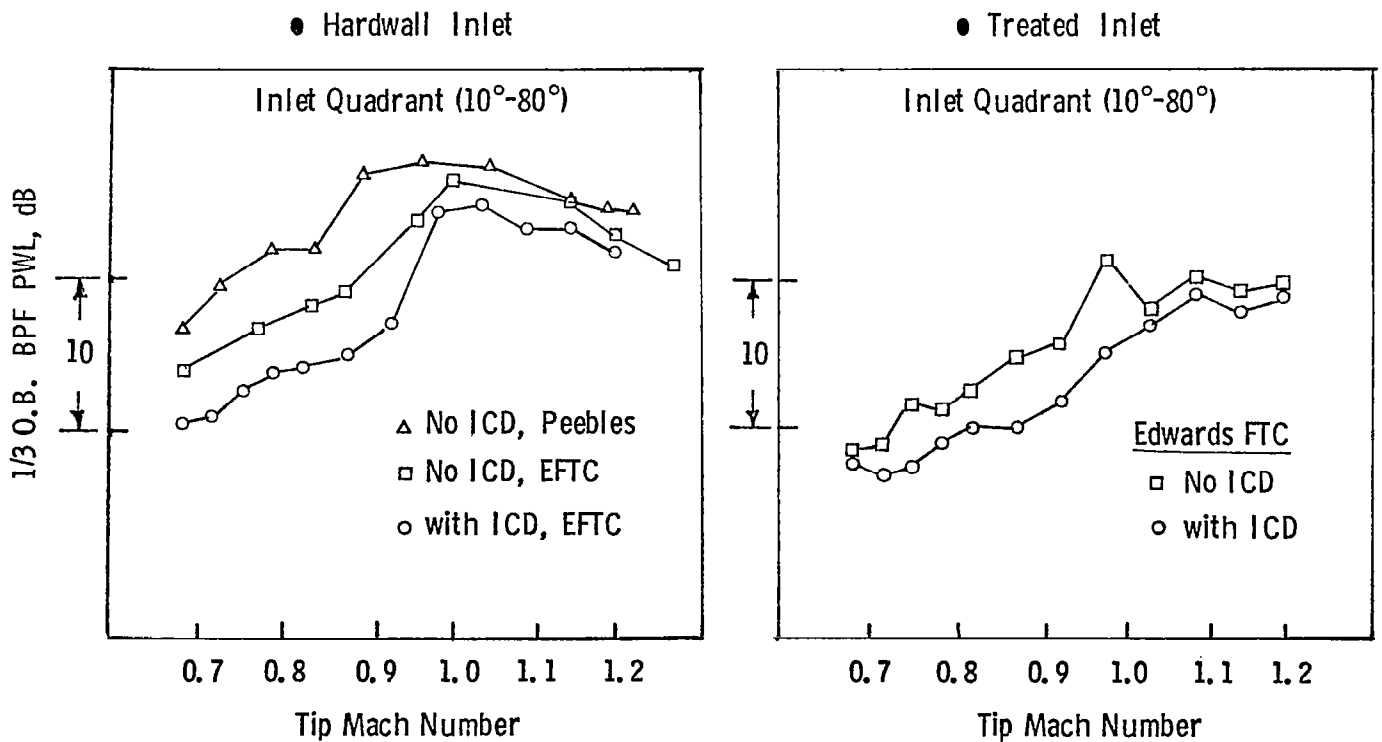


Figure 34.- CF6-80A ICD test results.

TAKE-OFF RATING	2200 LB THRUST
MAXIMUM FAN (N1) SPEED	16000 RPM
MAXIMUM COMPRESSOR (N2) SPEED	32000 RPM
BYPASS RATIO (MAX)	3.3
FAN PRESSURE RATIO (MAX)	1.5
ROTOR DIAMETER	21 INCHES
HUB/ROTOR TIP RATIO	.4
ROTOR BLADES	28
BYPASS STATOR VANES	66
* CORE STATOR VANES	71
BYPASS ROTOR-STATOR SPACING	1.83
** CORE ROTOR-STATOR SPACING	.63

- \* PRODUCTION ENGINE HAS 33 CORE STATOR VANES
- \*\* PRODUCTION ENGINE CORE ROTOR-STATOR SPACING IS .28

Figure 35.- JT15D-1 design features.

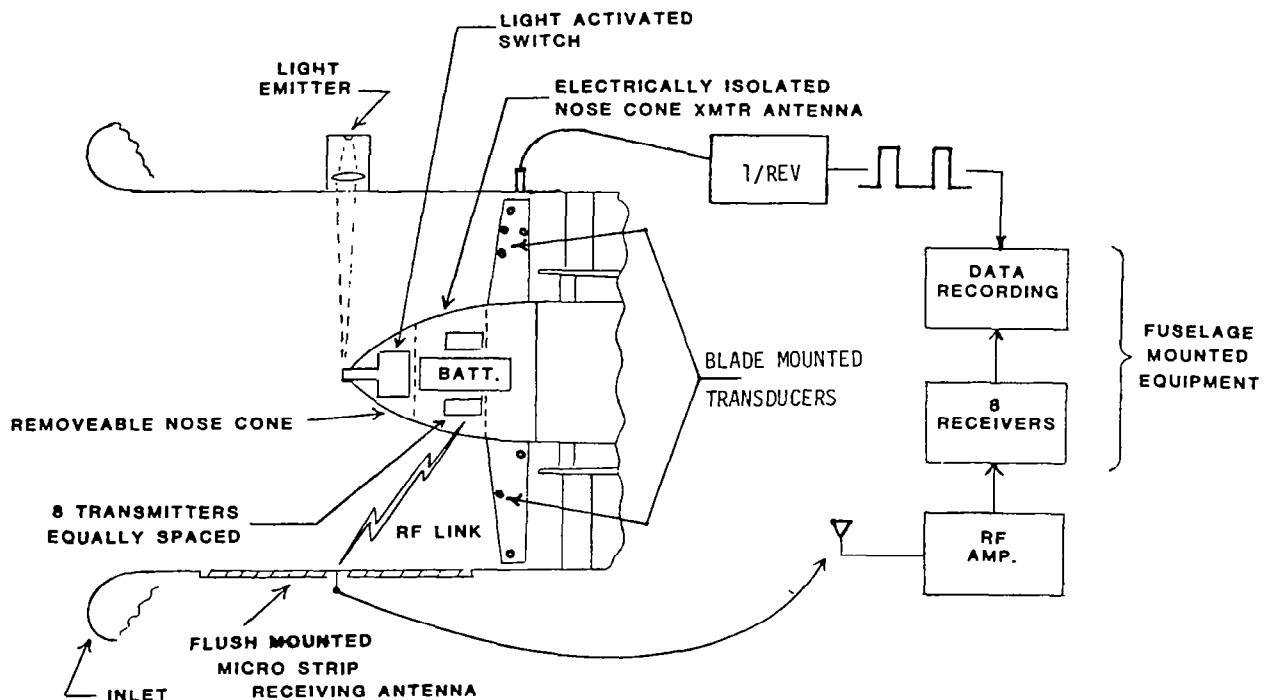


Figure 36.- JT15D BMT telemeter conceptual arrangement.

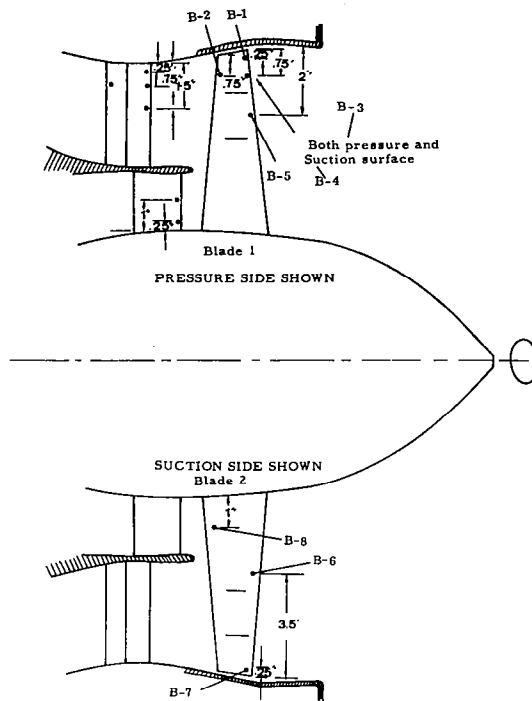


Figure 37.- JT15D-1 transducer locations and designations.

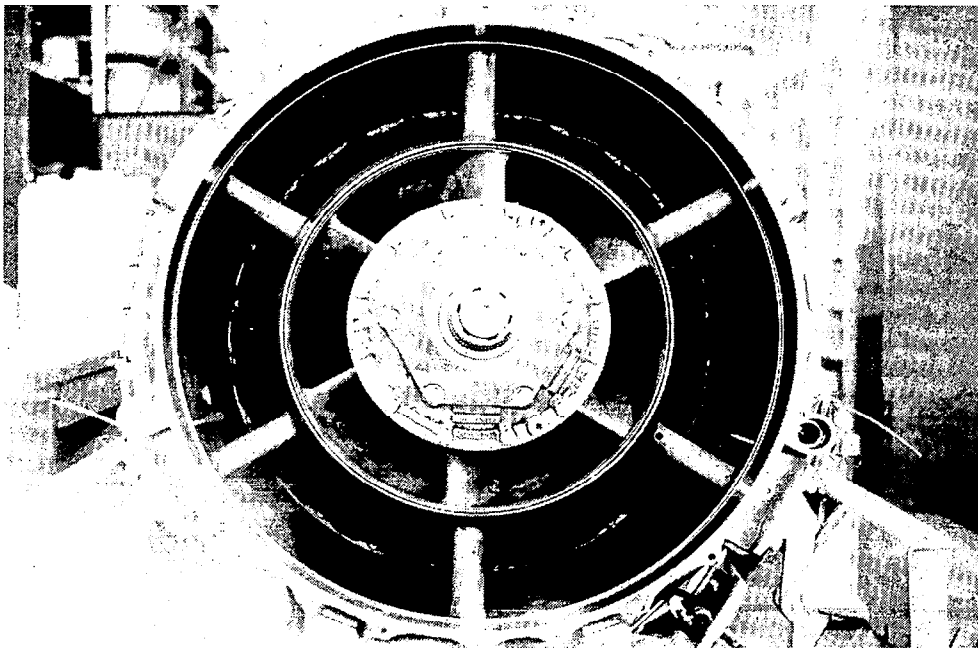


Figure 38.- Support struts for JT15D-1 engine.



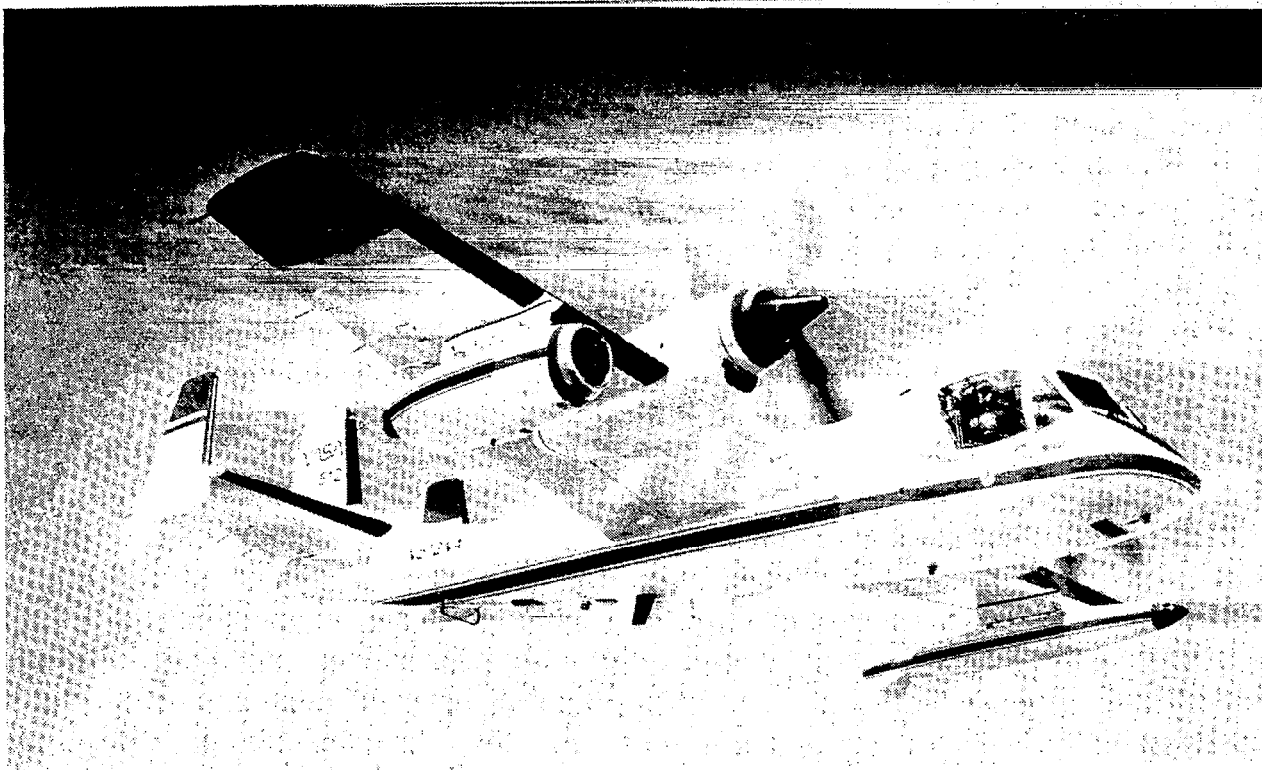


Figure 39.- OV-1B/JT15D test aircraft.

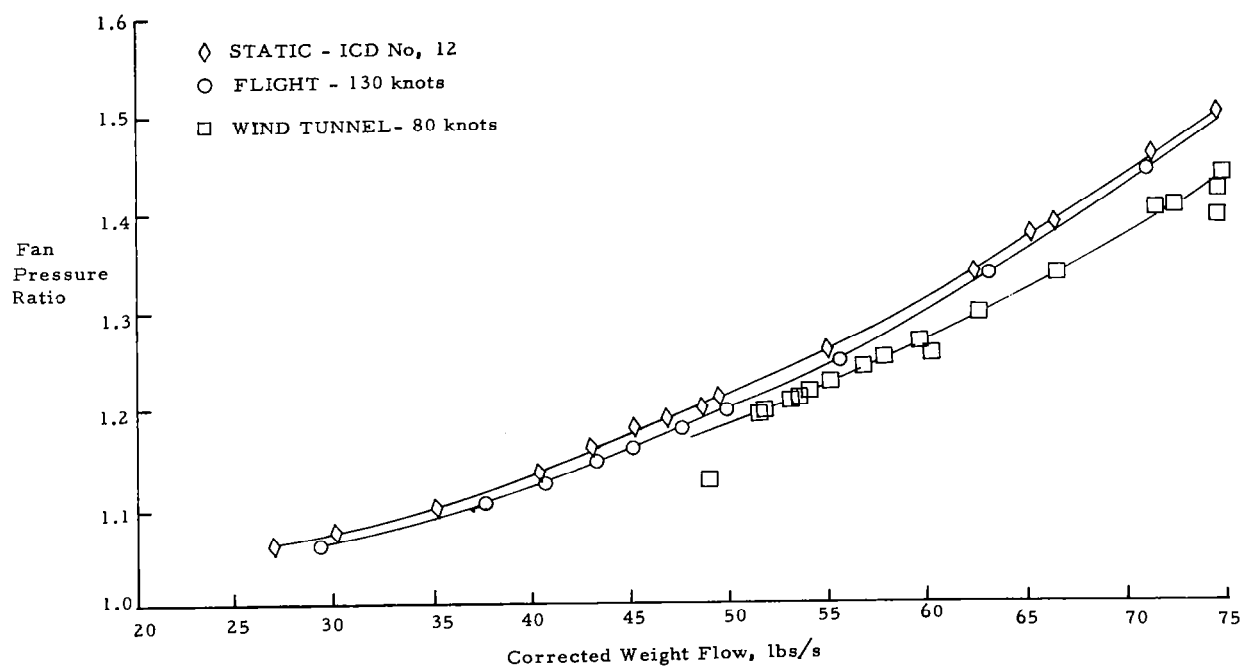


Figure 40.- Fan operation comparisons for JT15D with hardwall inlet.

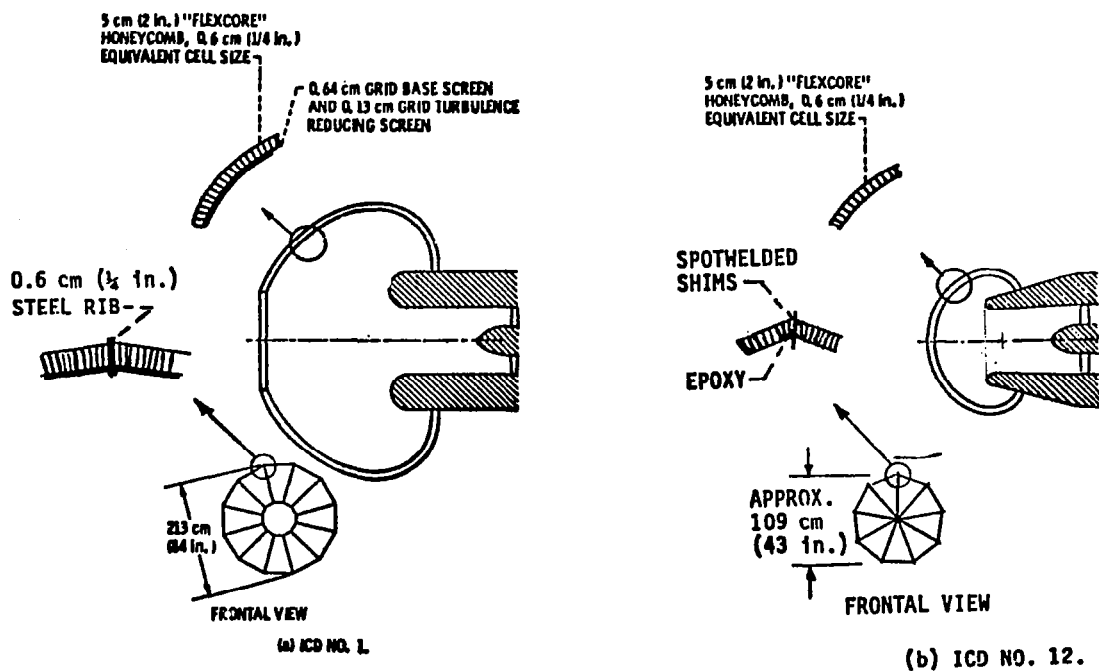


Figure 41.- Inflow control devices tested on the JT15D-1 on the LeRC outdoor static engine.

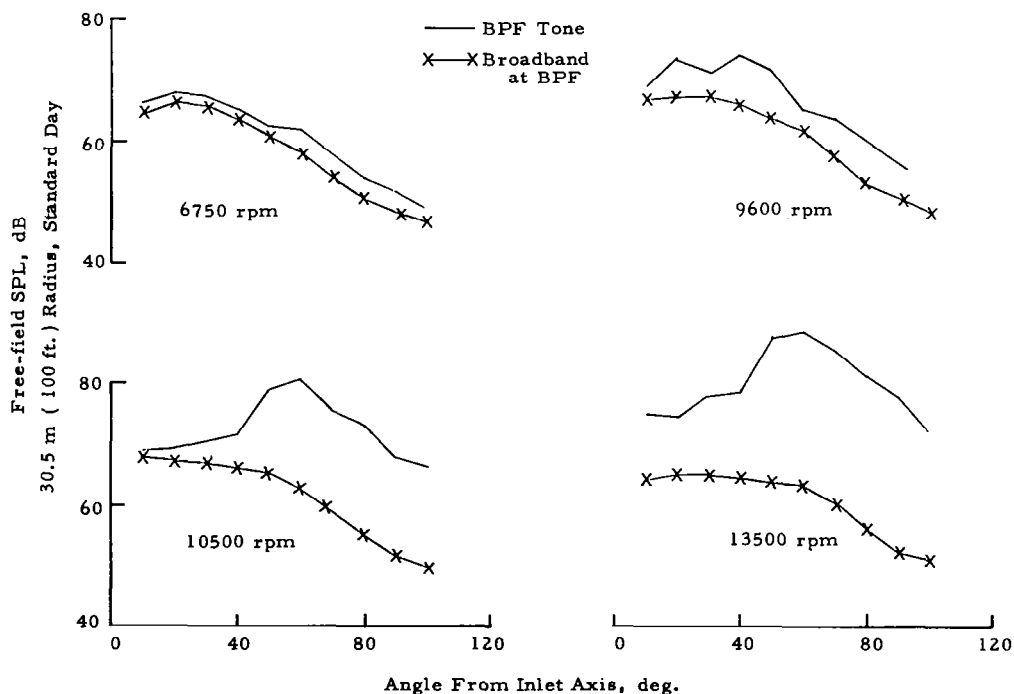
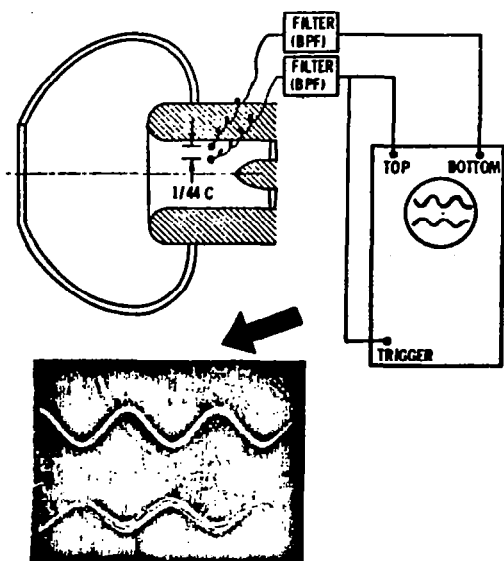


Figure 42.- BPF directivity with bellmouth inlet and ICD no. 1.



Experiment to confirm  $m = 22$  mode in duct.

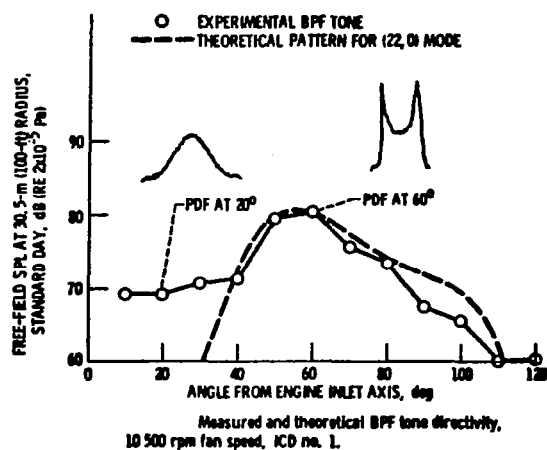


Figure 43.- Validation of presence of  $m = 22$  mode; 10,500 rpm fan speed; ICD no. 1.

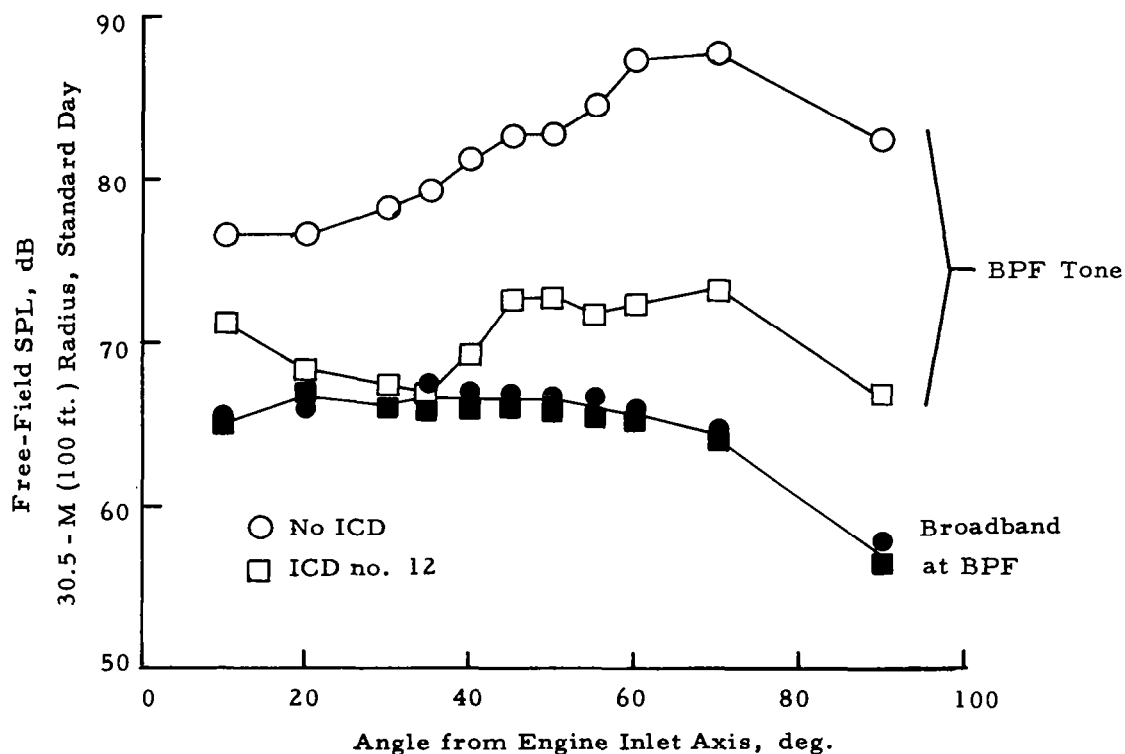


Figure 44.- BPF directivity with "flight" inlet; NF  $\approx$  10,800 rpm.

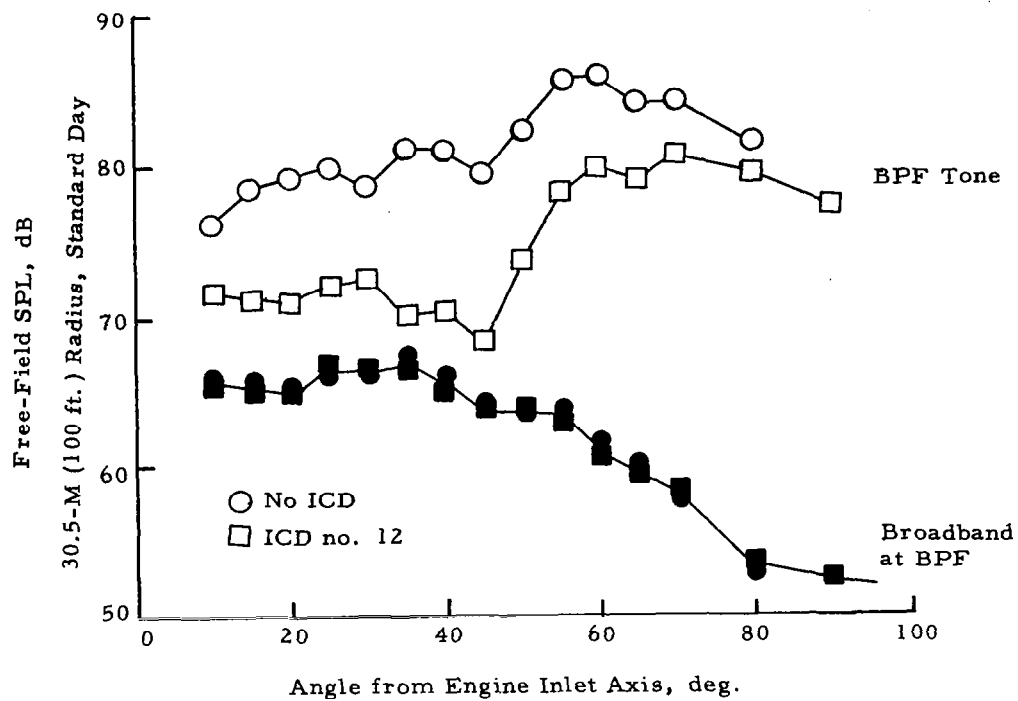


Figure 45.- BPF directivity with 41 rods; NF = 6750 rpm.

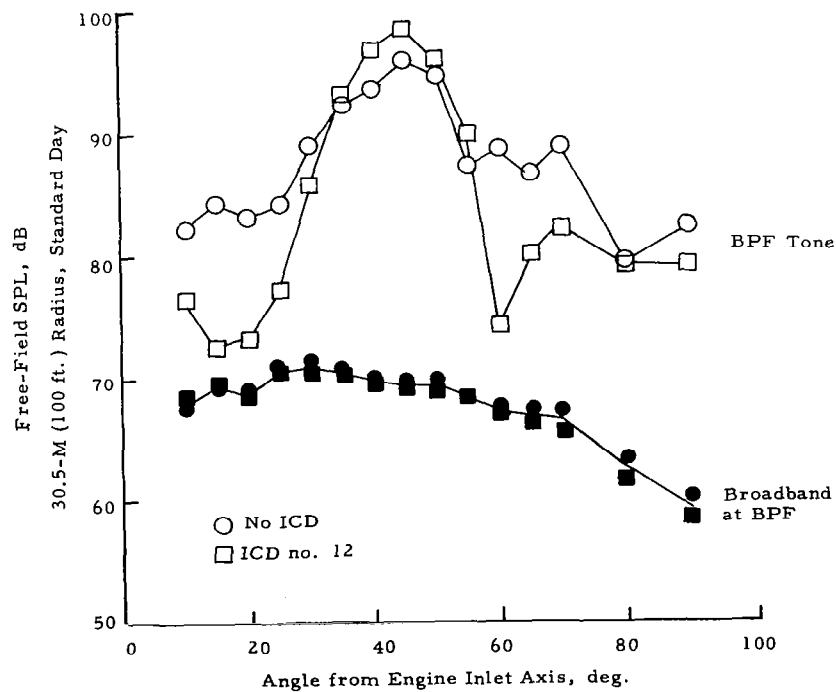


Figure 46.- BPF directivity with 41 rods; NF = 10,800 rpm.

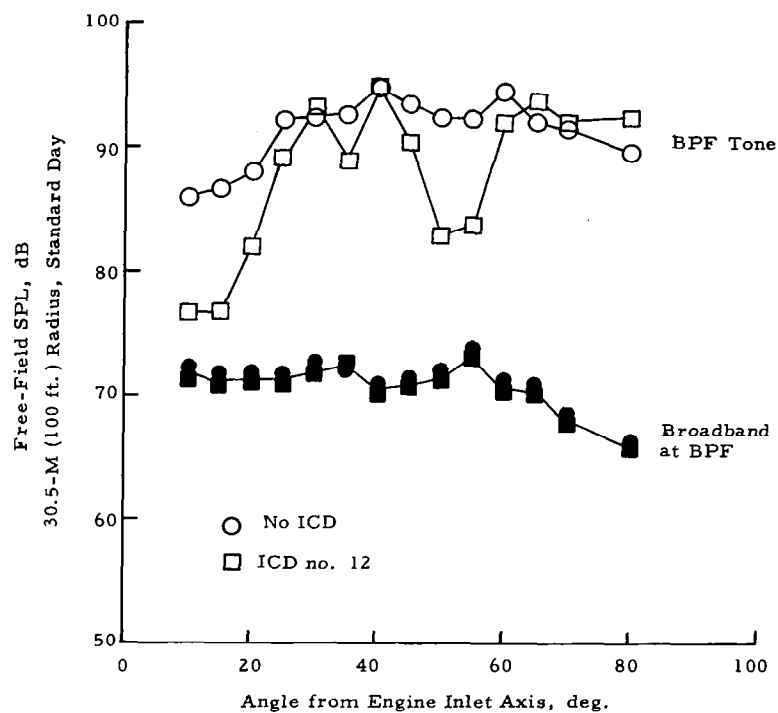


Figure 47.- BPF directivity with 41 rods; NF = 13,500 rpm.

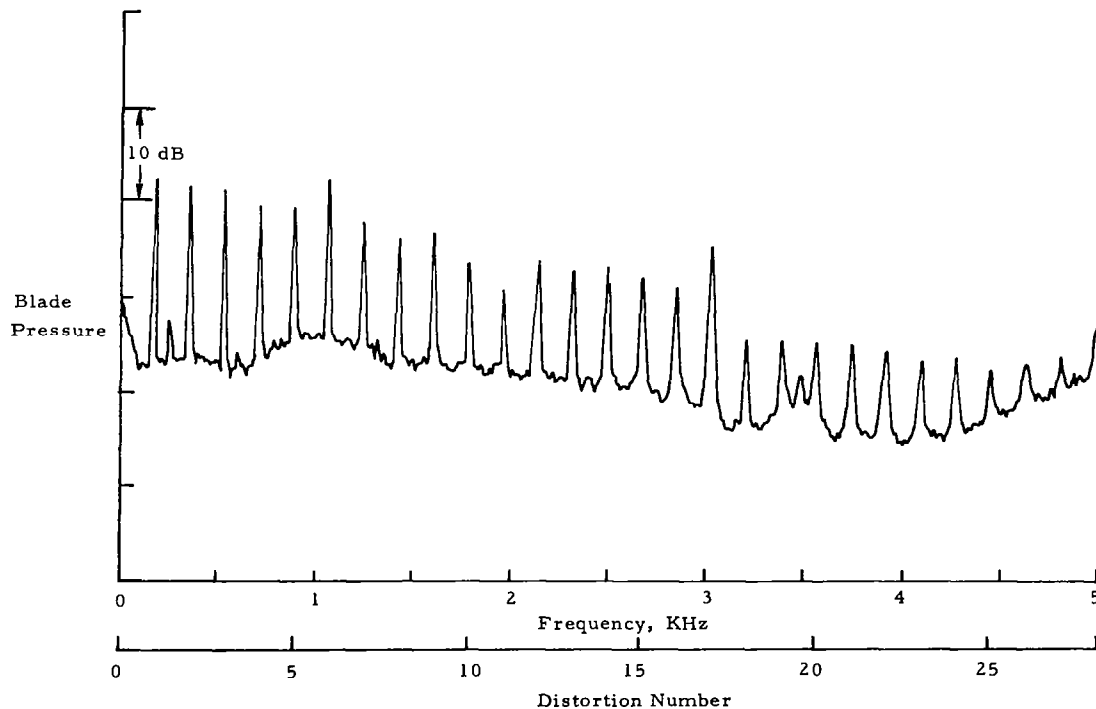


Figure 48.- BMT (B-3) power spectrum; no ICD; flight inlet.

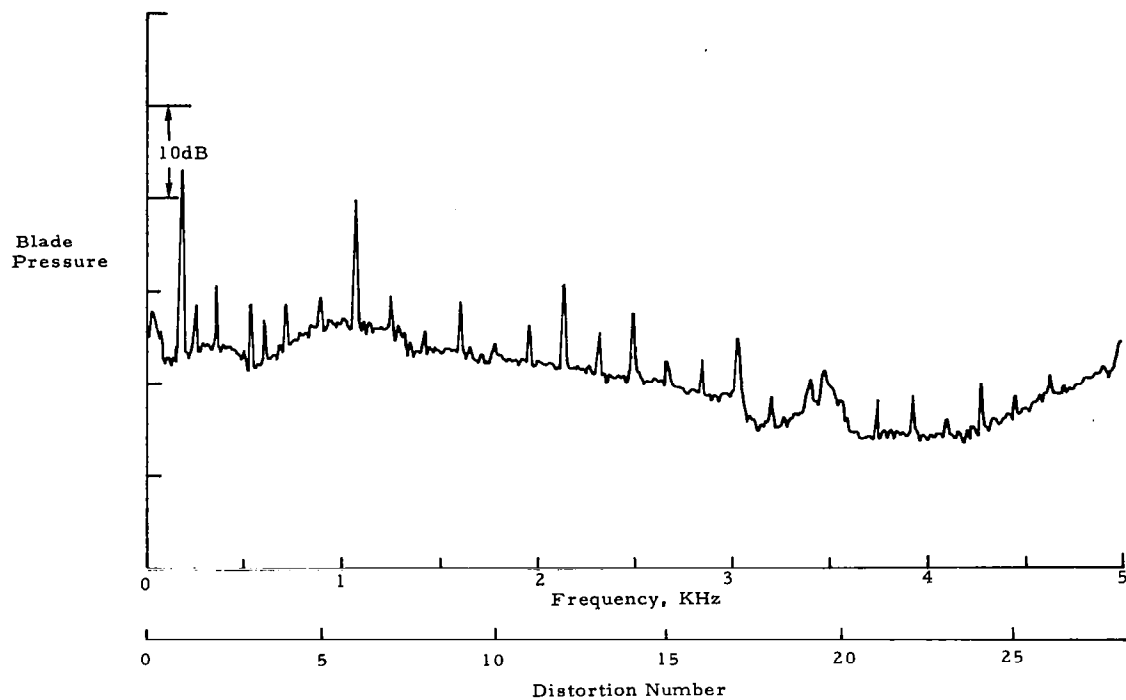


Figure 49.- BMT (B-3) power spectrum; ICD no. 12; flight inlet.

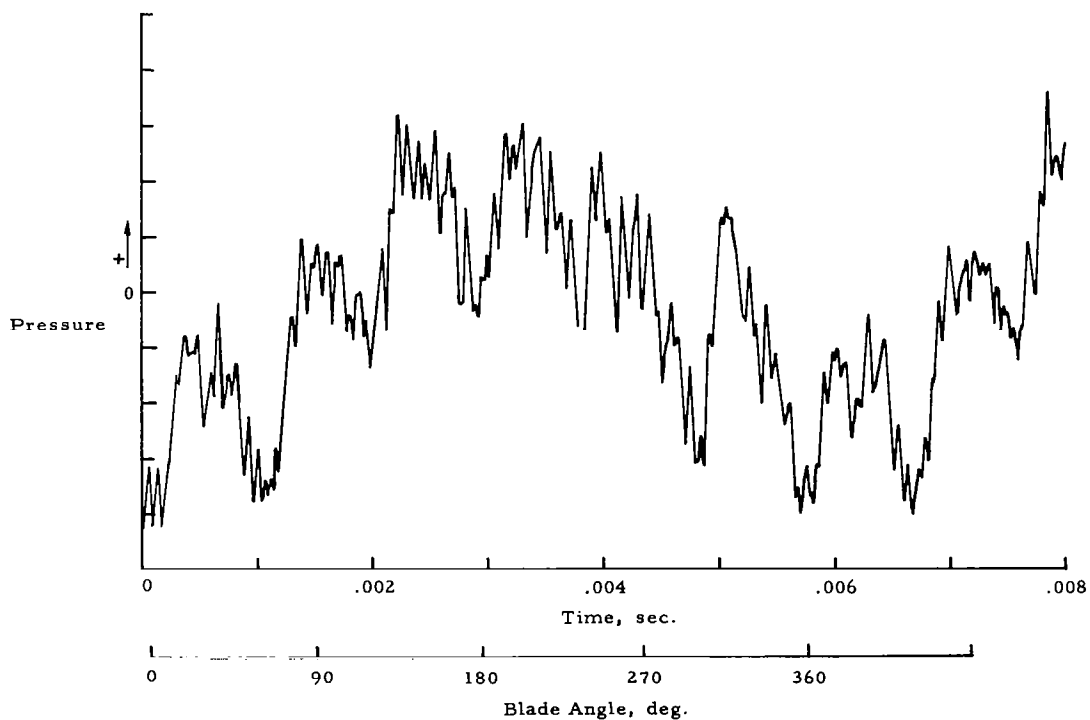


Figure 50.- BMT (B-3) mean pressure; ICD no. 12; flight inlet.

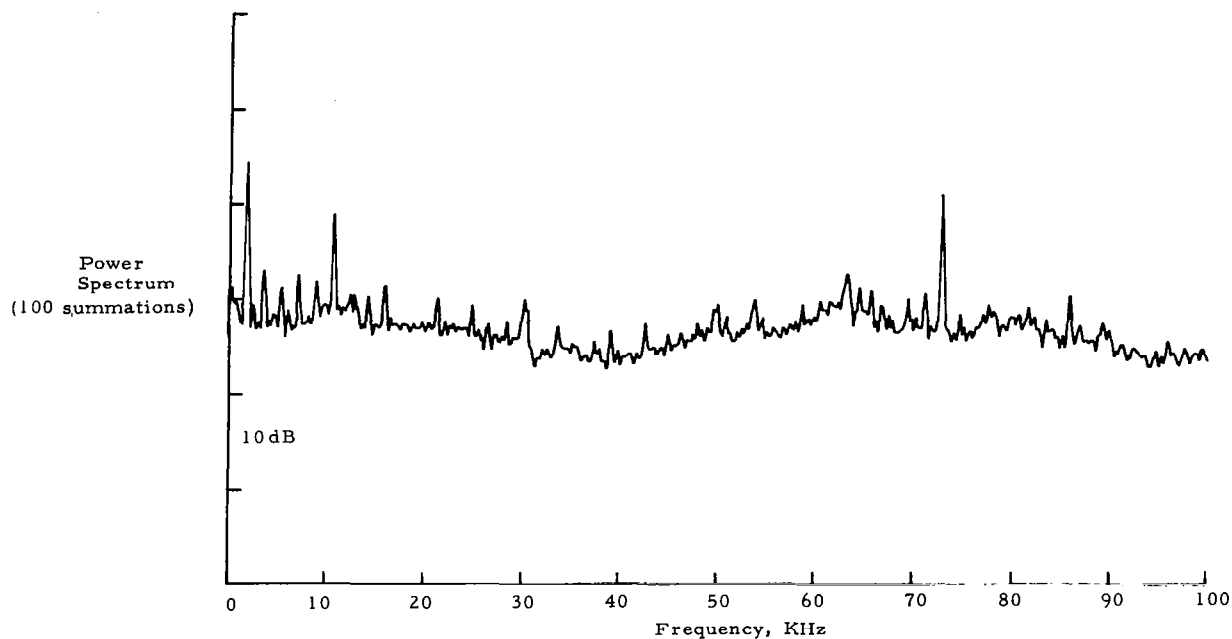
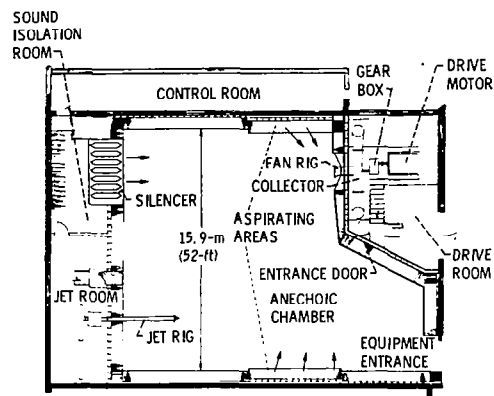
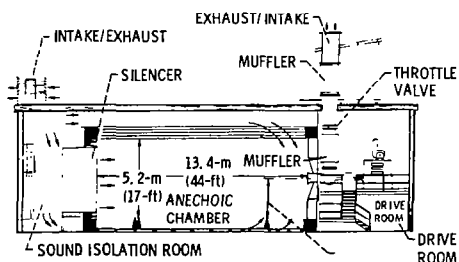


Figure 51.- BMT spectrum of 41-rods experiment; ICD no. 1; bell inlet.



(a) Noise facility floor plan.



(b) Noise facility elevation view.

Figure 52.- NASA LeRC anechoic chamber.

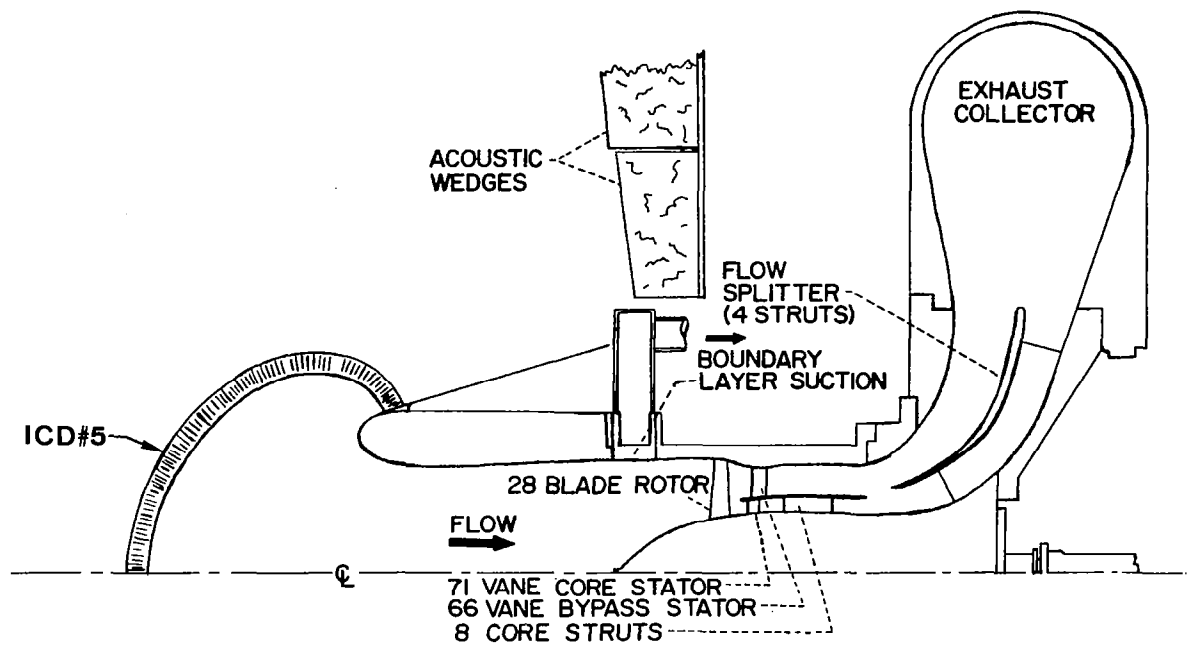


Figure 53.- JT15D fan in Lewis anechoic chamber.

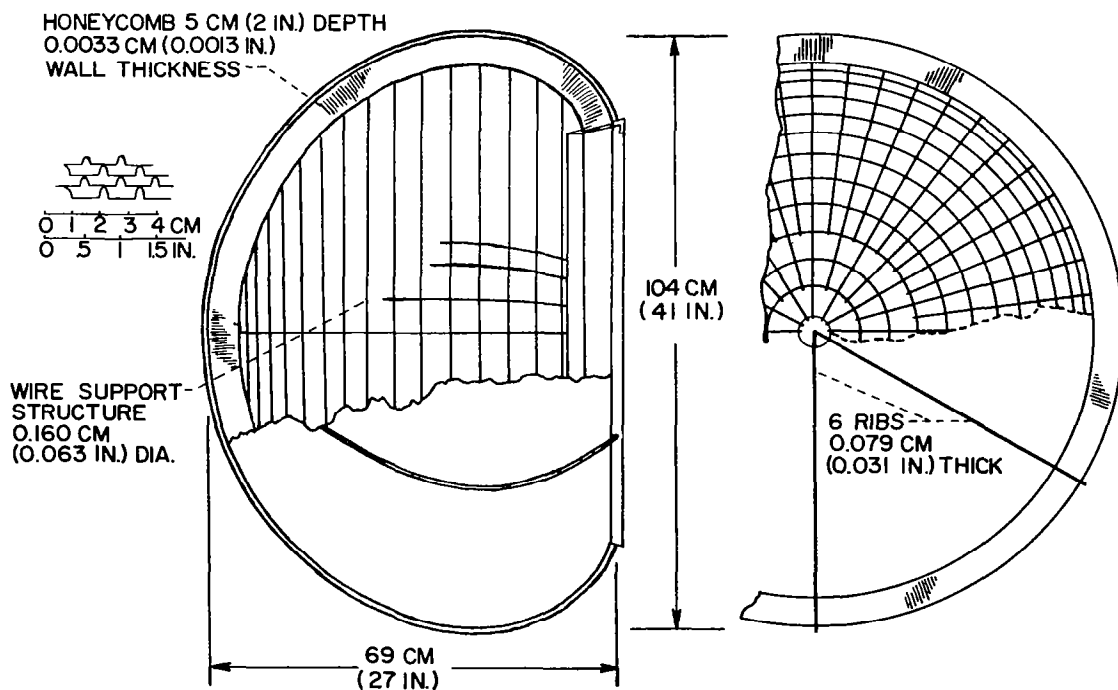


Figure 54.- ICD no. 5 construction details.



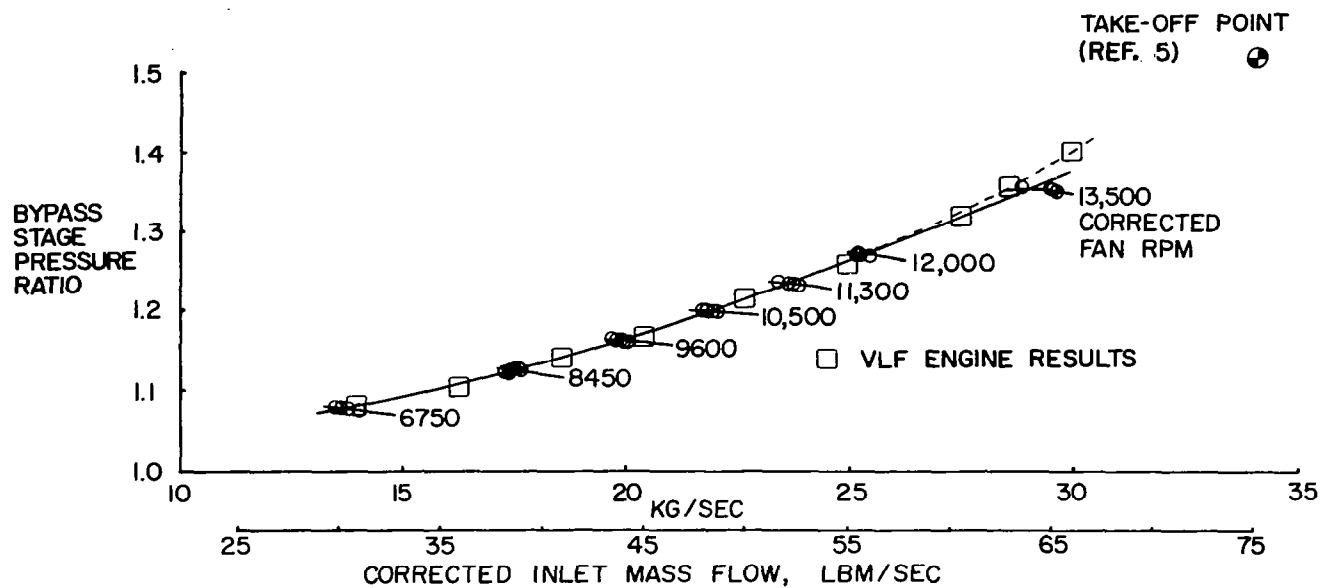


Figure 55.- JT15D fan - standard operating line.

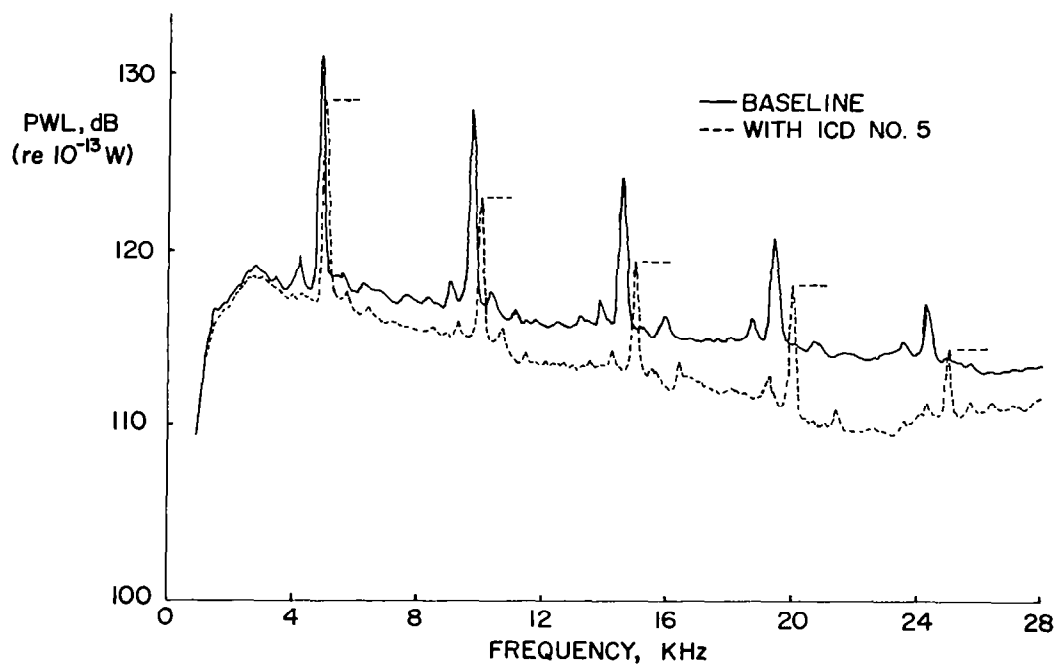


Figure 56.- JT15D fan sound power spectra; 10,500 corrected rpm.

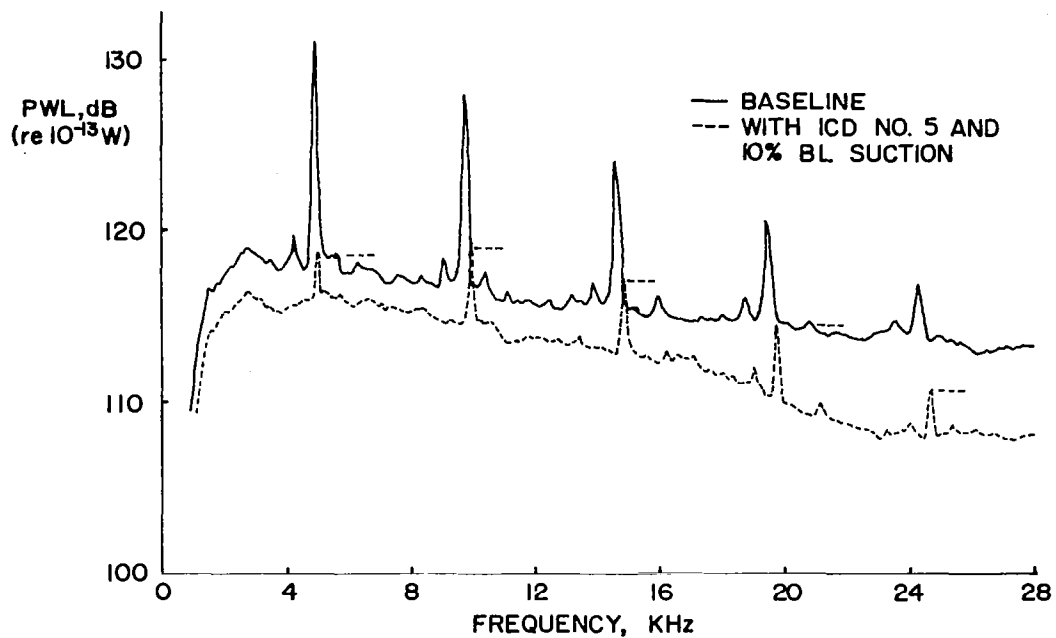


Figure 57.- JT15D fan sound power spectra with baseline suction;  
10,500 corrected rpm.

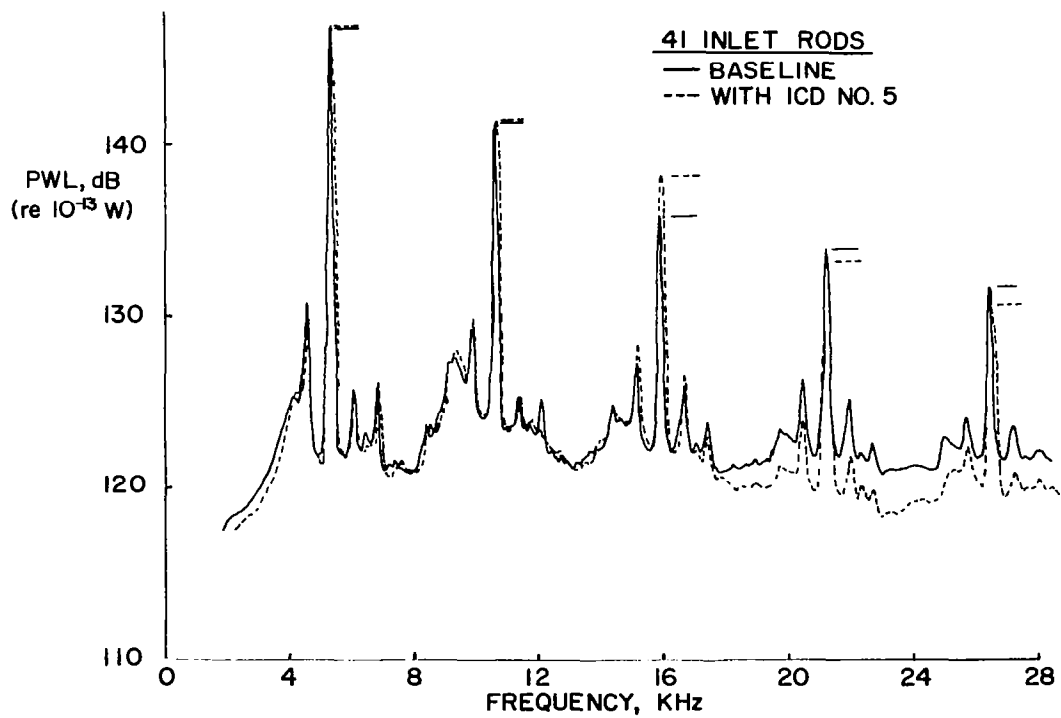


Figure 58.- JT15D fan sound power spectra; 11,300 corrected rpm.

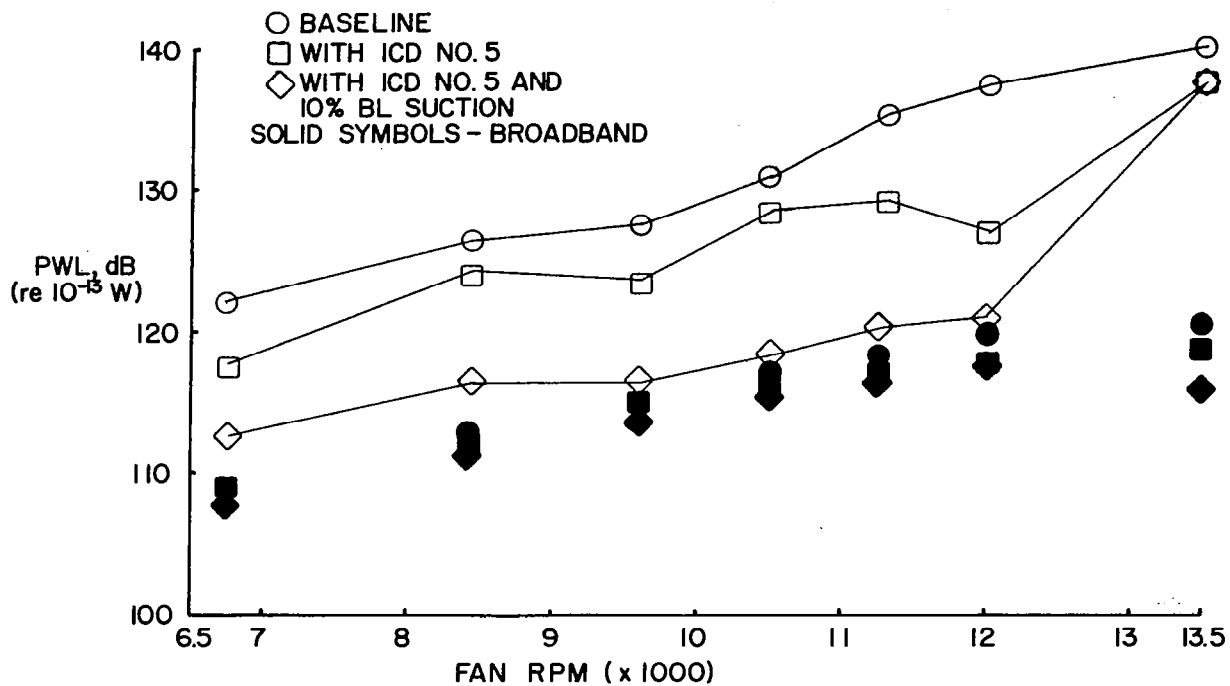


Figure 59.- JT15D fan blade passage tone power.

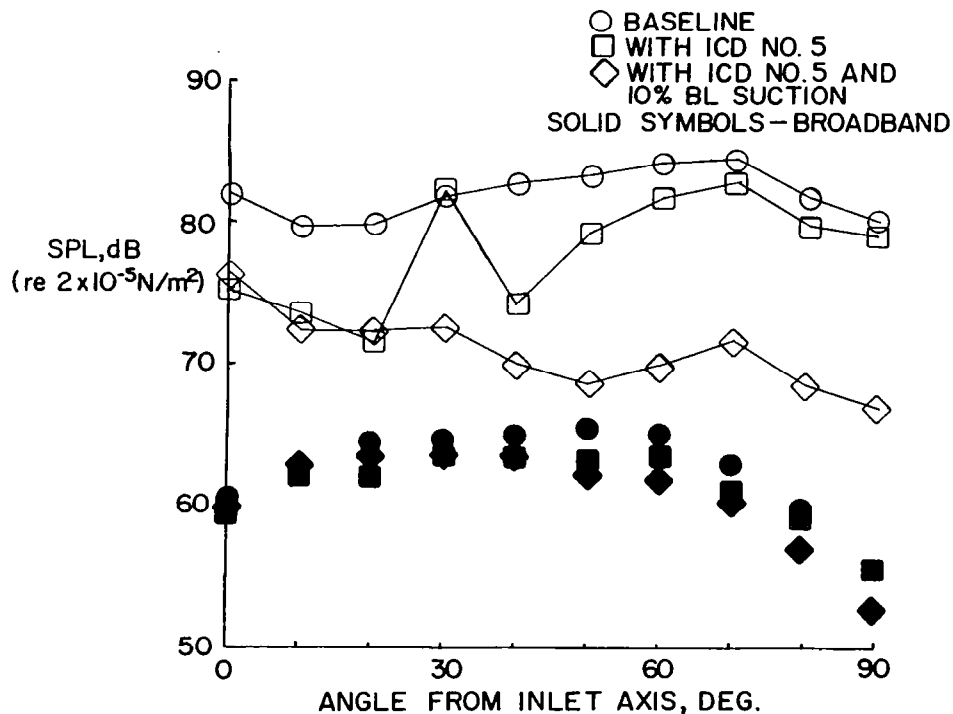


Figure 60.- JT15D fan blade passage tone directivity; 10,500 corrected rpm.

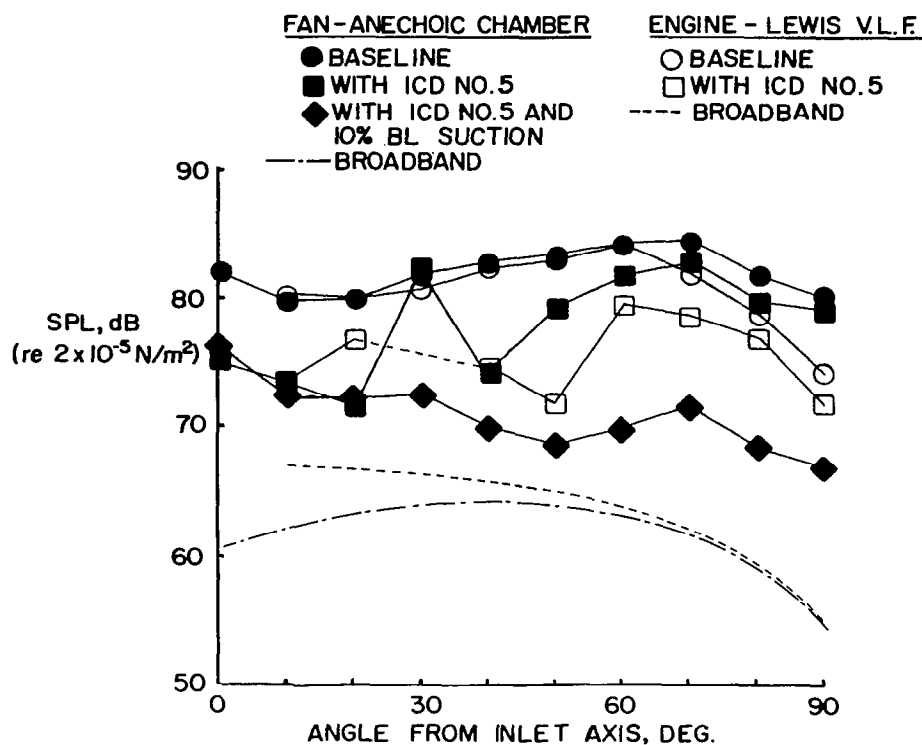


Figure 61.- Blade passage tone directivity; 10,500 corrected rpm.

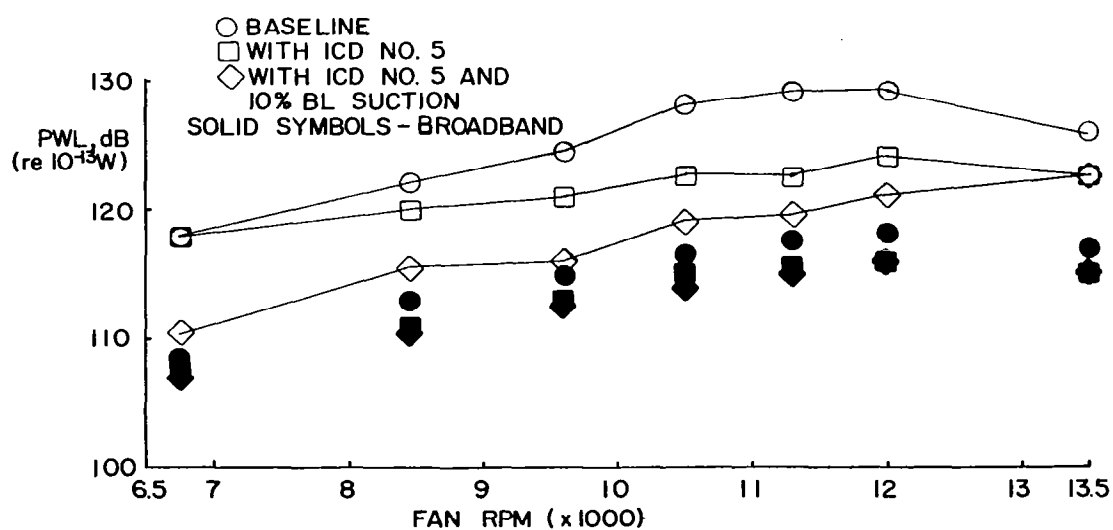


Figure 62.- JT15D fan first overtone power.

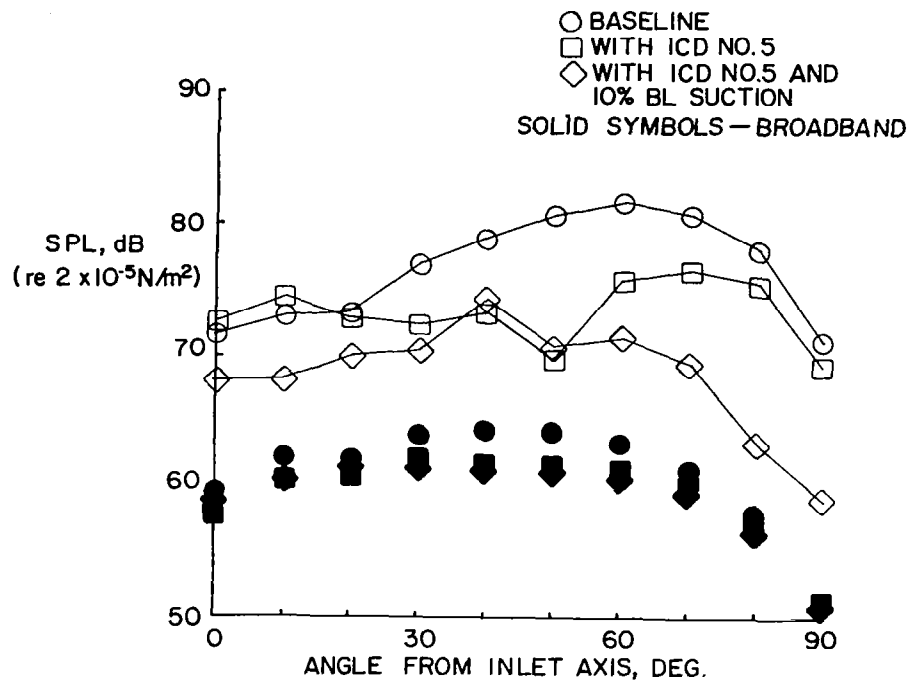


Figure 63.- JT15D fan first overtone directivity; 10,500 corrected rpm.

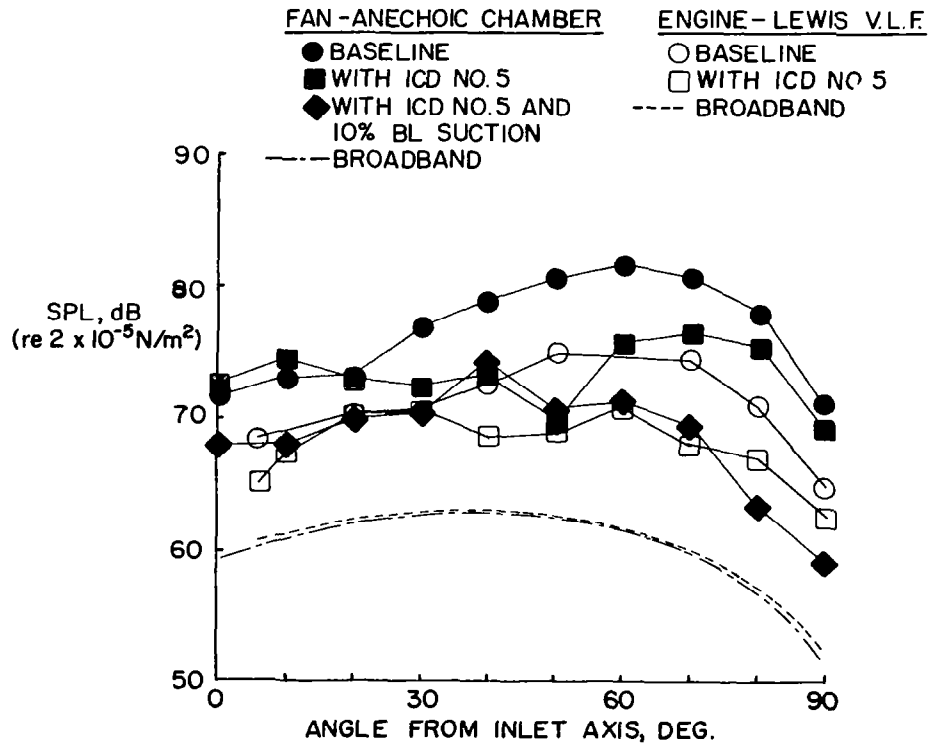


Figure 64.- First overtone directivity; 10,500 corrected rpm.

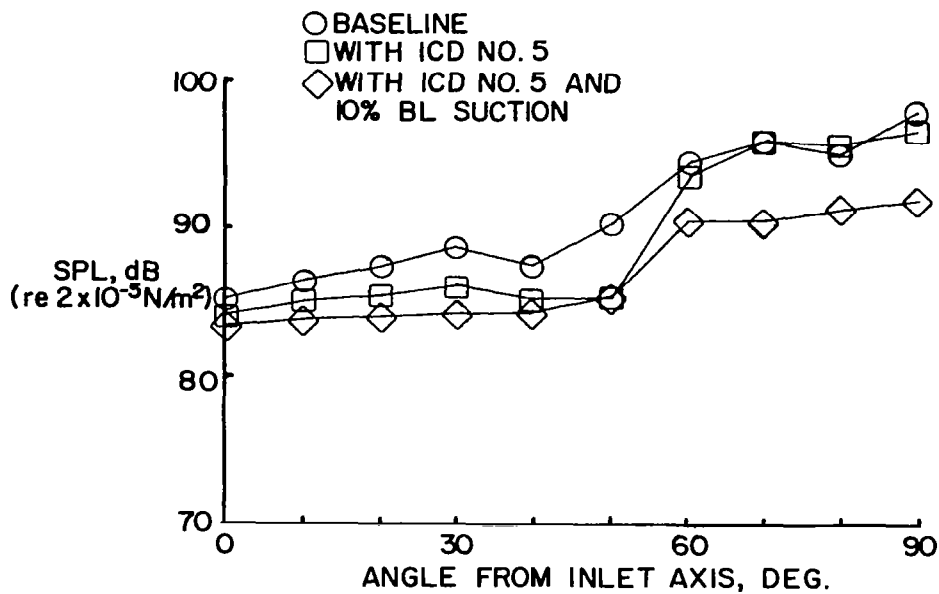


Figure 65.- JT15D fan multiple pure tone directivity; 13,500 corrected rpm.

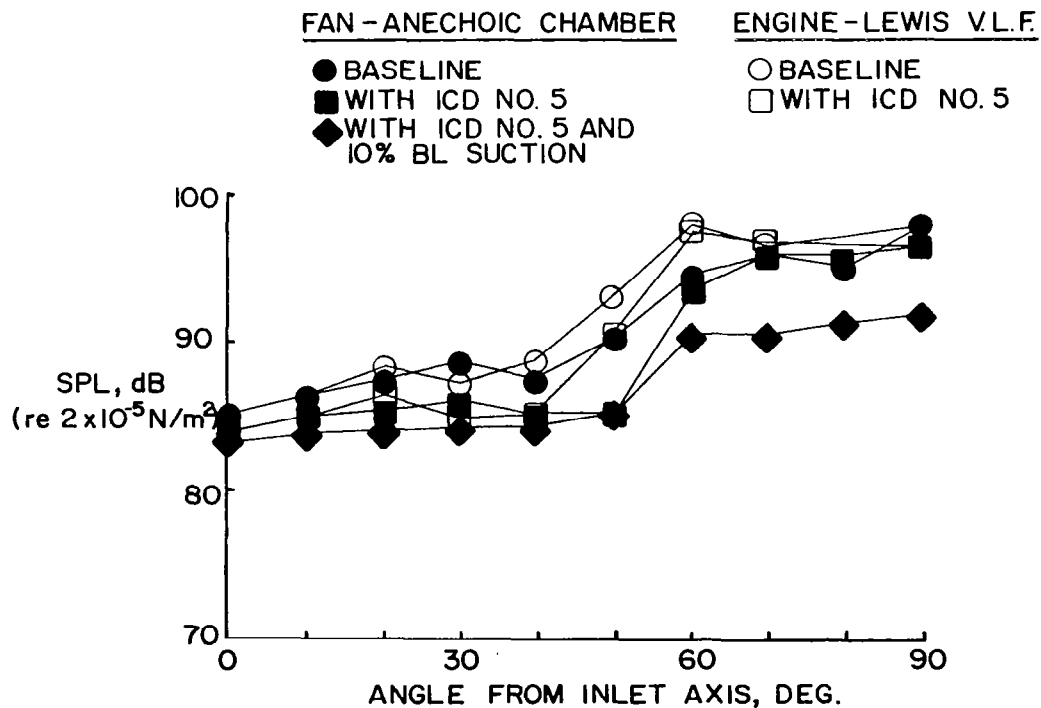


Figure 66.- Multiple pure tone directivity; 13,500 corrected rpm.

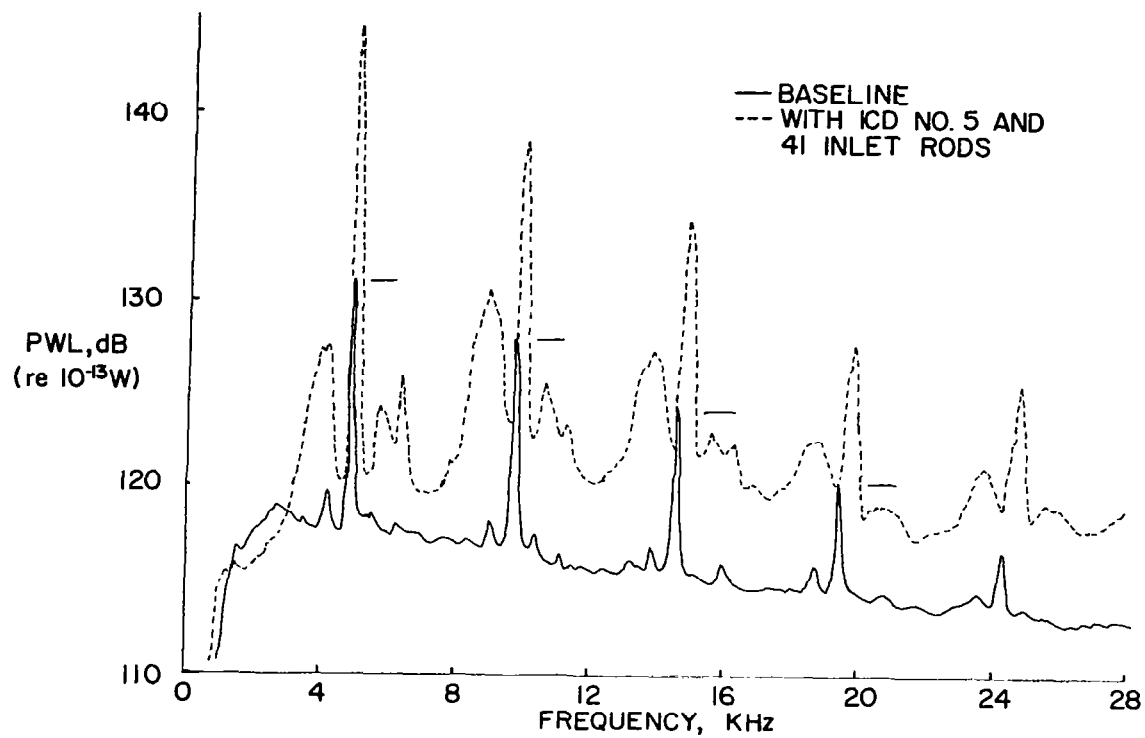


Figure 67.- JT15D fan sound power spectra; 10,500 corrected rpm.

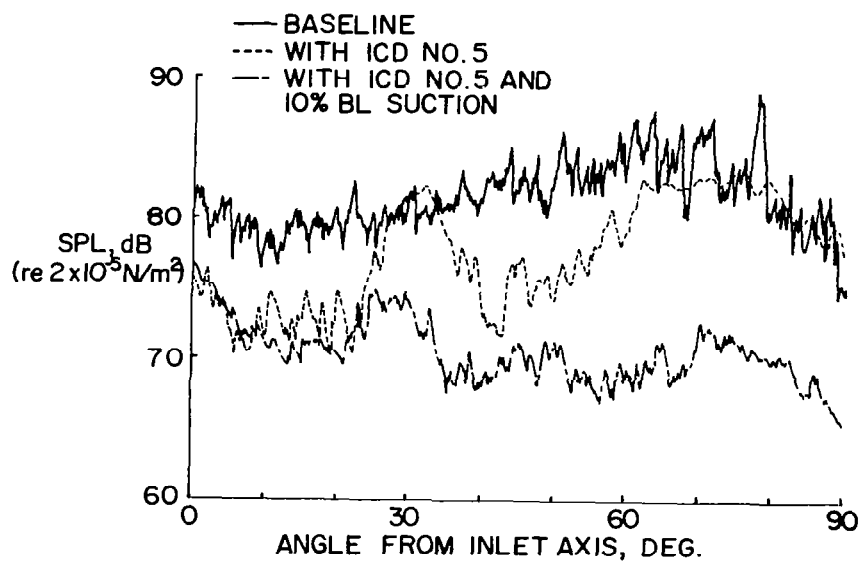


Figure 68.- JT15D fan boom microphone blade passage tone directivity; 10,500 corrected rpm.

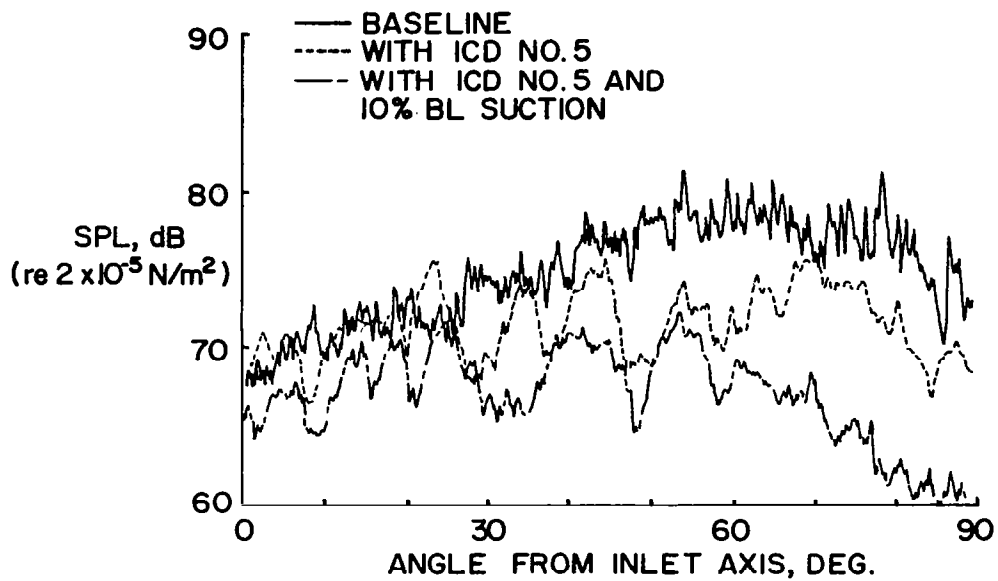


Figure 69.- JT15D fan boom microphone first tone directivity; 10,500 corrected rpm.

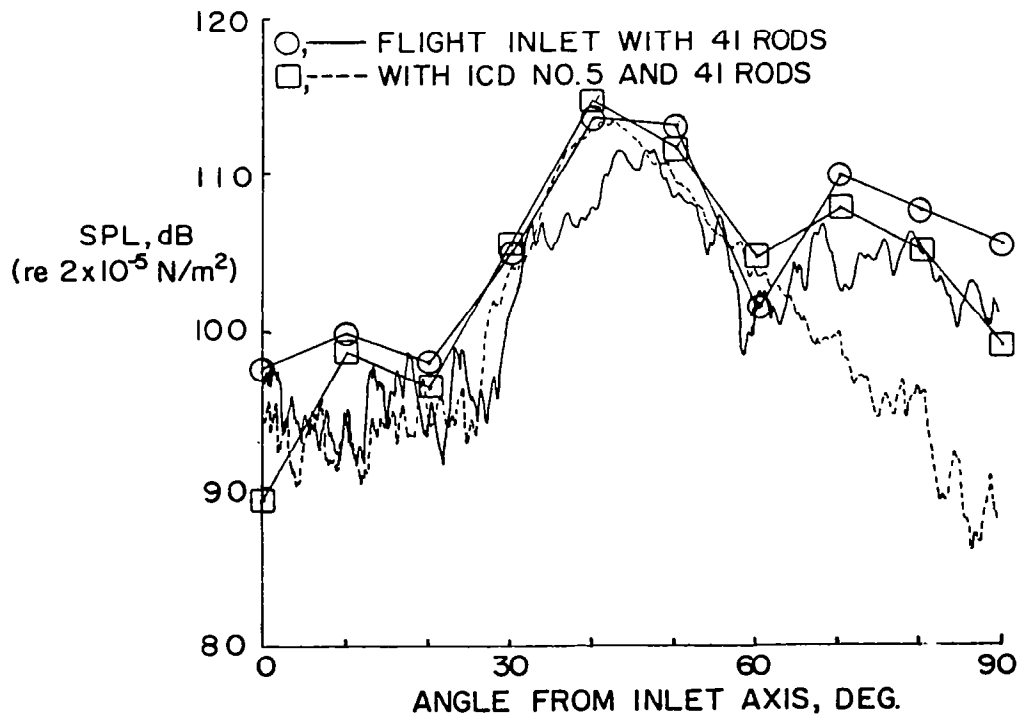


Figure 70.- JT15D fan boom microphone blade passage tone directivity; 10,500 corrected rpm.



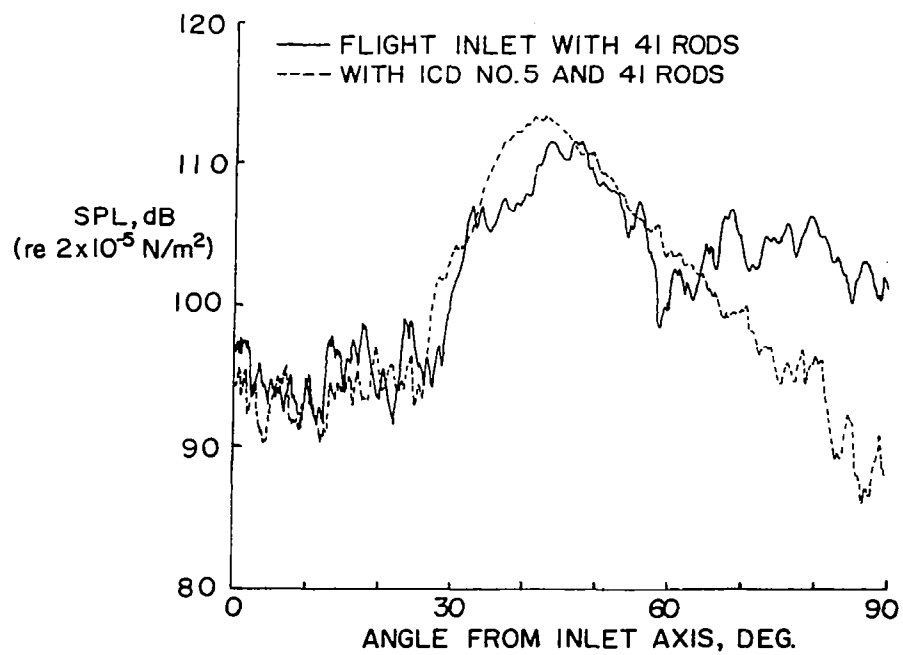


Figure 71.- JT15D fan boom microphone blade passage tone directivity; 10,500 corrected rpm.

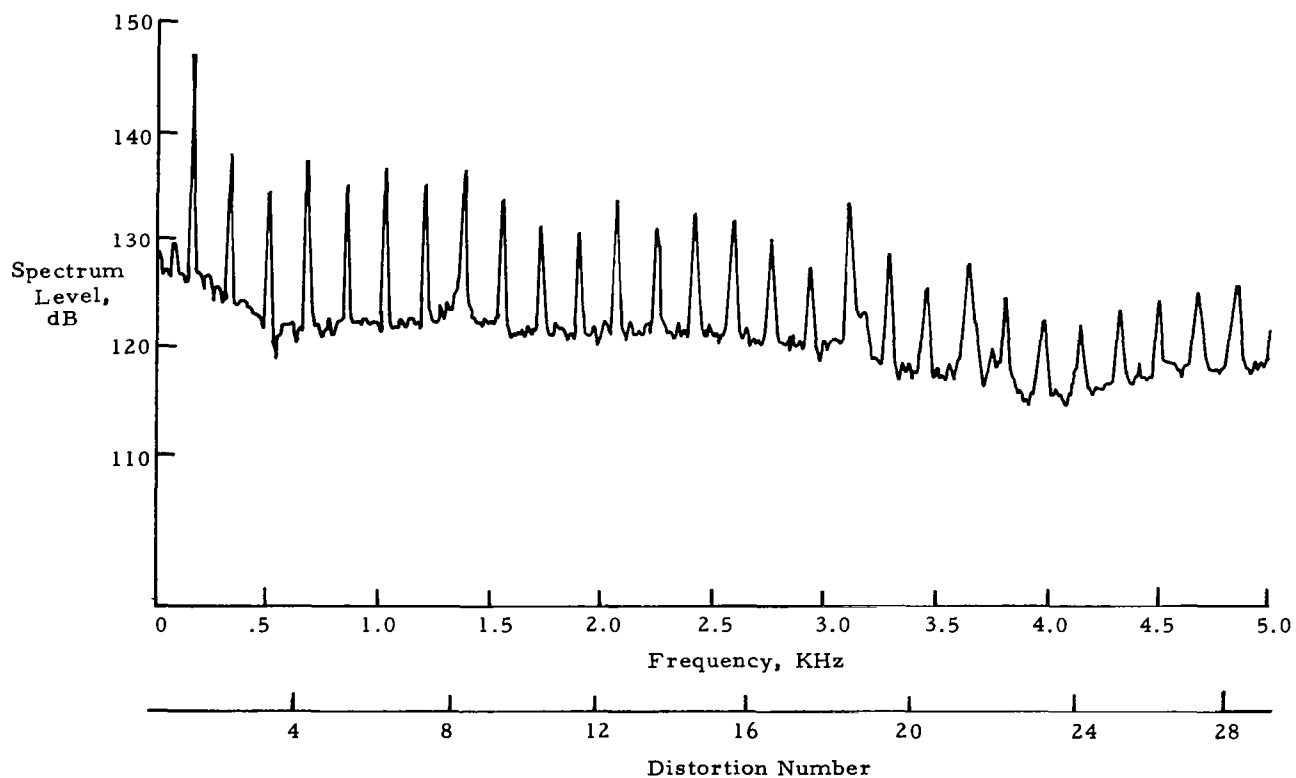


Figure 72.- B-3 power spectra - baseline.

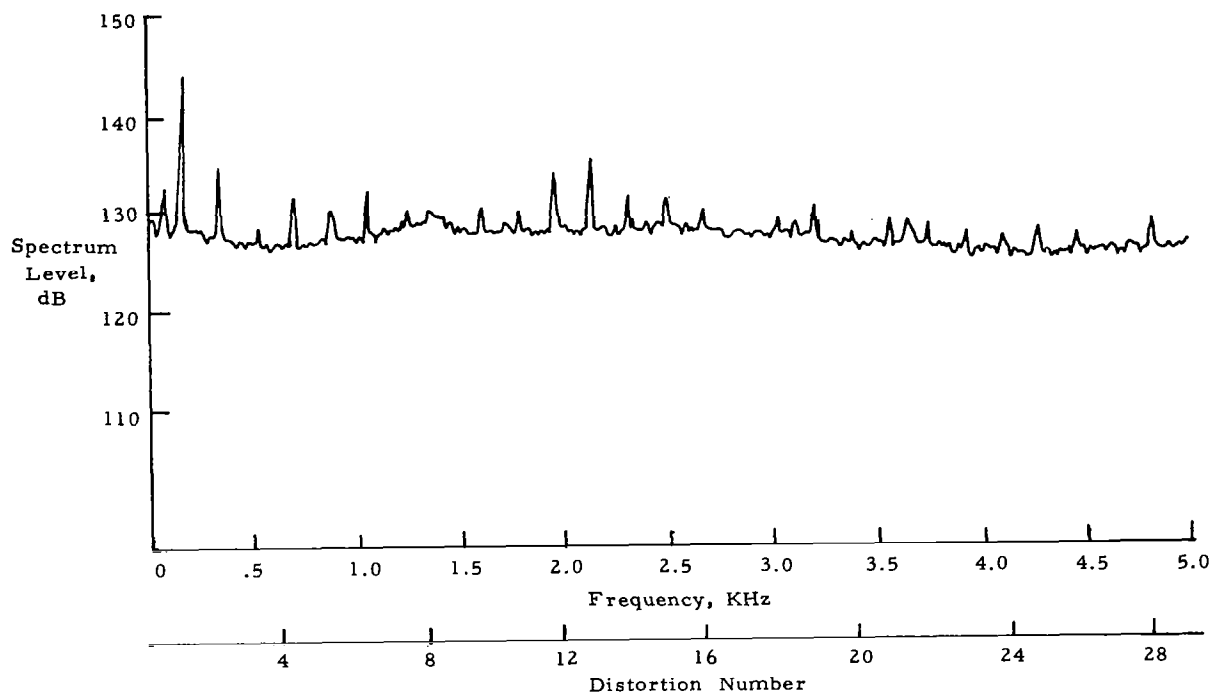


Figure 73.- B-3 power spectra - ICD no. 5.

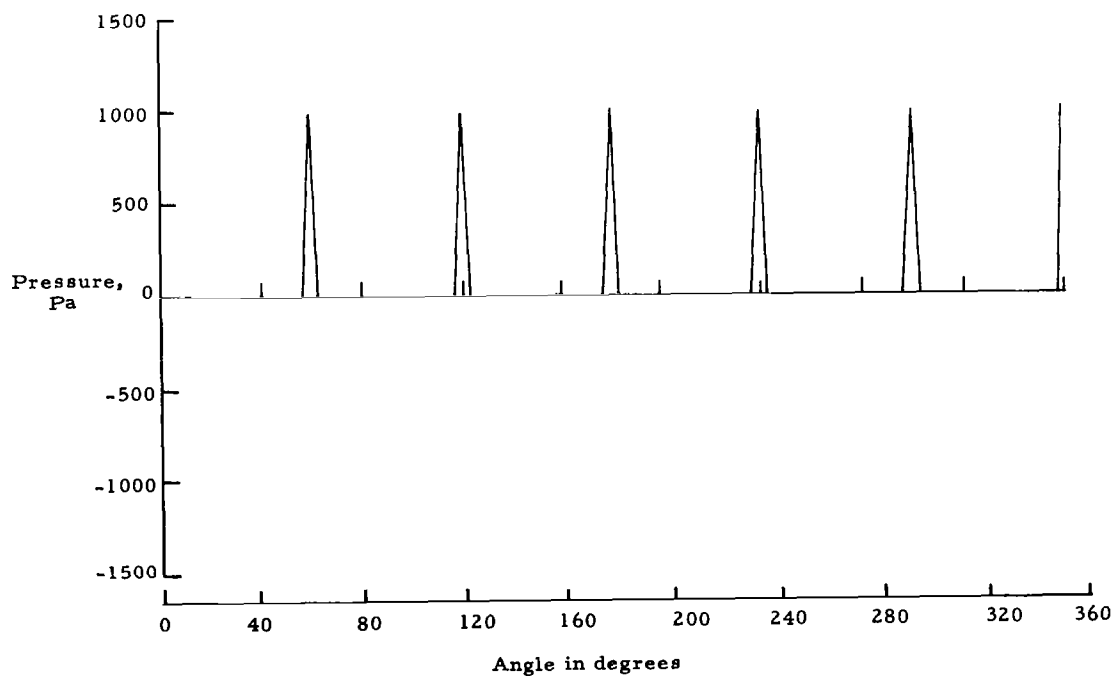


Figure 74.- Impulse pattern no. 1.

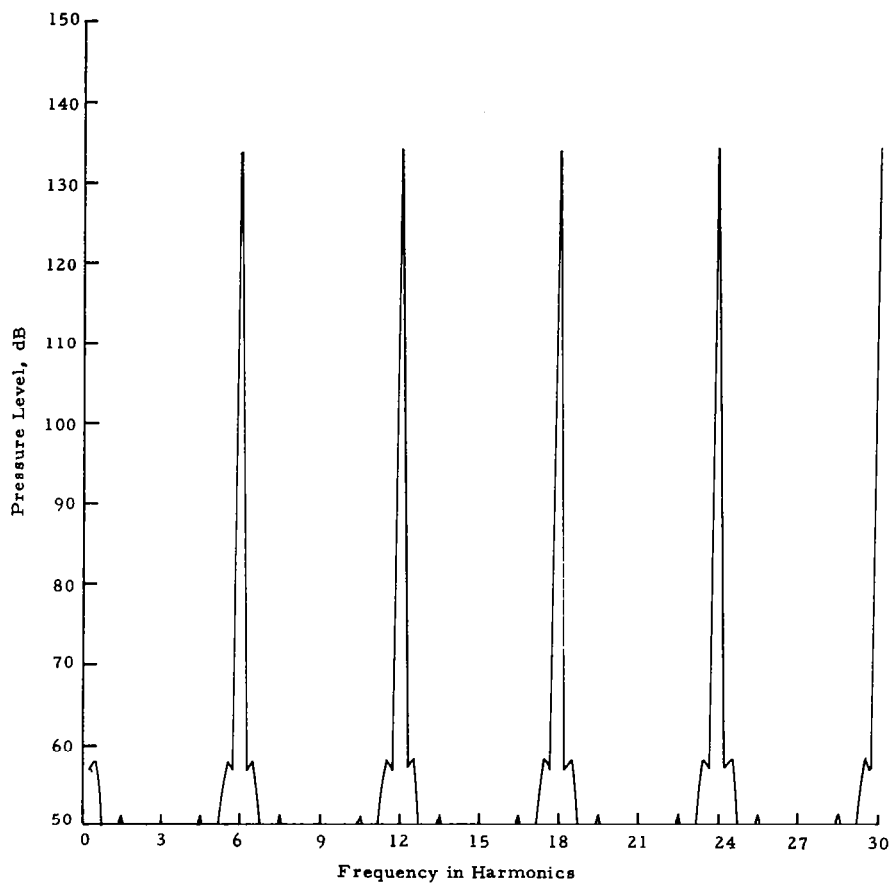


Figure 75.- Impulse pattern no. 1 - spectrum.

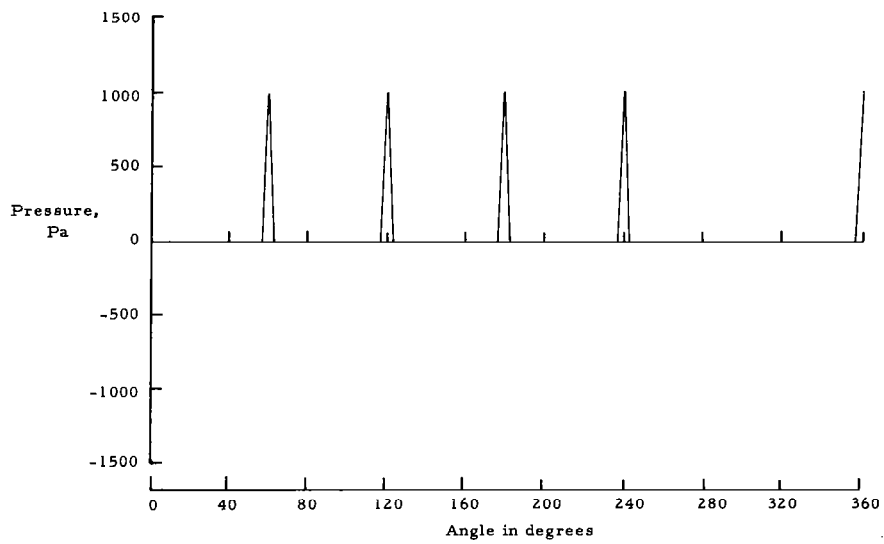


Figure 76.- Impulse pattern no. 2.

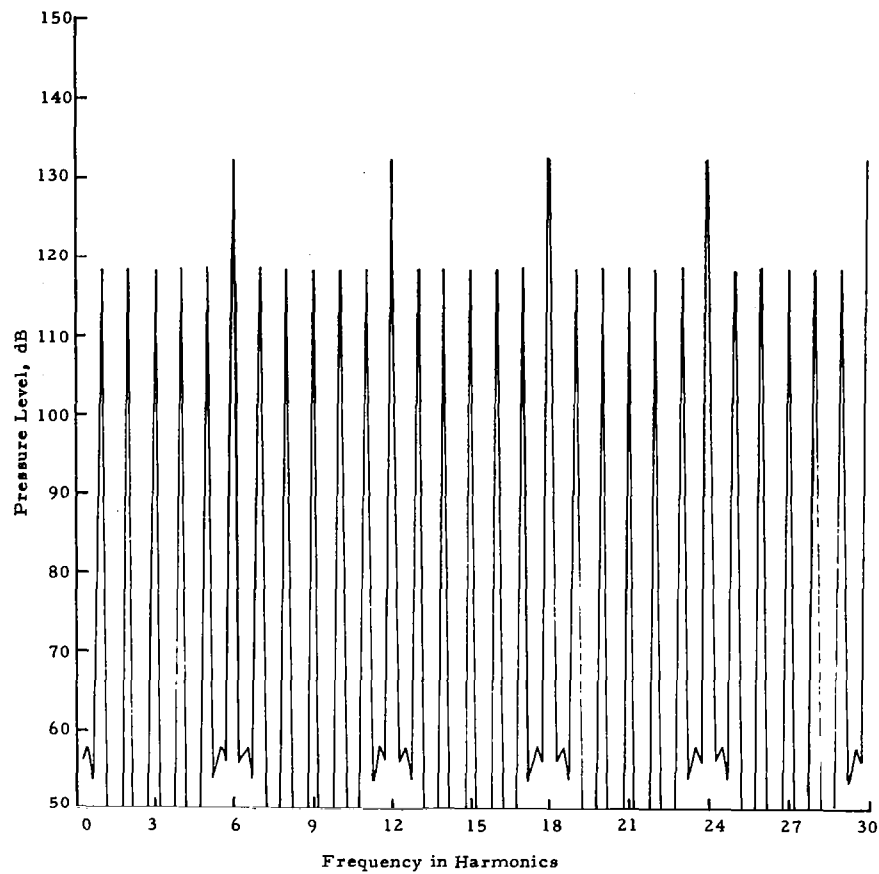


Figure 77.- Impulse pattern no. 2 - spectrum.

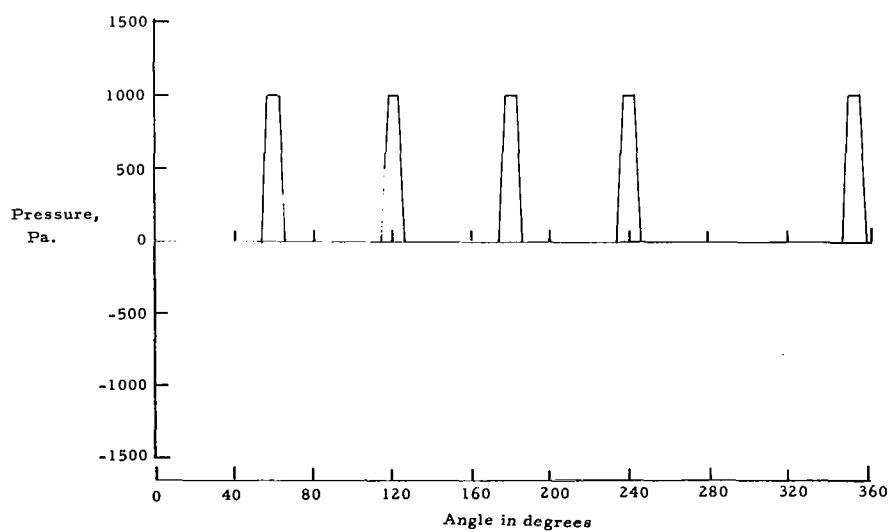


Figure 78.- Impulse pattern no. 4.

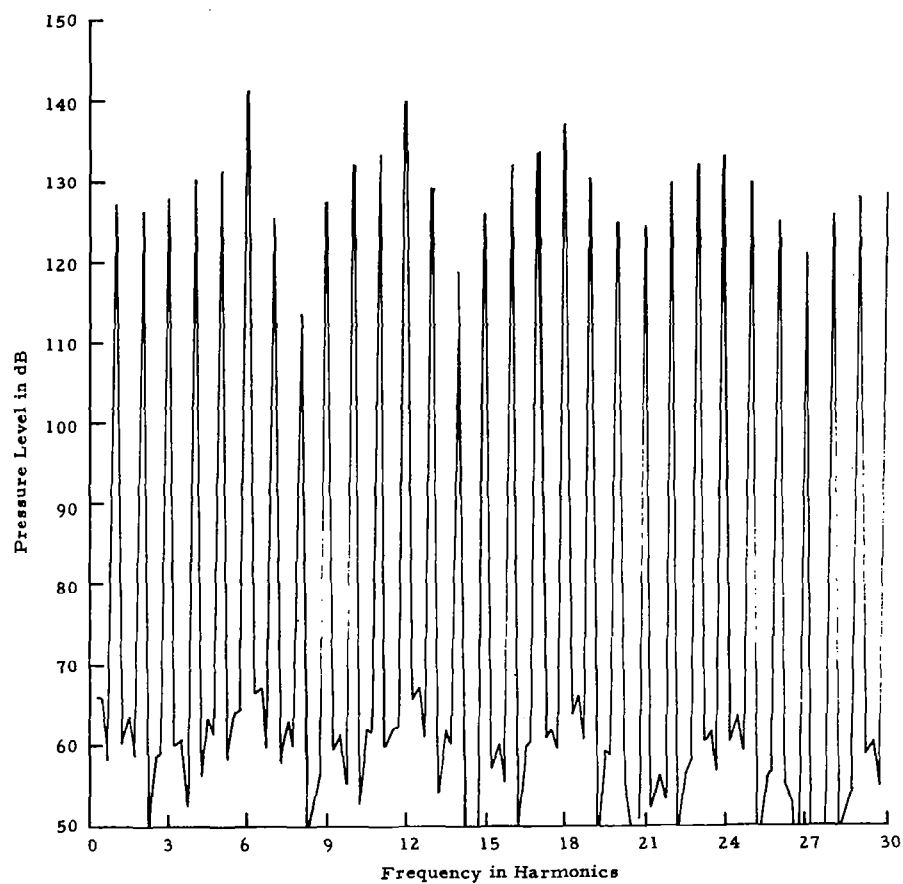


Figure 79.- Impulse pattern no. 4 - spectrum.

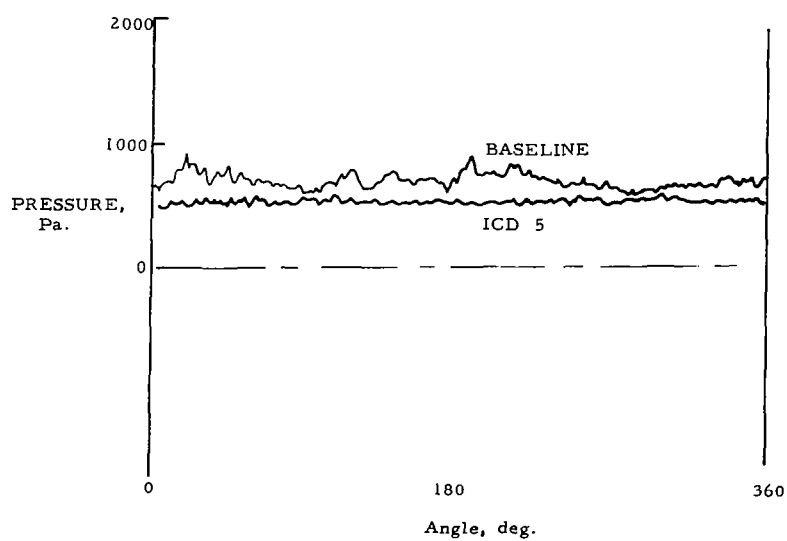


Figure 80.- B-3 rms pressure.

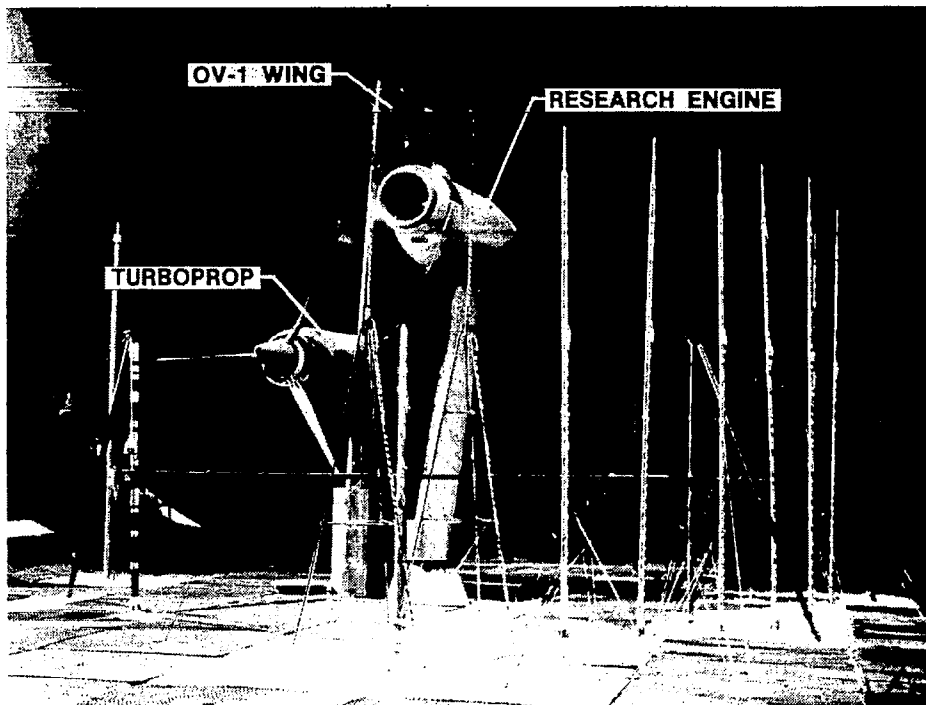


Figure 81.- Research engine with OV-1 turboprop/wing assembly.

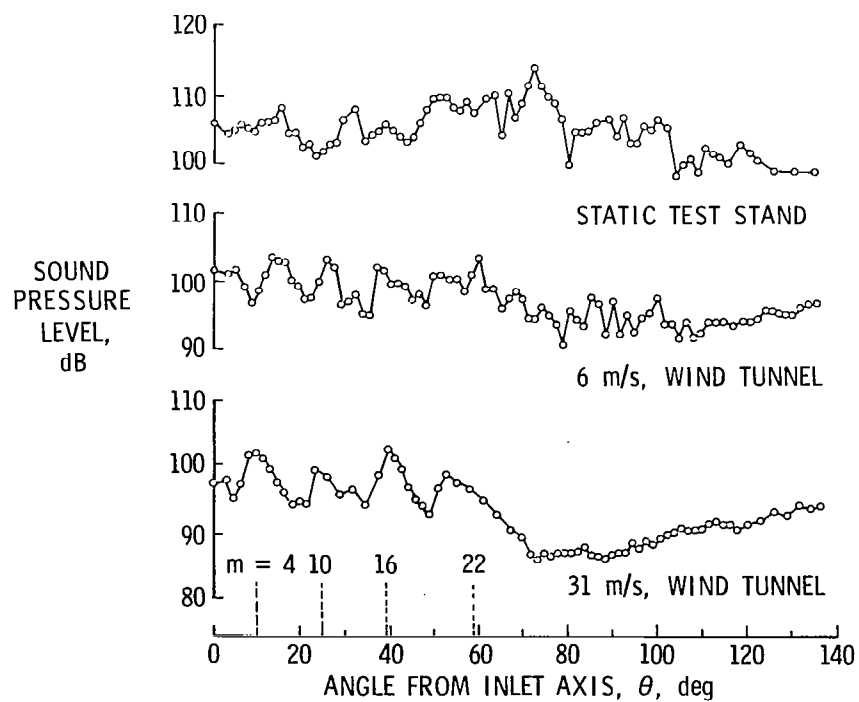


Figure 82.- Blade passing frequency (BPF) directivity patterns;  $N_1 = 12,000$  rpm.

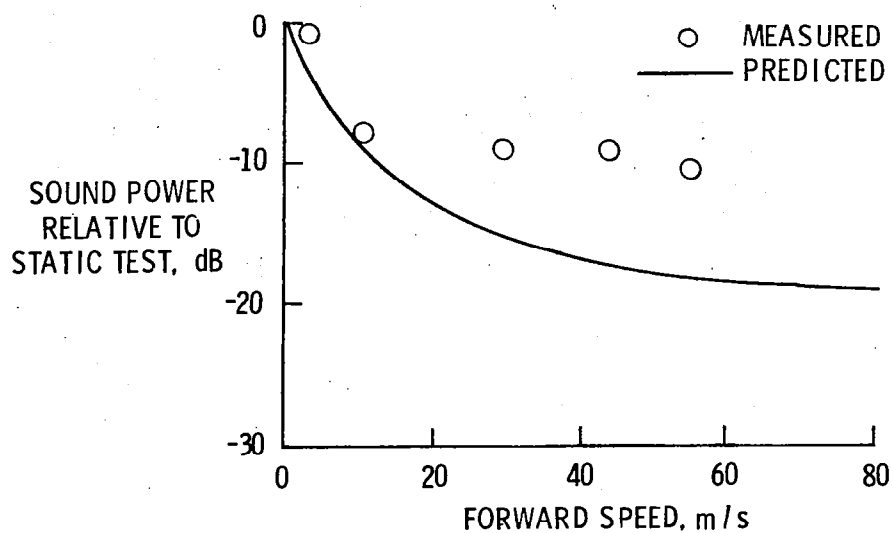


Figure 83.- Variation of acoustic sound power with forward speed;  $N_1 = 10,500$  rpm.

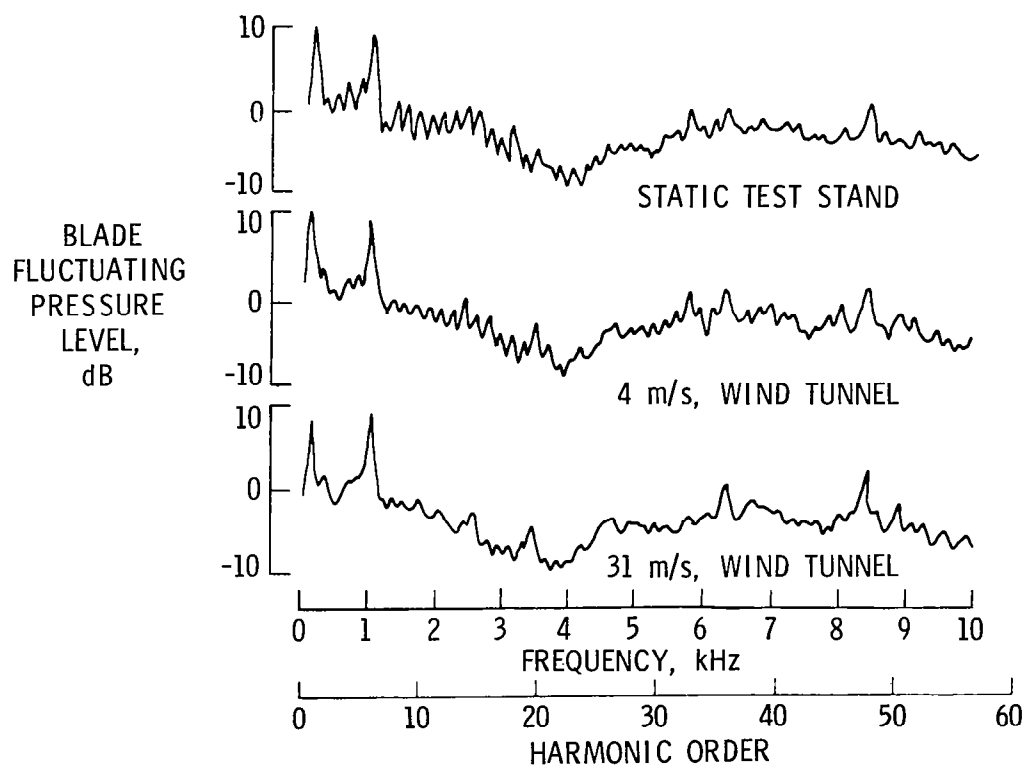


Figure 84.- Blade mounted transducer (BMT) pressure spectra.

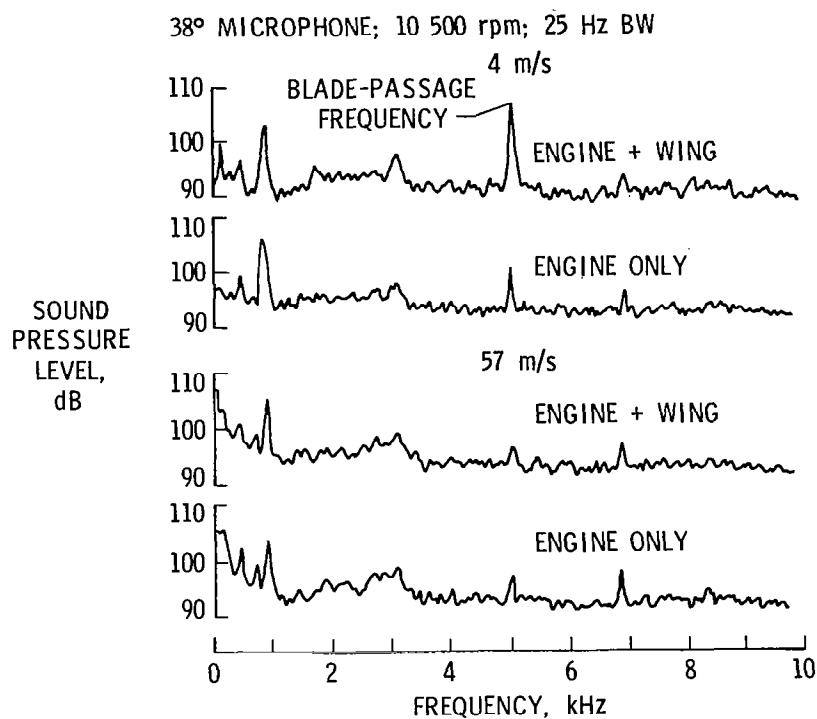


Figure 85.- Effect of OV-1 wing on acoustic spectra.

- INVESTIGATE FLIGHT SIMULATION EFFECTIVENESS ON FORWARD-RADIATED FAN NOISE THROUGH BACK-TO-BACK TESTING:
  1. 40x80 FT. AMES WIND TUNNEL
  2. OUTDOOR STATIC TEST STAND - NO TCS (ICS)
  3. OUTDOOR STATIC TEST STAND - WITH TCS (ICS)
- INVESTIGATE INLET DESIGN EFFECTS
- INVESTIGATE INLET TREATMENT EFFECTS
- INVESTIGATE FAN OPERATING LINE EFFECTS

Figure 86.- Scope of G.E./Ames program.



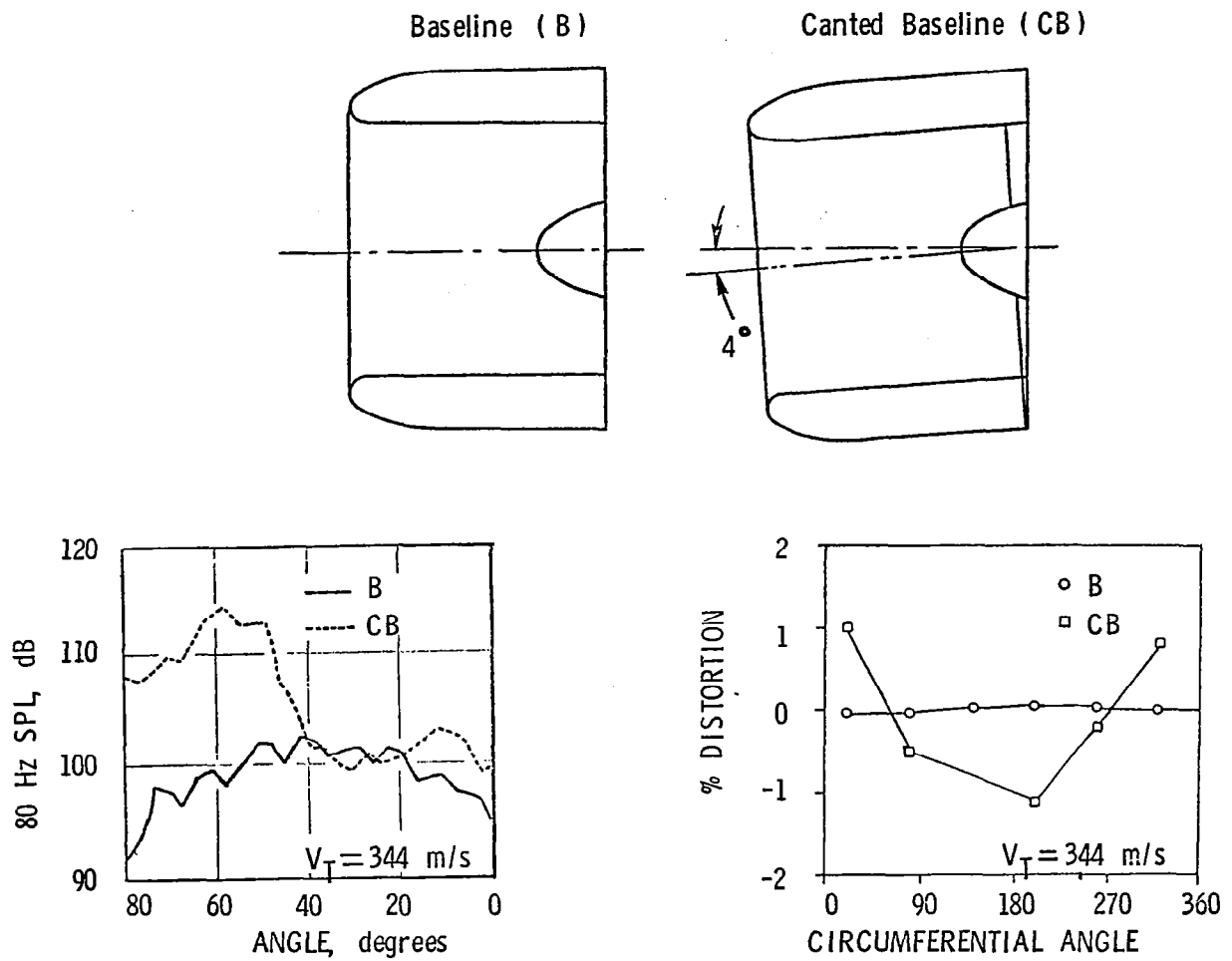


Figure 87.- Canted baseline summary.

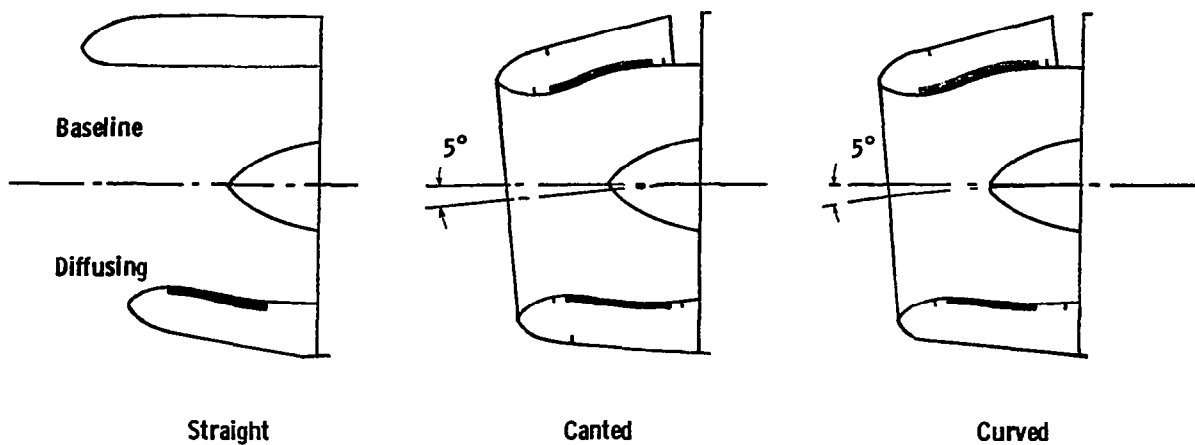
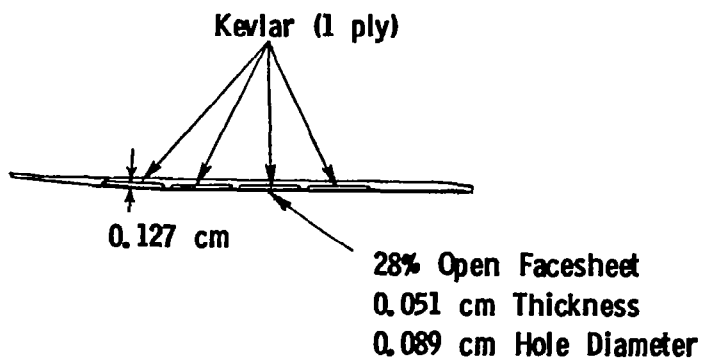
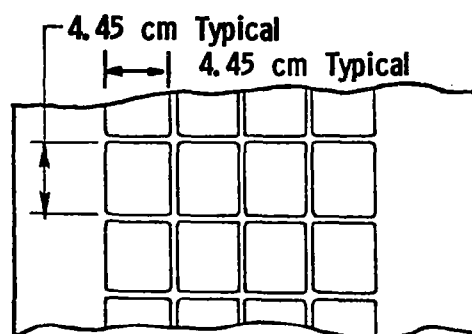


Figure 88.- Wind tunnel inlets.



(a) Axial treatment deployment.



(b) Projection of treatment deployment.

Figure 89.- Inlet treatment details.

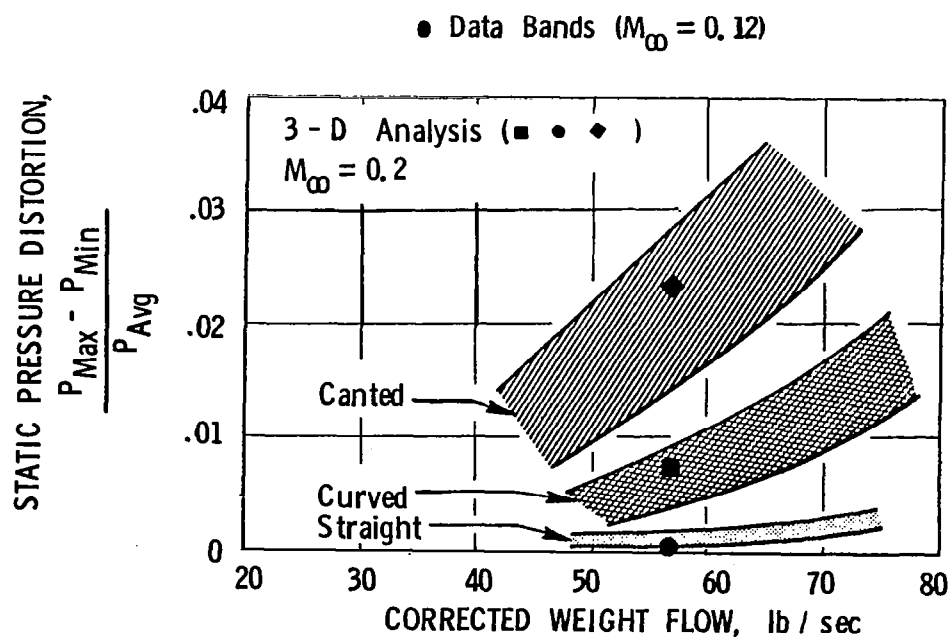


Figure 90.- Static pressure distortion - Ames inlets.

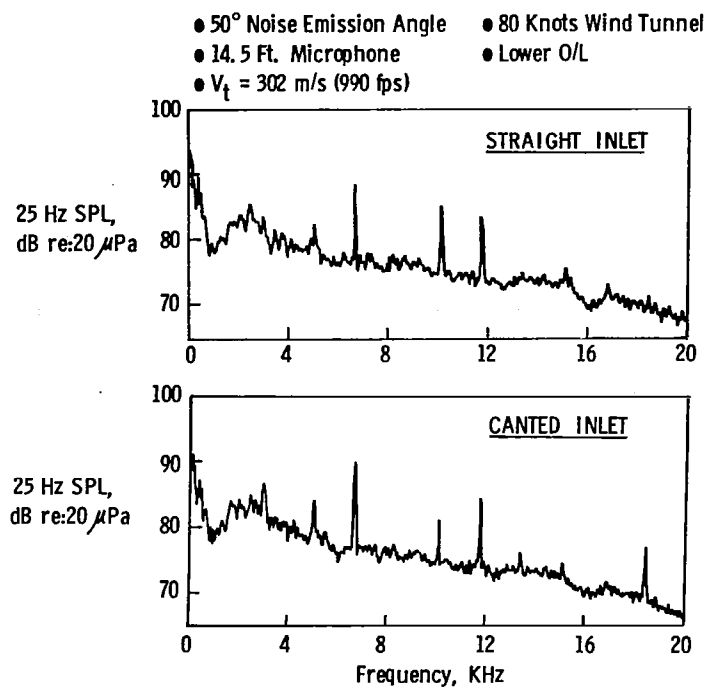


Figure 91.- Comparison of canting and straight diffusing with treated inlet - narrowband spectra.

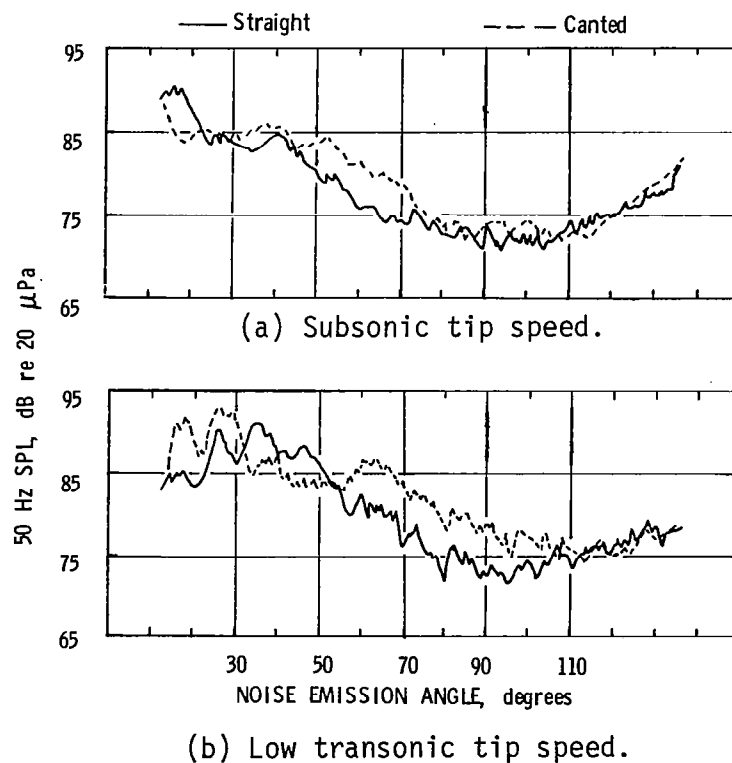


Figure 92.- Comparison of BPF directivities for straight and canted diffusing with treated inlets.

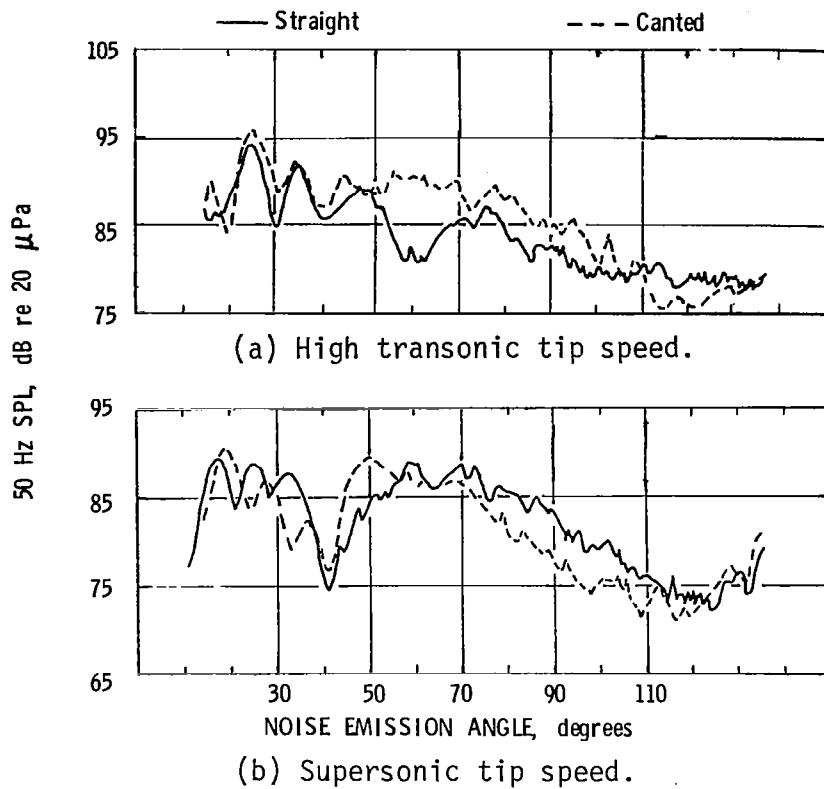


Figure 93.- Comparison of BPF directivities for straight and canted diffusing with treated inlets (higher speeds).

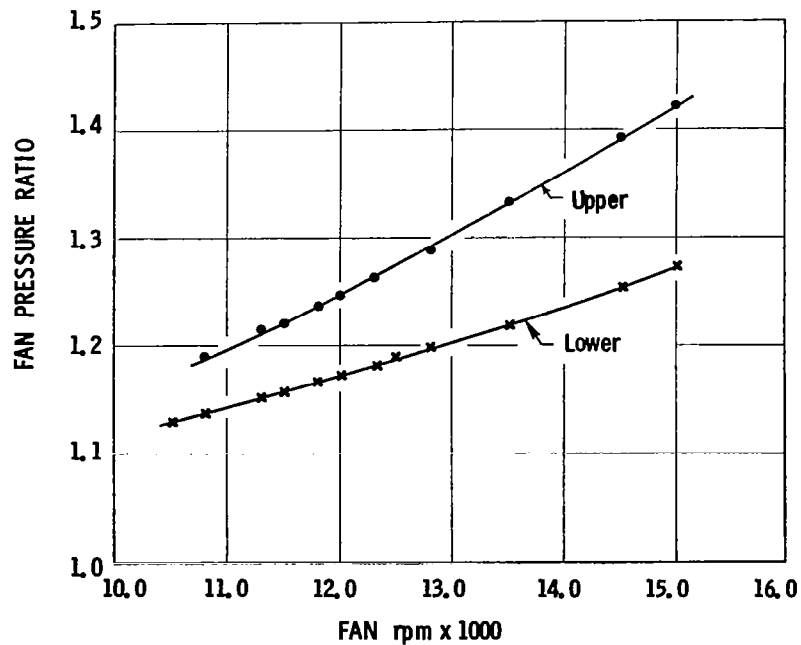


Figure 94.- Two fan operating lines tested.

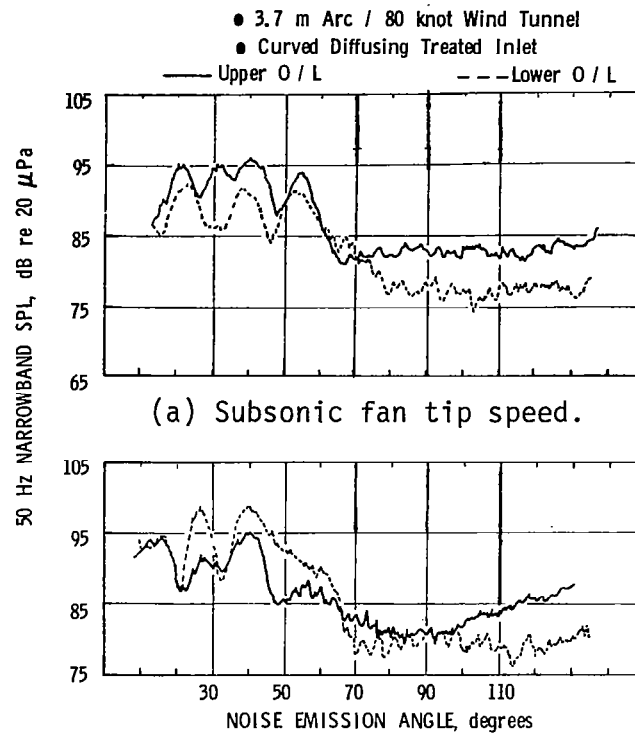


Figure 95.- Narrowband BPF directivities.

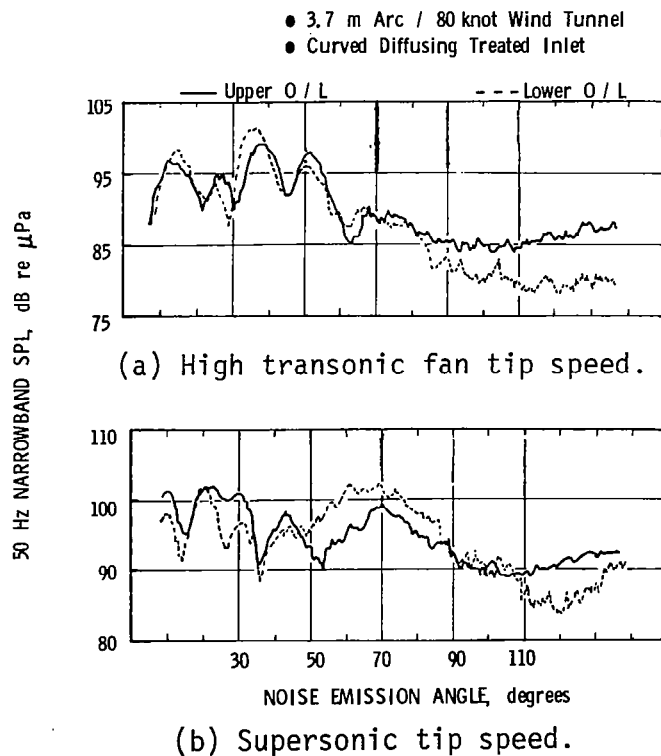


Figure 96.- Narrowband BPF directivities (higher speeds).

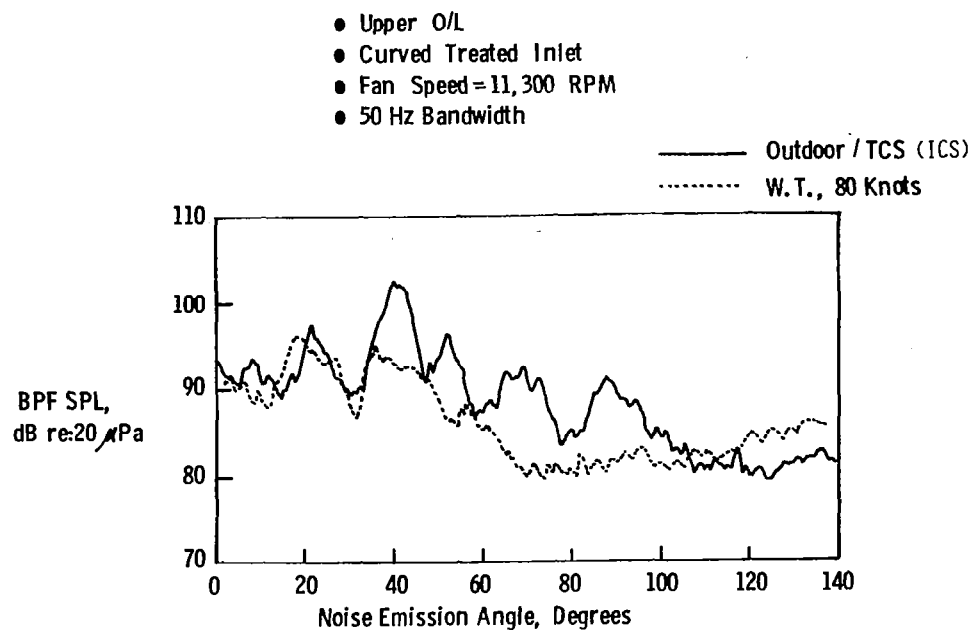


Figure 97.- Comparison of wind tunnel and outdoor BPF directivities.

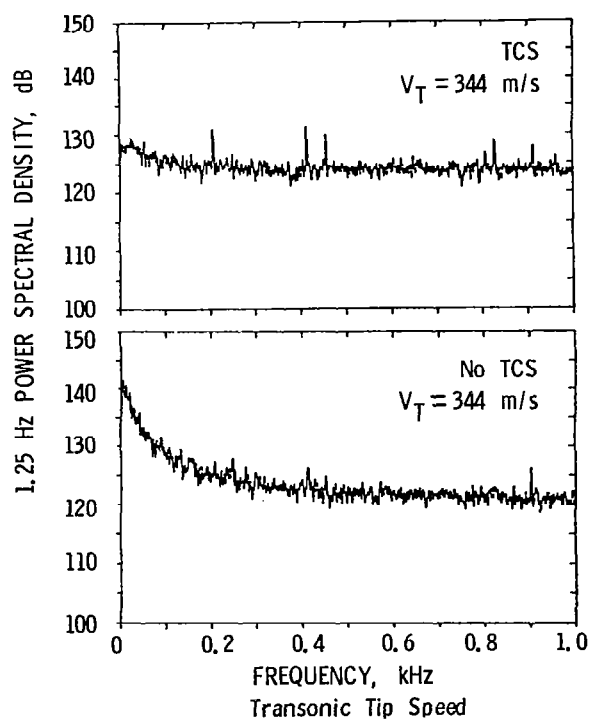


Figure 98.- Comparative turbulence spectra for TCS (ICS) and no-TCS tests.

(No ICS - ICS)

● Straight Diffusing Hard - Wall Inlet

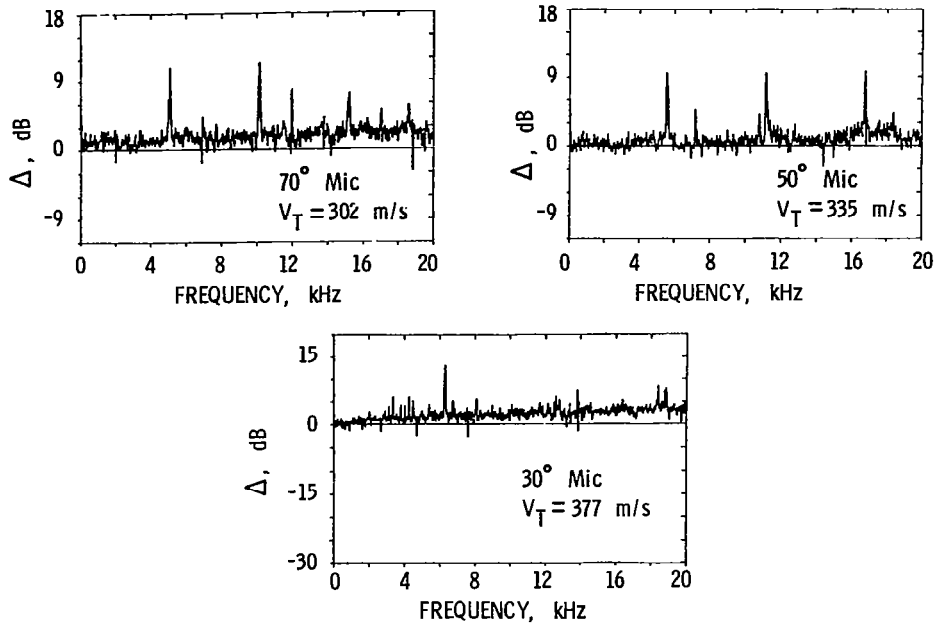


Figure 99.- Spectral differences (25 Hz).

- 11,800 RPM
- Upper Operating Line

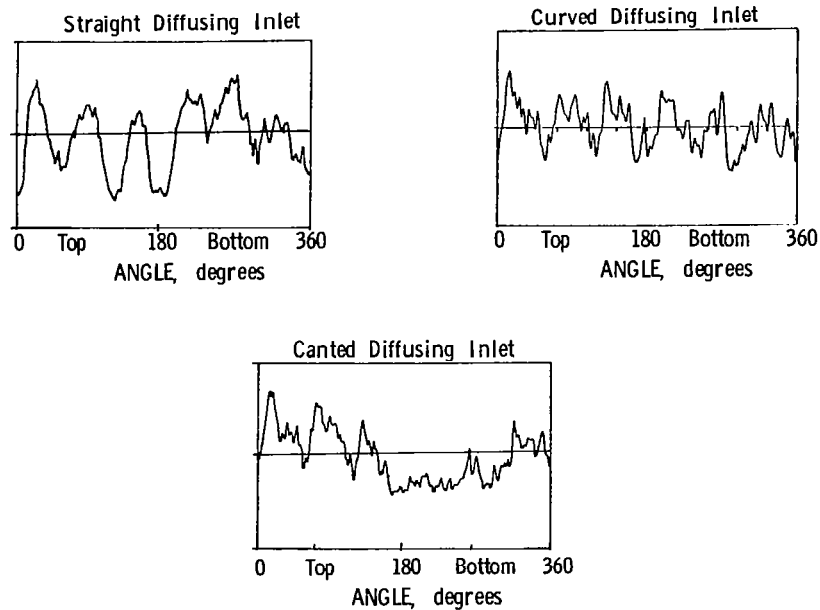


Figure 100.- BMT I - averaged waveforms.

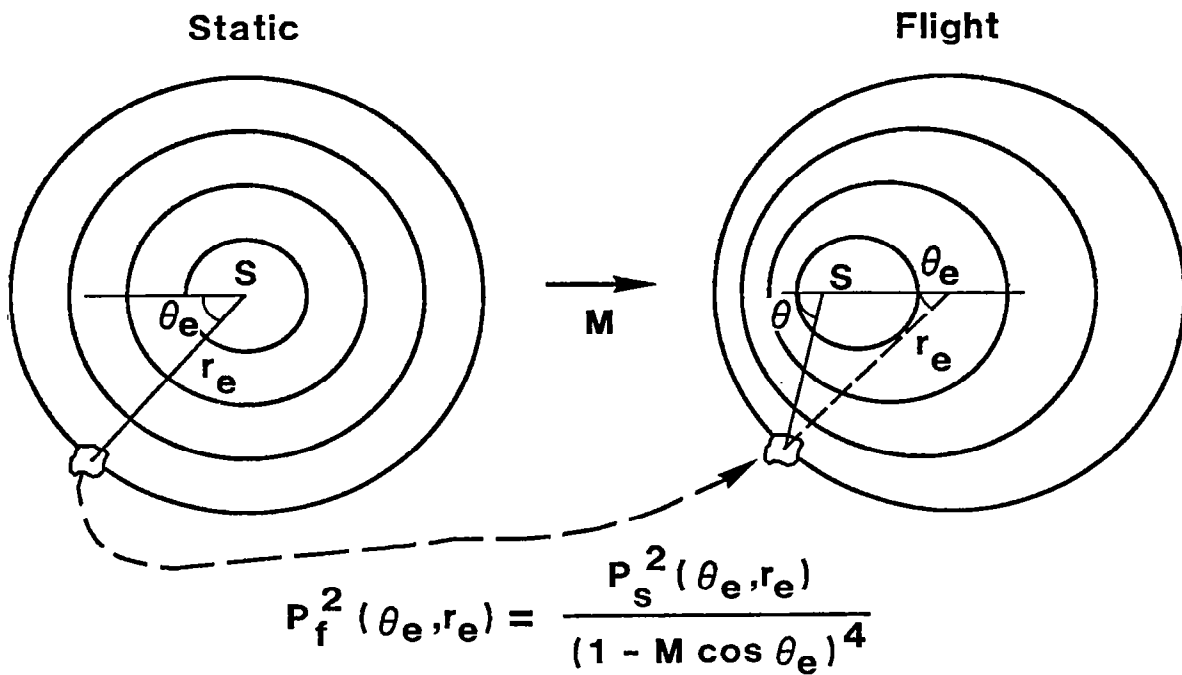


Figure 101.- Common dipole correction.

$$\frac{\partial \epsilon}{\partial t} + \nabla \cdot \underline{l} = 0$$

$$\epsilon \equiv \frac{P'^2}{2\rho_0 c_0} + \frac{\rho_0}{2} v'^2 + \underline{M} \cdot \underline{v}' \frac{P'}{c_0}$$

$$\underline{l} \equiv P' \underline{v}' + \underline{M} \frac{P'^2}{\rho_0 c_0} + \rho_0 c_0 \underline{M} \cdot \underline{v}' \underline{v}' + \underline{M} \underline{M} \cdot \underline{v}' P'$$

Figure 102.- Energy flow in moving fluid.



Pressure and velocity perturbations are simply related

$$P' \hat{k} = \rho_o c_o \underline{v}'$$

$$\epsilon = \frac{P'^2}{\rho_o c_o^2} (1 + \underline{M} \cdot \hat{k})$$

$$\underline{l} = c_o (\hat{k} + \underline{M}) \epsilon$$

Figure 103.- Energy in far field.

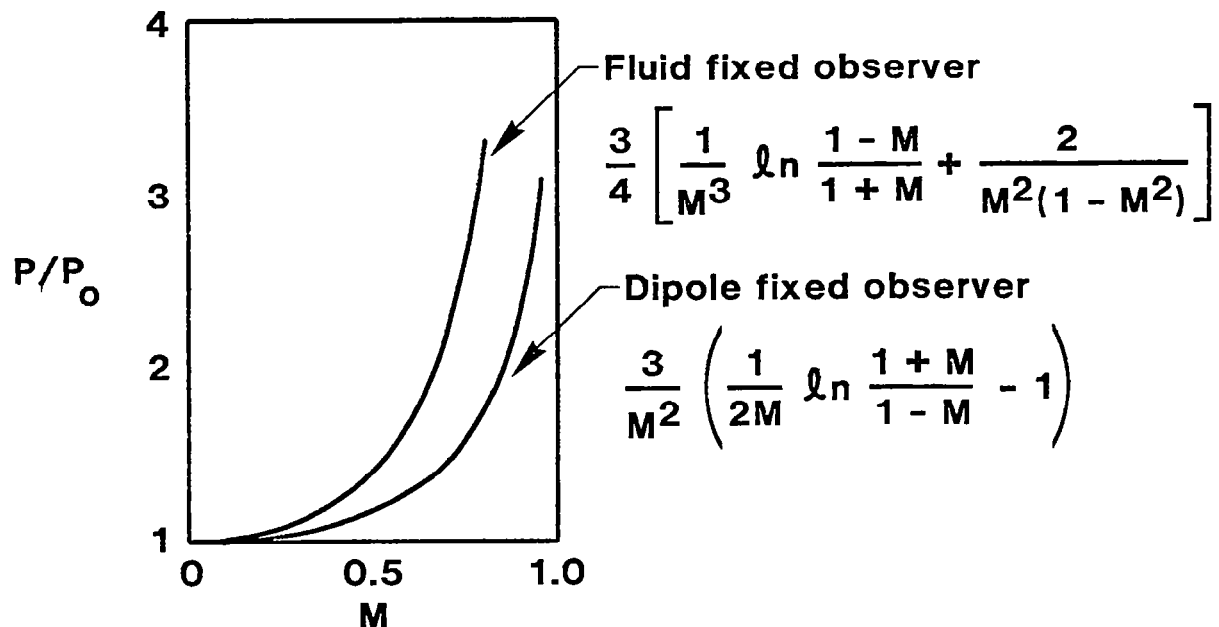
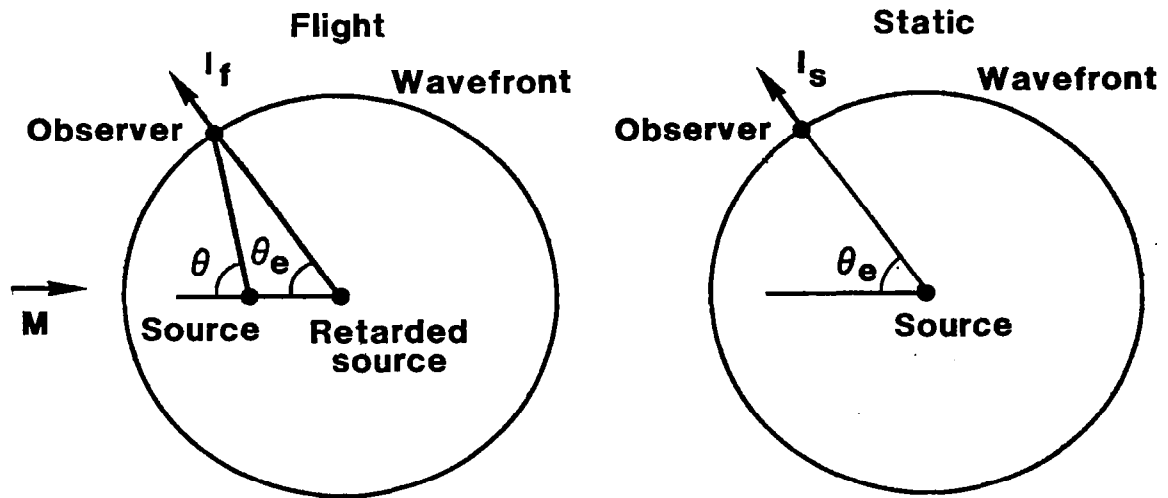
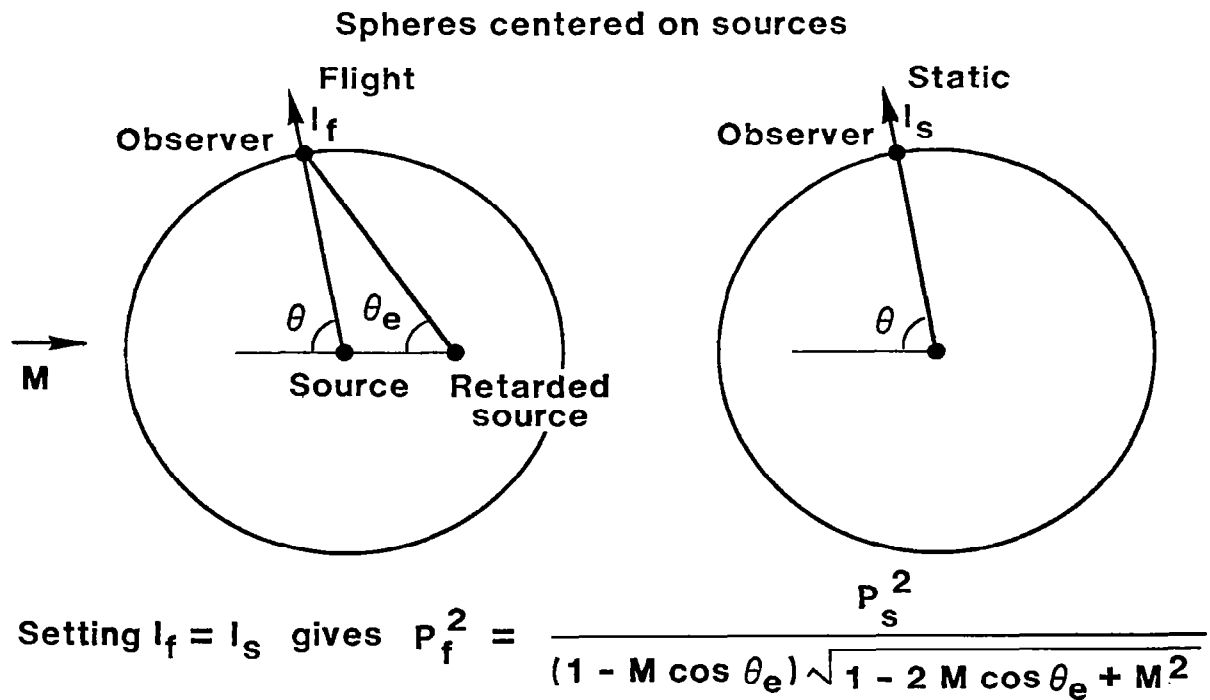


Figure 104.- Power radiated by dipole in flow relative to fixed dipole.



Setting  $I_f = I_s$  gives  $P_f^2 = \frac{P_s^2}{(1 - M \cos \theta_e)^2}$

Figure 105.- Equate intensities on wavefronts.



Setting  $I_f = I_s$  gives  $P_f^2 = \frac{P_s^2}{(1 - M \cos \theta_e) \sqrt{1 - 2 M \cos \theta_e + M^2}}$

Figure 106.- Recommended expression for  $P_f^2$ .

- Continued improvement required in methodology for projecting static data to flight, including convective amplification effects
- Preliminary wind tunnel experiment
  - Model fan in UTRC tunnel
  - Measurable effect
  - Constant fan noise source achieved
  - Limited to one speed and flight Mach no.
  - Approximate nose cone corrections used

Figure 107.- Experimental status.

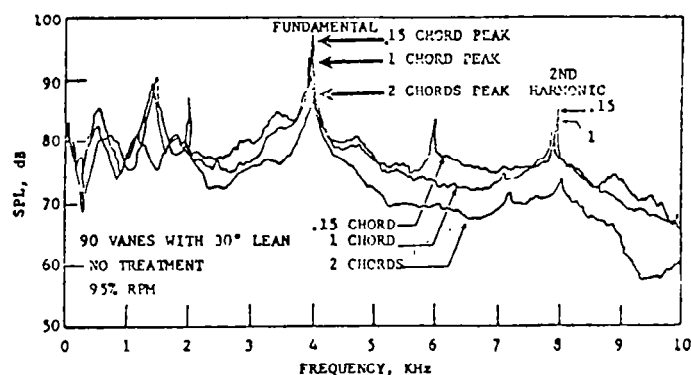


Figure 108.- Effect of rotor-stator spacing on measured far-field SPL spectrum. (From ref. 8.)

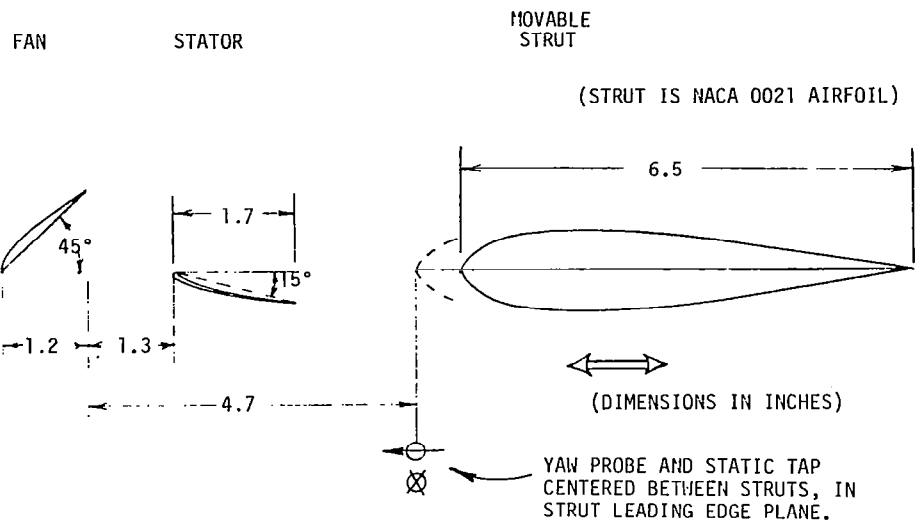


Figure 109.- Rotor blade, stator vane, and strut arrangement in research compressor rig.

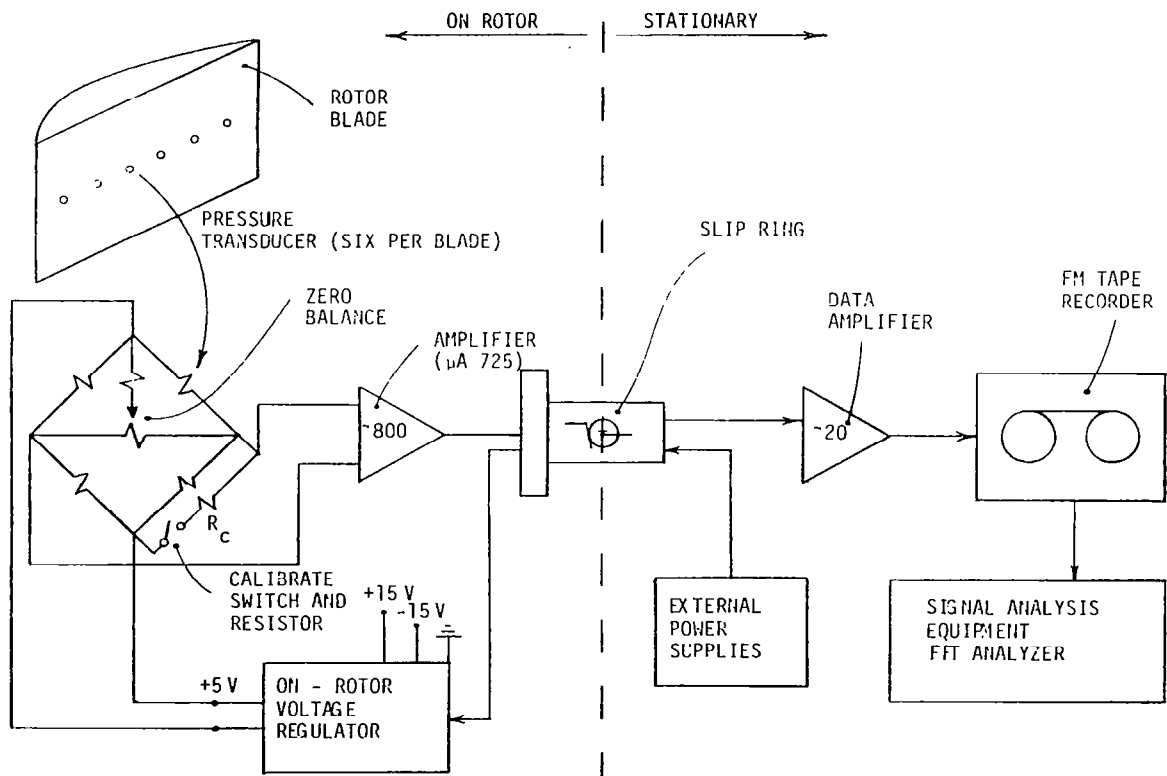


Figure 110.- Block diagram of on-rotor pressure measurement, recording, and analysis system.

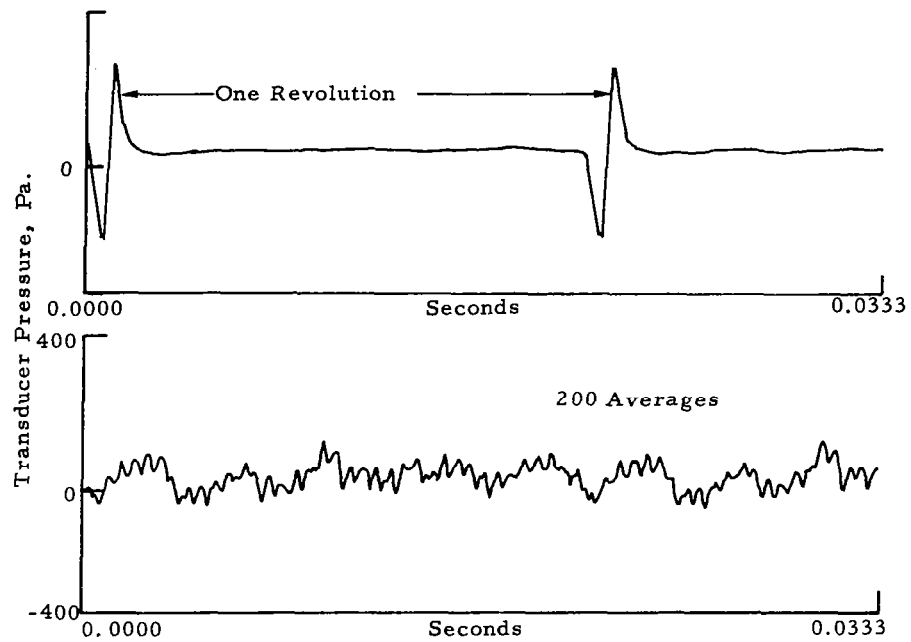


Figure 111.- Pressure signal and revolution indicator for transducer no. 2 with downstream struts in place.

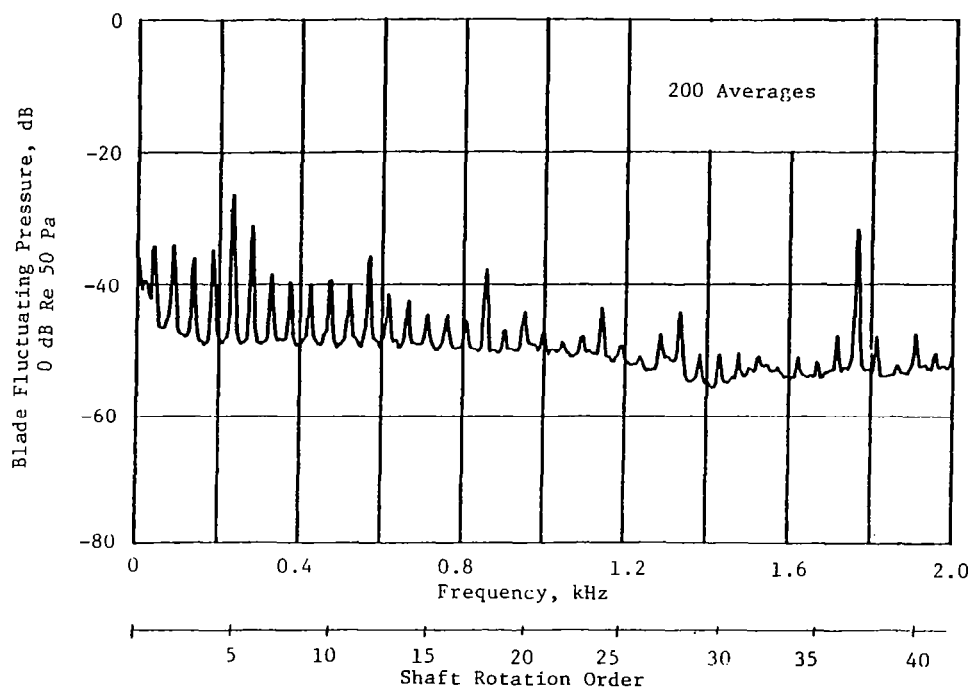


Figure 112.- Transducer no. 2, 0- to 2-kHz spectrum, downstream struts in place.

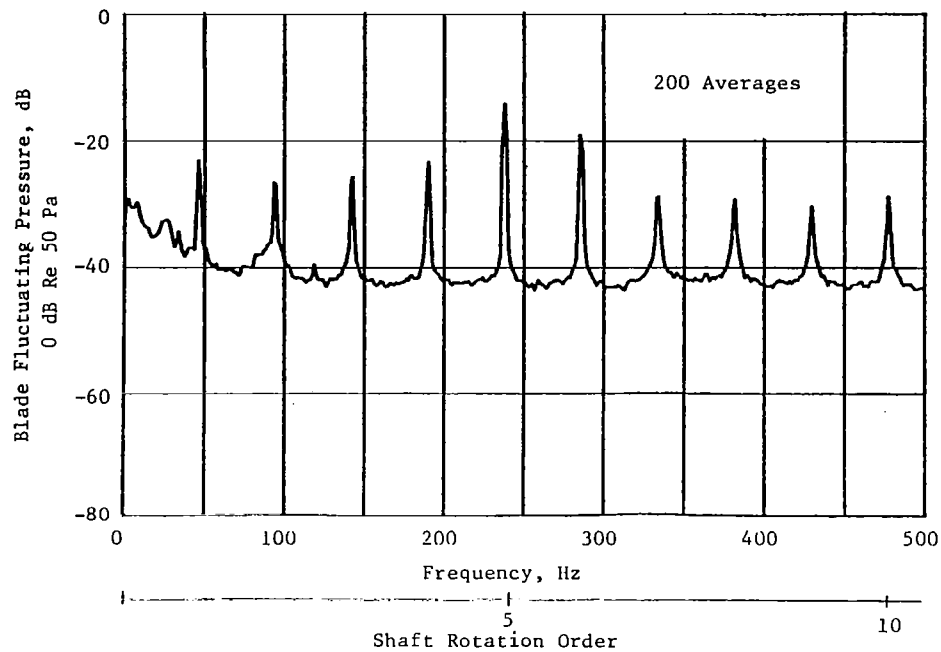


Figure 113.- Transducer no. 2, 0- to 500-Hz spectrum, downstream struts in place.

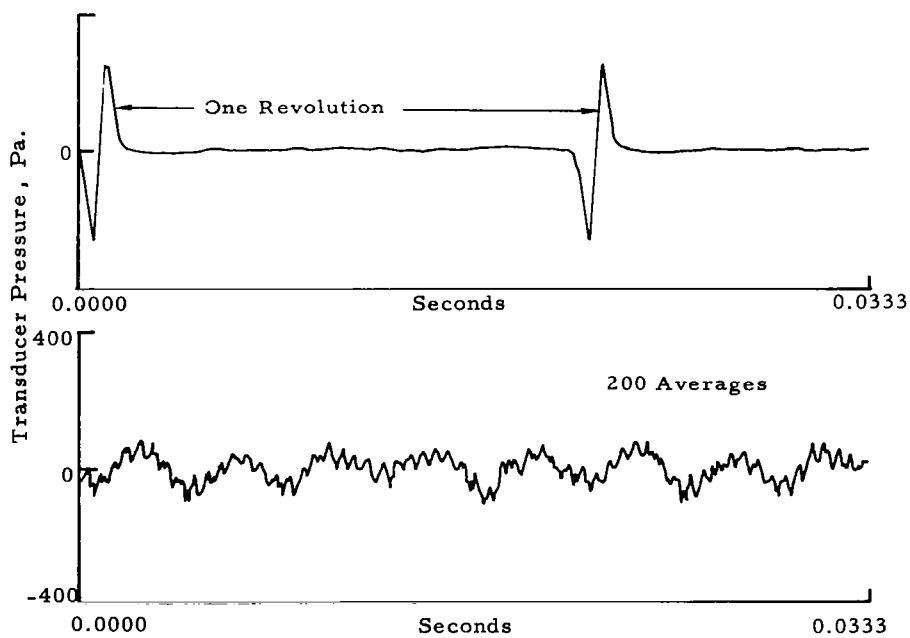


Figure 114.- Pressure signal and revolution indicator for transducer no. 6 with downstream struts in place.

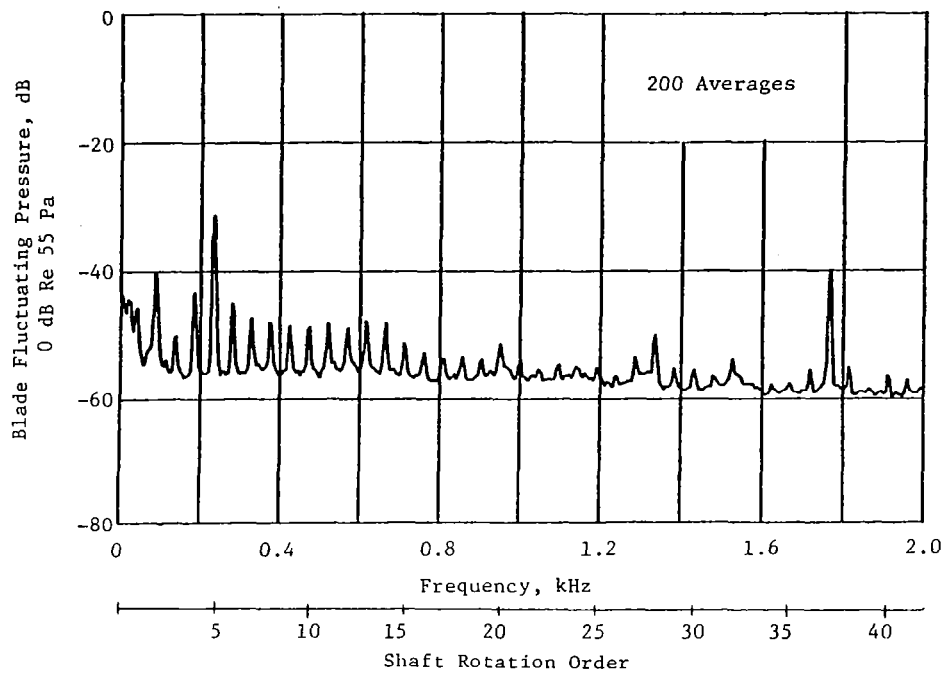


Figure 115.- Transducer no. 6, 0- to 2-kHz spectrum, downstream struts in place.

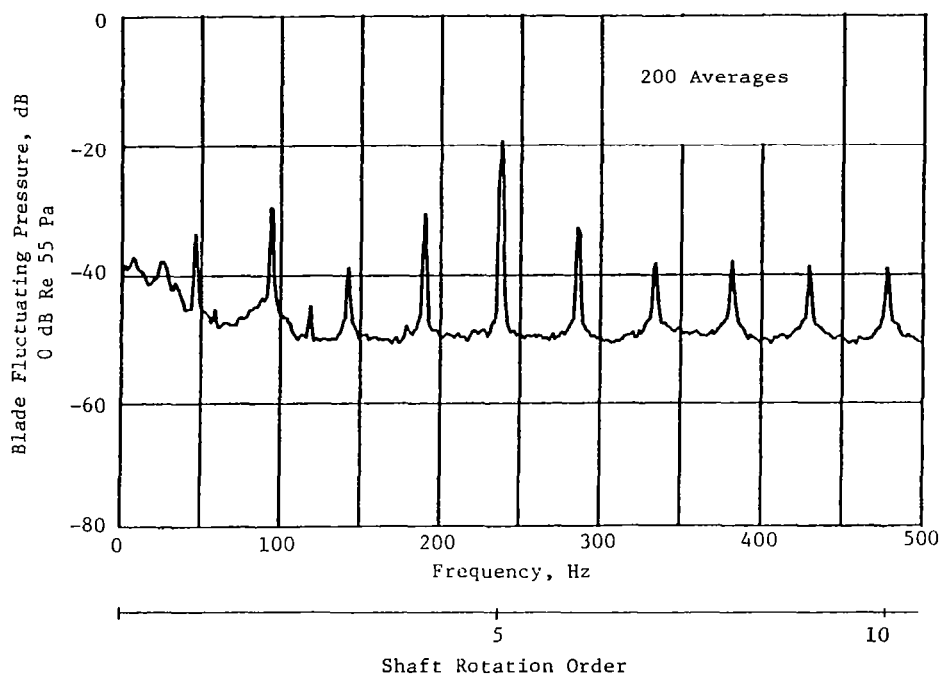


Figure 116.- Transducer no. 6, 0- to 500-Hz spectrum, downstream struts in place.

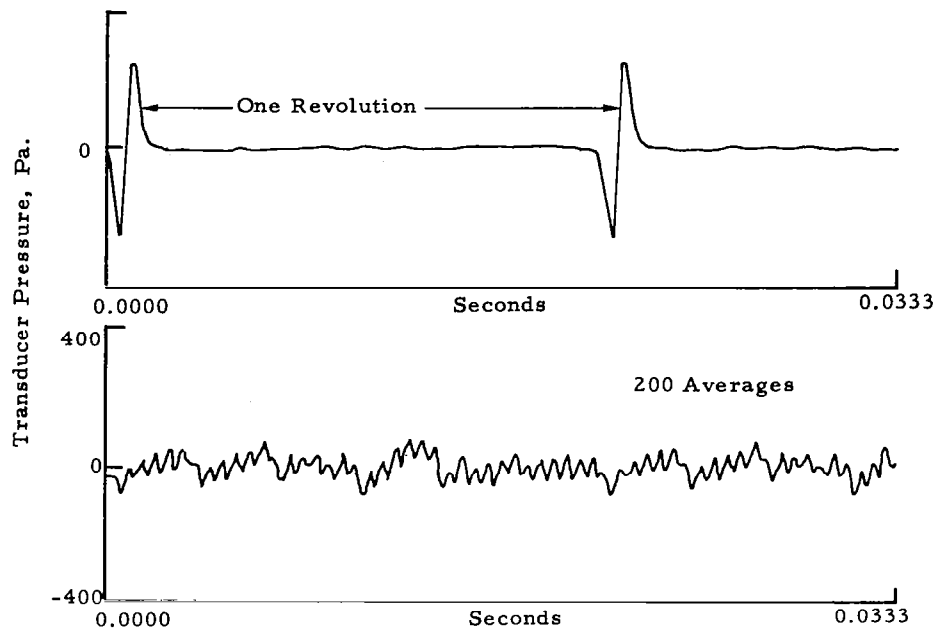


Figure 117.- Pressure signal and revolution indicator for transducer no. 2 with downstream struts removed.

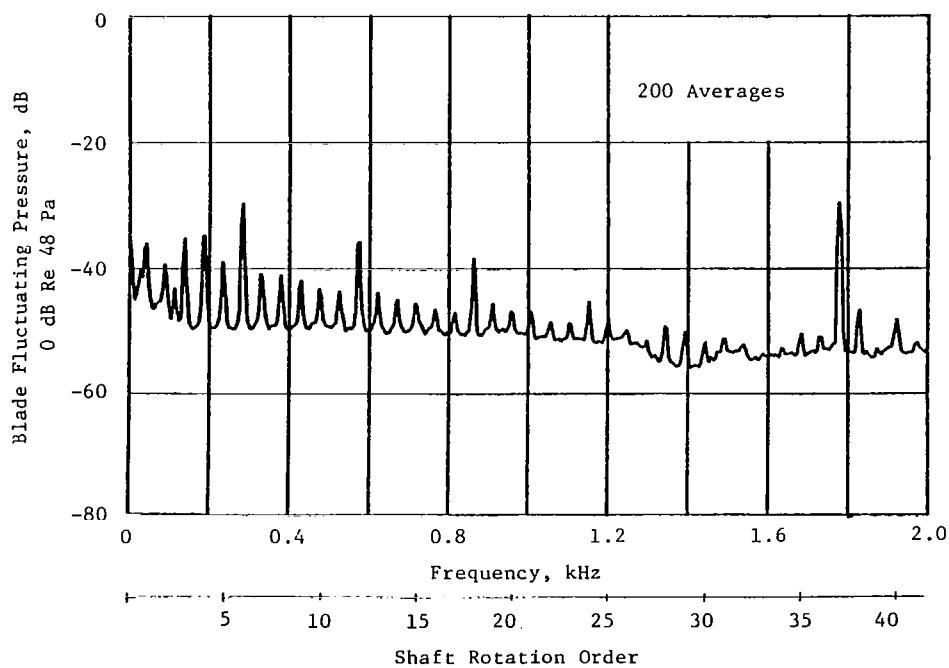


Figure 118.- Transducer no. 2, 0- to 2-kHz spectrum, downstream struts removed.



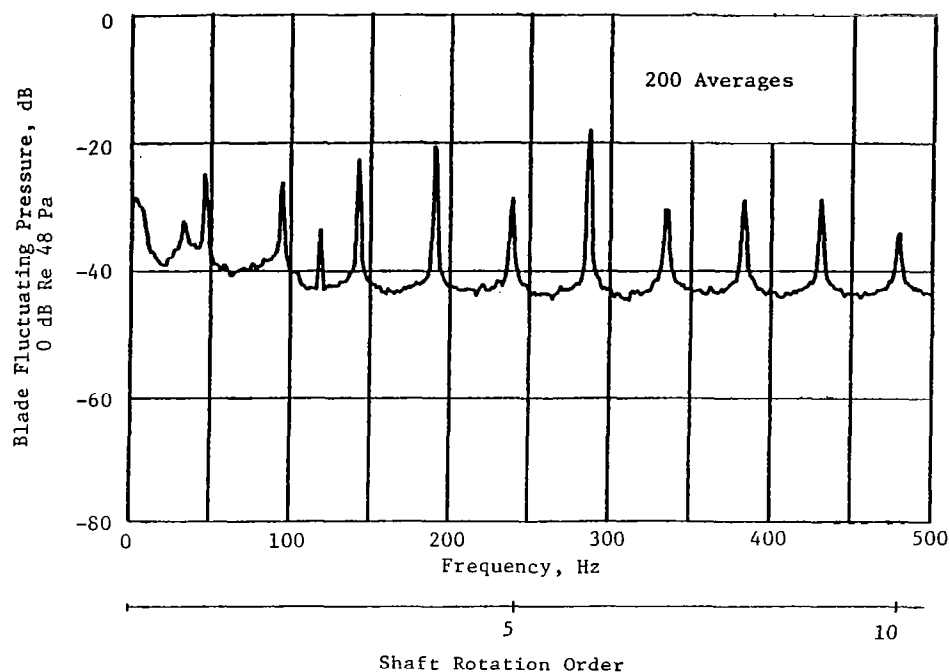


Figure 119.- Transducer no. 2, 0- to 500-Hz spectrum, downstream struts removed.

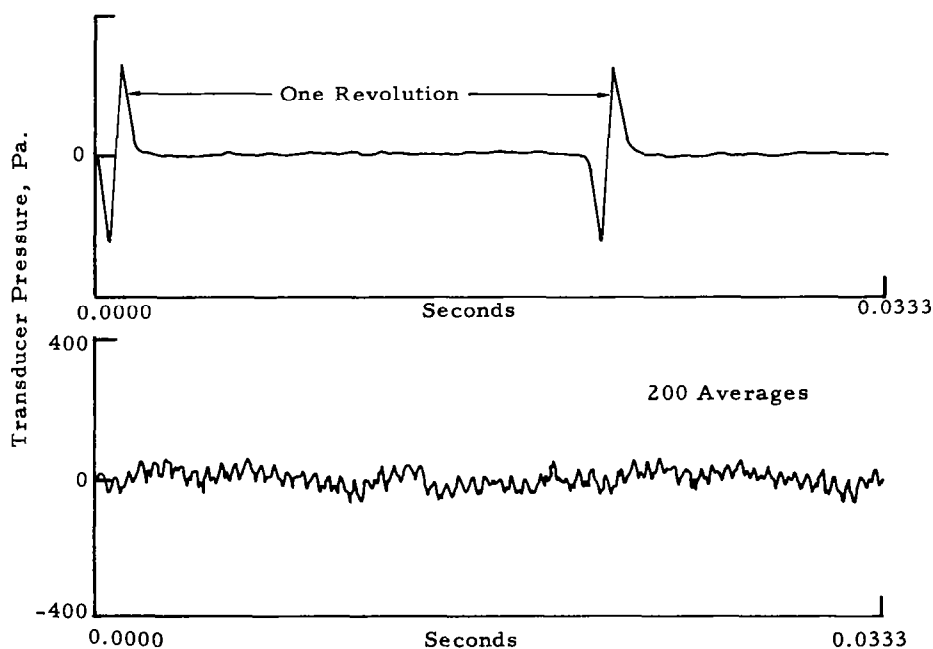


Figure 120.- Pressure signal and revolution indicator for transducer no. 6 with downstream struts removed.

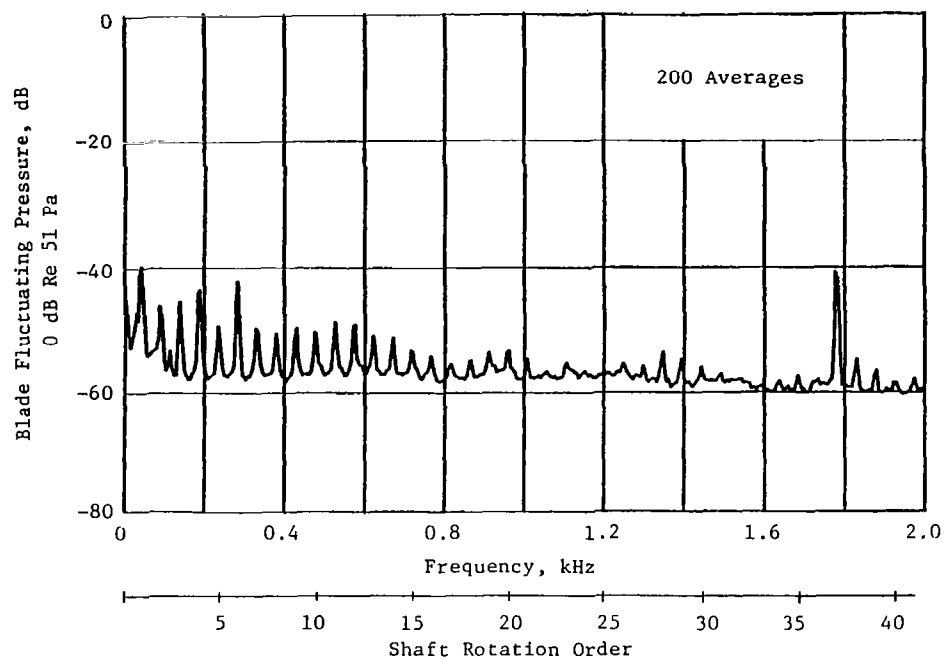


Figure 121.- Transducer no. 6, 0- to 2-kHz spectrum, downstream struts removed.

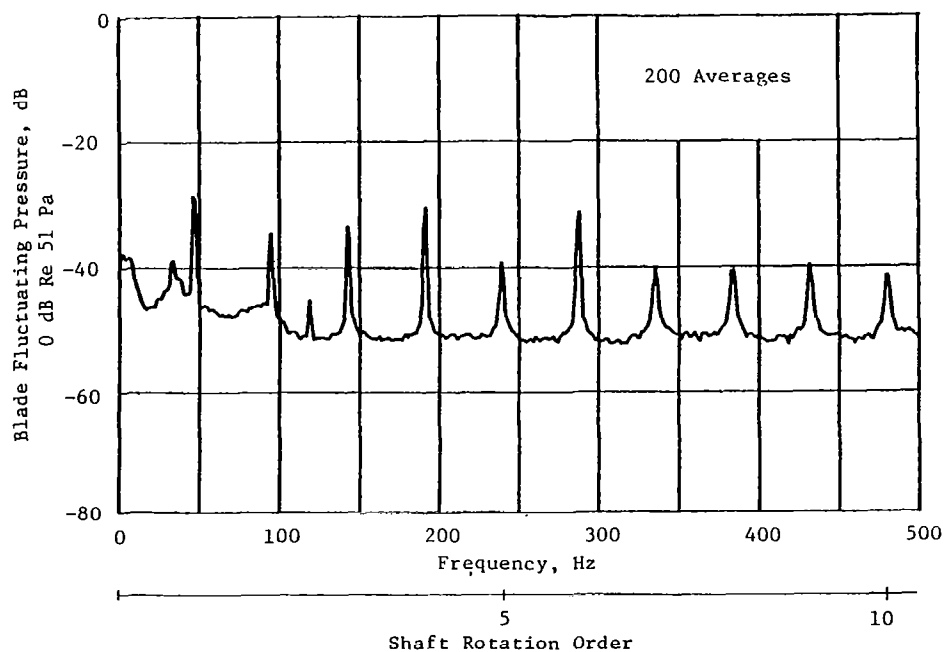


Figure 122.- Transducer no. 6, 0- to 500-Hz spectrum, downstream struts removed.

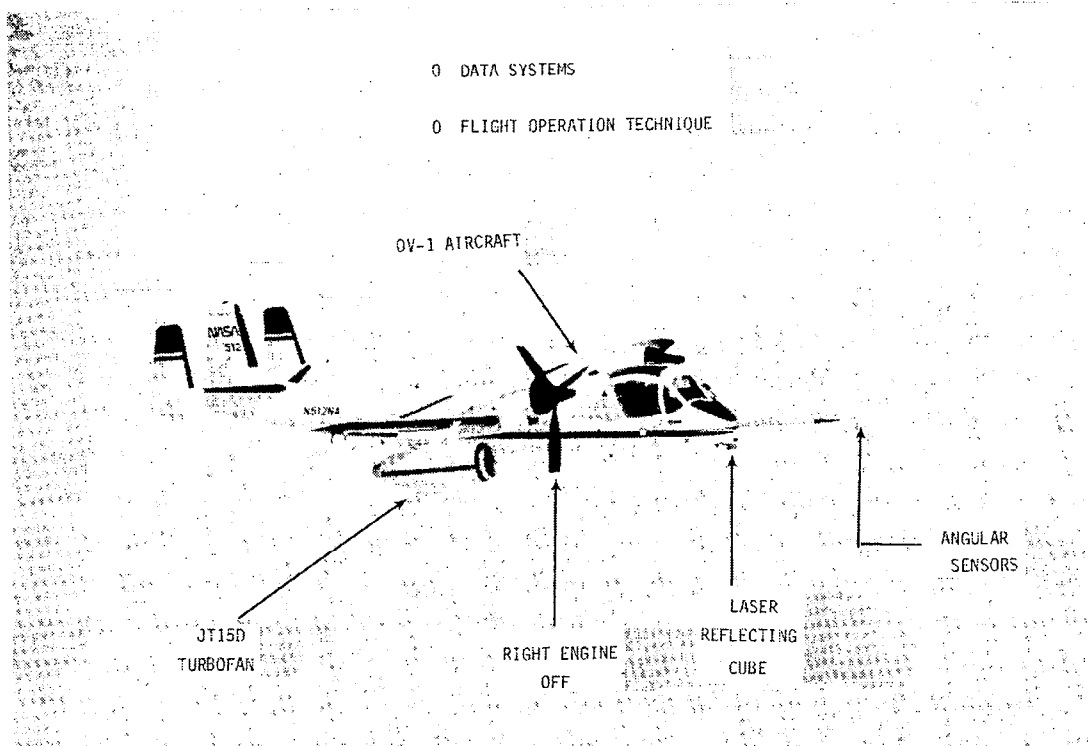


Figure 123.- Test aircraft.

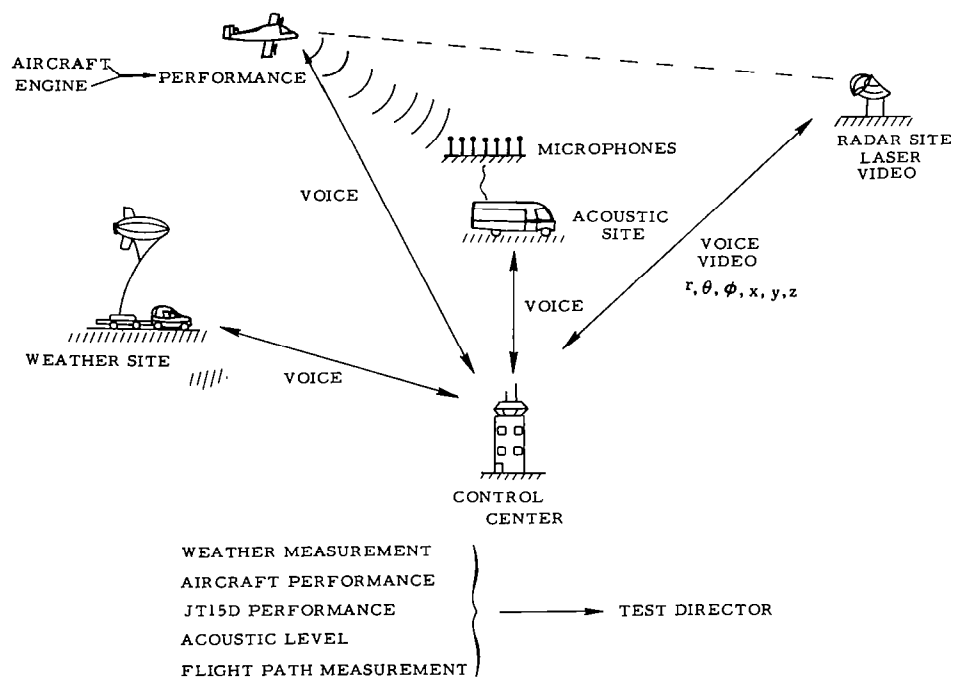


Figure 124.- Flight operations technique.

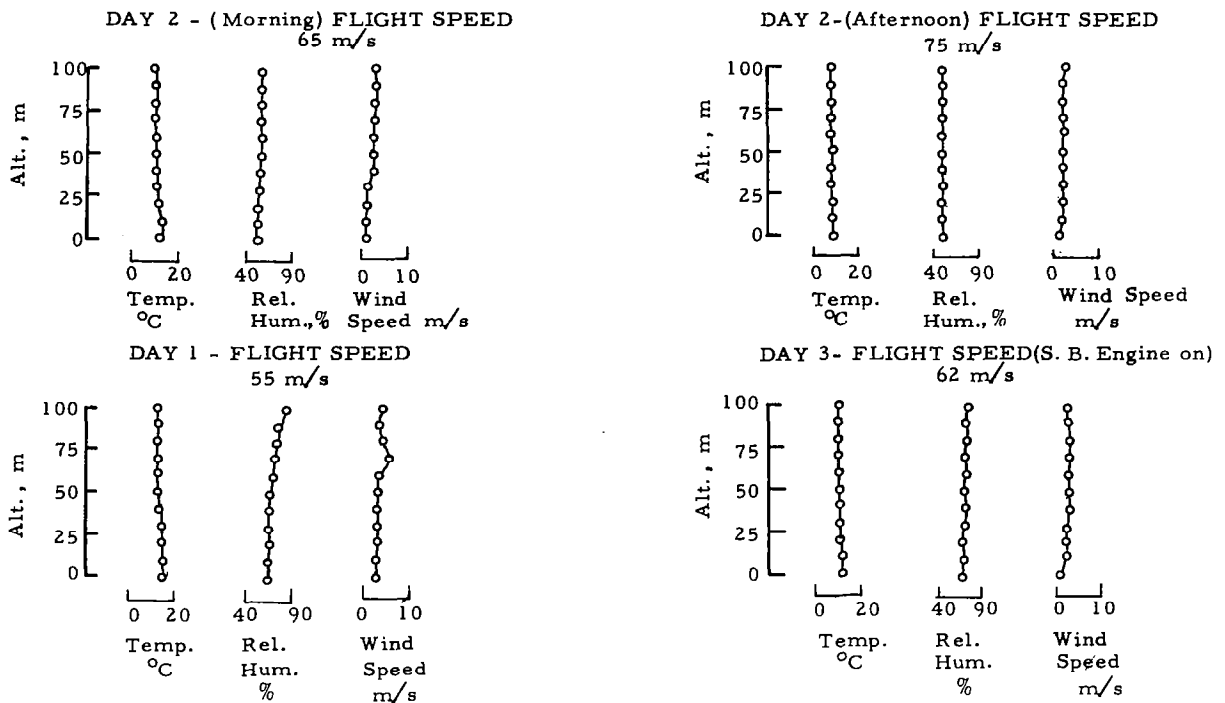


Figure 125.- Typical weather profile for temperature, relative humidity, and wind speed.

- PILOT
  - FLY THE AIRCRAFT
  - ANGLE OF ATTACK, SLIDE SLIP  
PITCH AND ROLL ATTITUDE
  - COMMUNICATIONS WITH TEST DIRECTOR
- JT15D ENGINE OPERATOR
  - MONITORS  $N_1$ ,  $N_2$ , FUEL FLOW, 1 PER REV AND  
ENGINE VIBRATION LEVEL
  - TWO ONBOARD TAPE RECORDERS
    - BLADE MOUNTED TRANSDUCERS
    - STATOR MOUNTED TRANSDUCERS
    - INDUCT MOUNTED TRANSDUCERS
    - JT15D ENGINE VARIABLES
  - COMMUNICATIONS WITH TEST DIRECTOR

Figure 126.- Duties of pilot and JT15D engine operator.

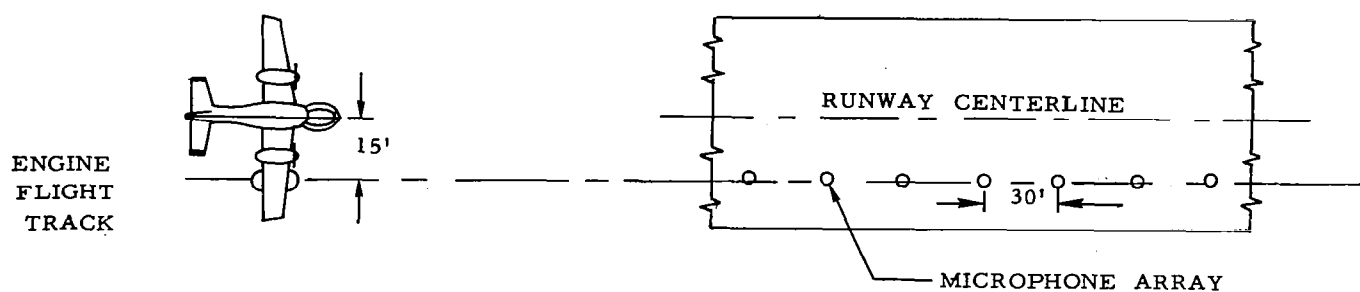


Figure 127.- Plan view of flight profile.

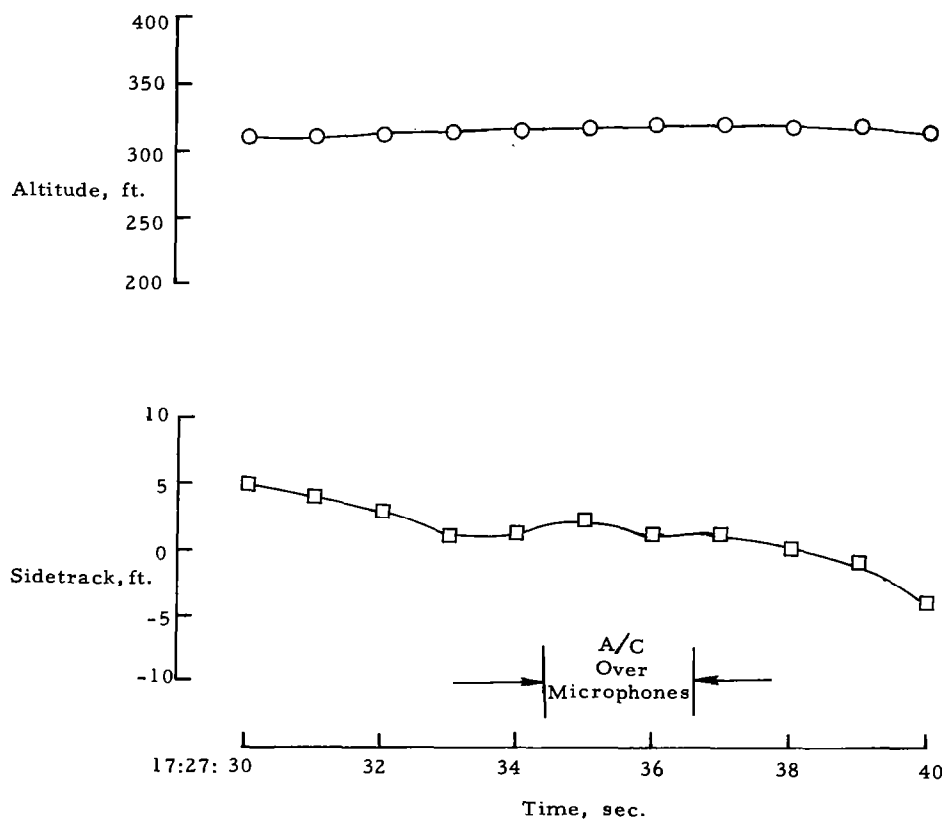
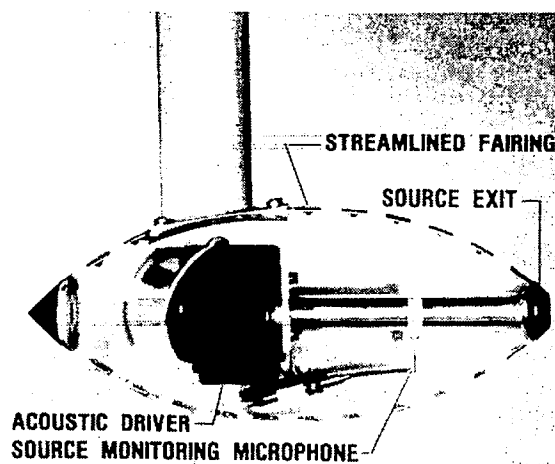


Figure 128.- Aircraft rectangular position response.



(a) Cutaway view of source.



(b) Source on aircraft in flight.

Figure 129.- Source and flight vehicle.

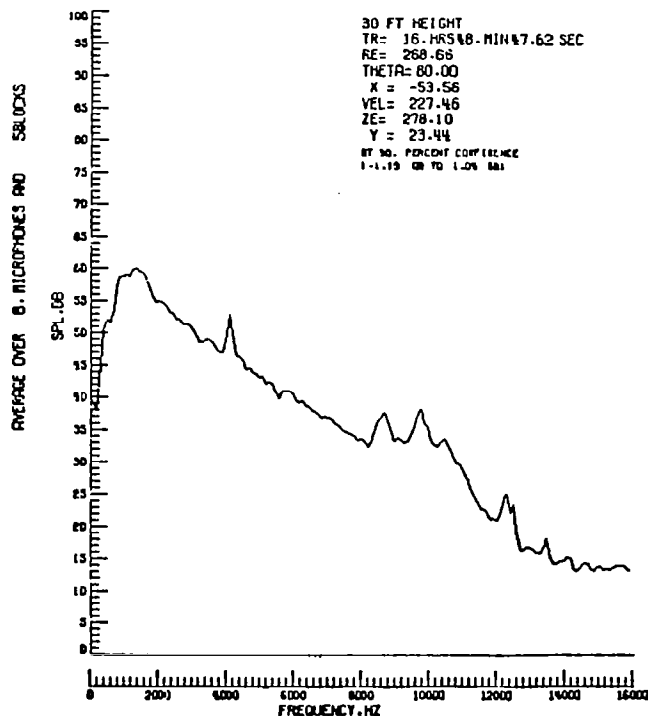


Figure 130.- Uncorrected flyover noise spectrum.

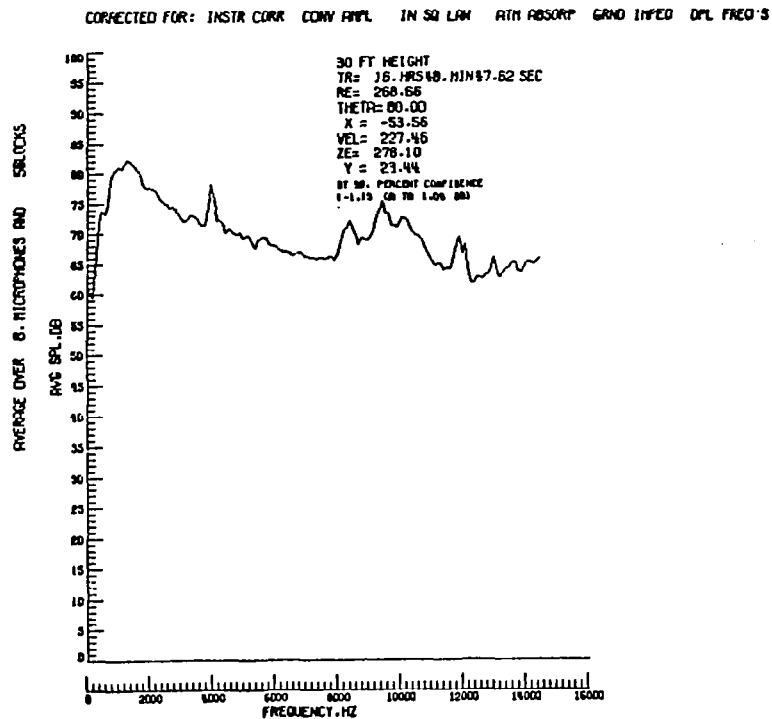


Figure 131.- Corrected flyover noise spectrum.

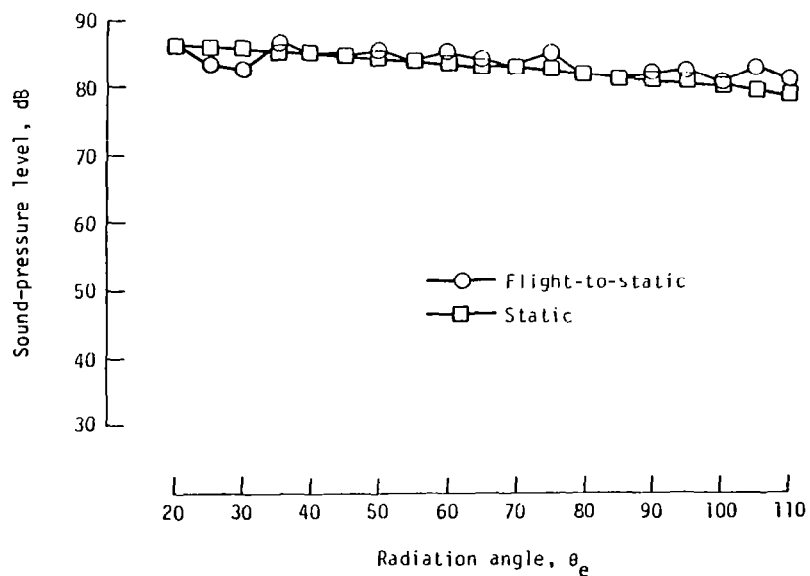


Figure 132.- Comparison of 4-kHz directivity of flight-to-static results and static results.

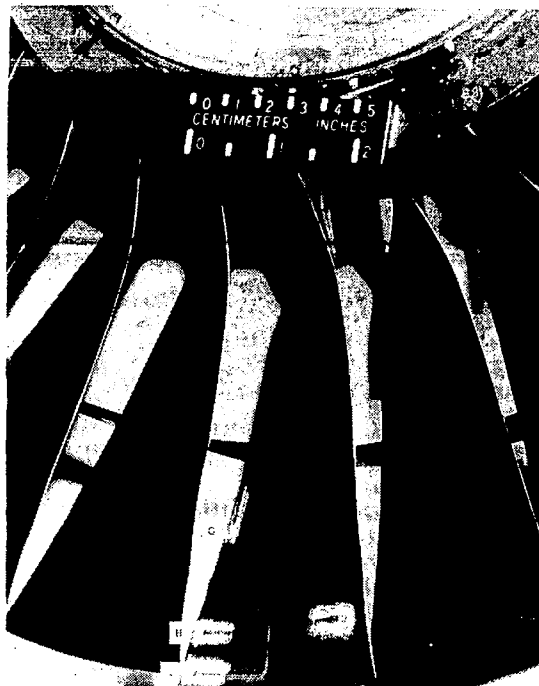


Figure 133.- Blade mounted transducer (BMT) locations on JT15D fan.

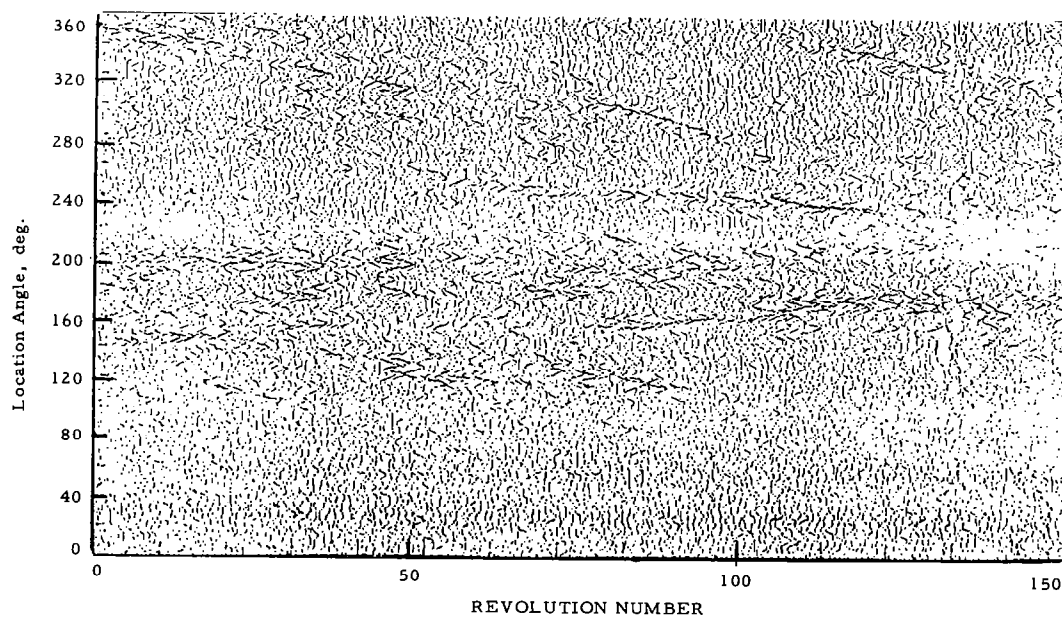


Figure 134.- Space time history of BMT H (Lewis B-3). Ames outdoor test; 13,500 rpm.



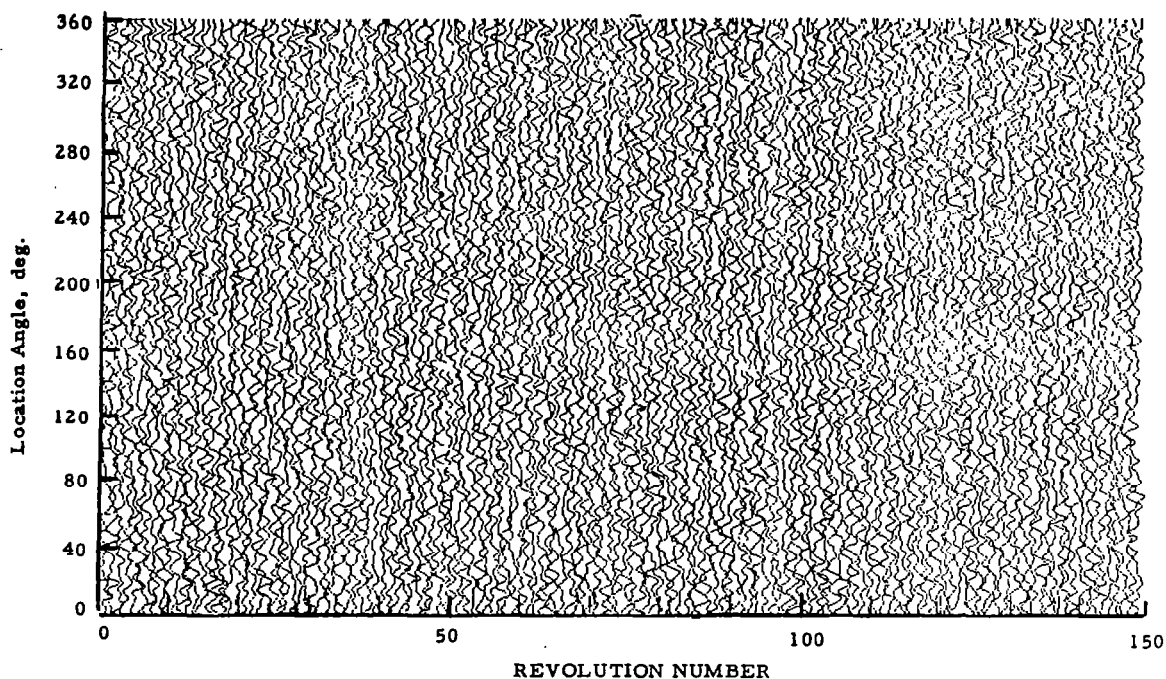


Figure 135.- Space time history of BMT H (Lewis B-3). Langley flight test; 13,000 rpm.

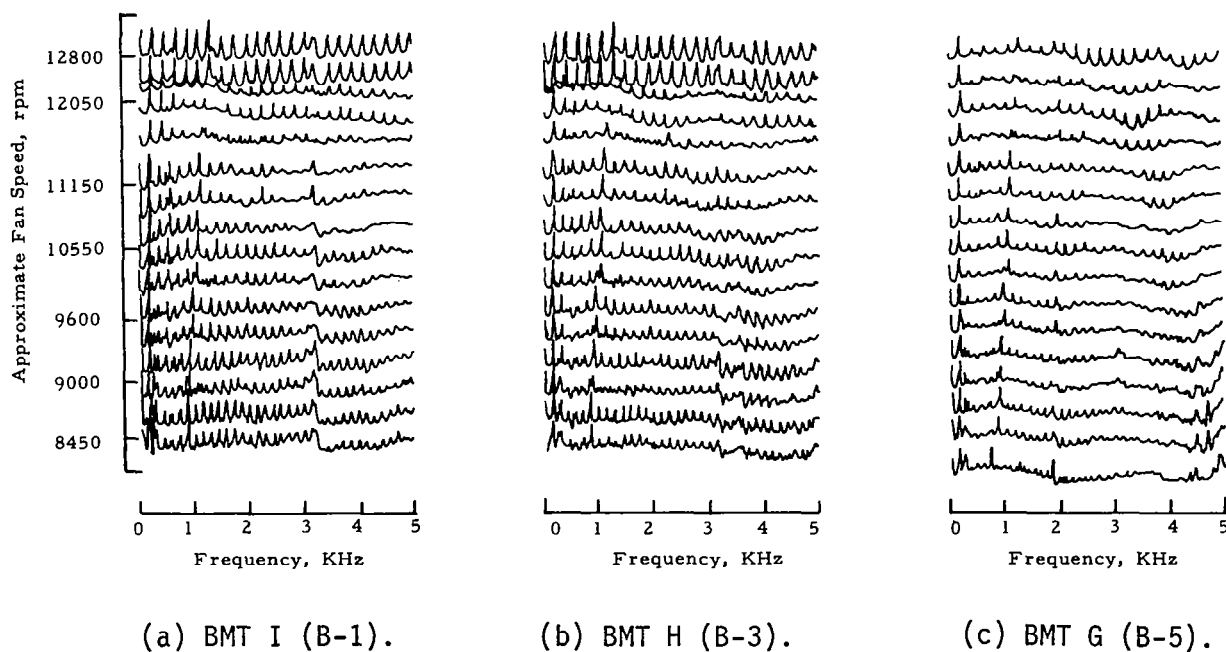


Figure 136.- BMT spectra from sweep of fan speed during Ames tunnel test (tunnel off).

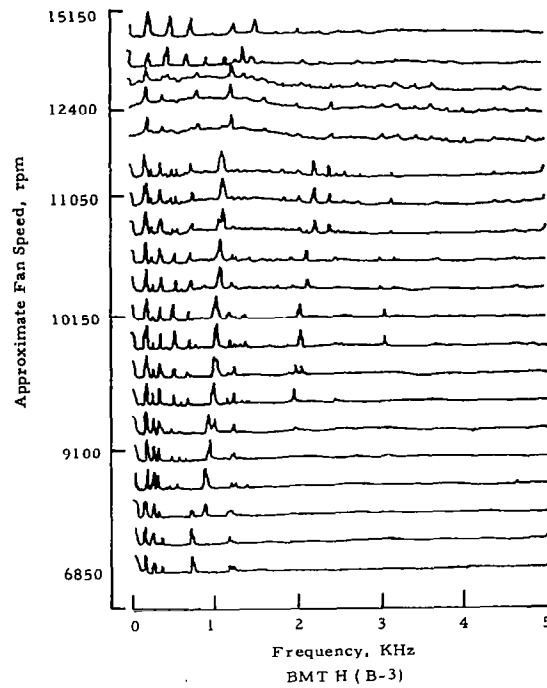
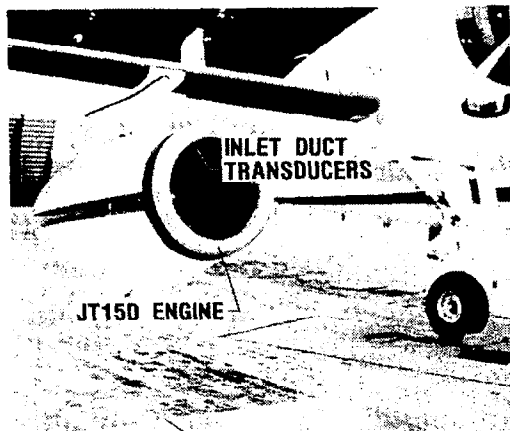
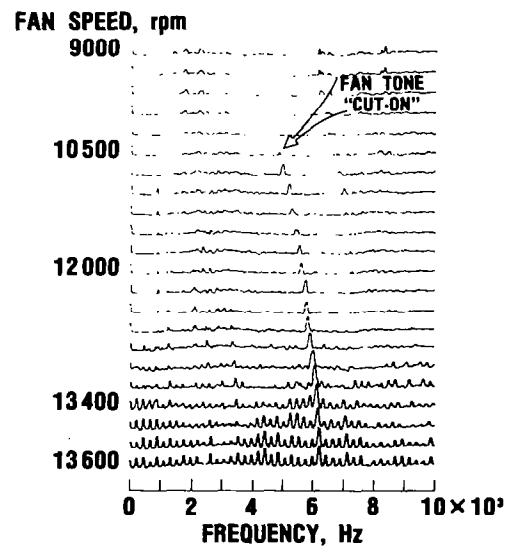


Figure 137.- BMT spectra from sweep of fan speed during flight; 67 m/s, BMT H (Lewis B-3).



(a) Modified OV-1 aircraft.



(b) Spectral time history, JT15D inlet duct.

Figure 138.- Fluctuating pressures in an inlet duct during flight.

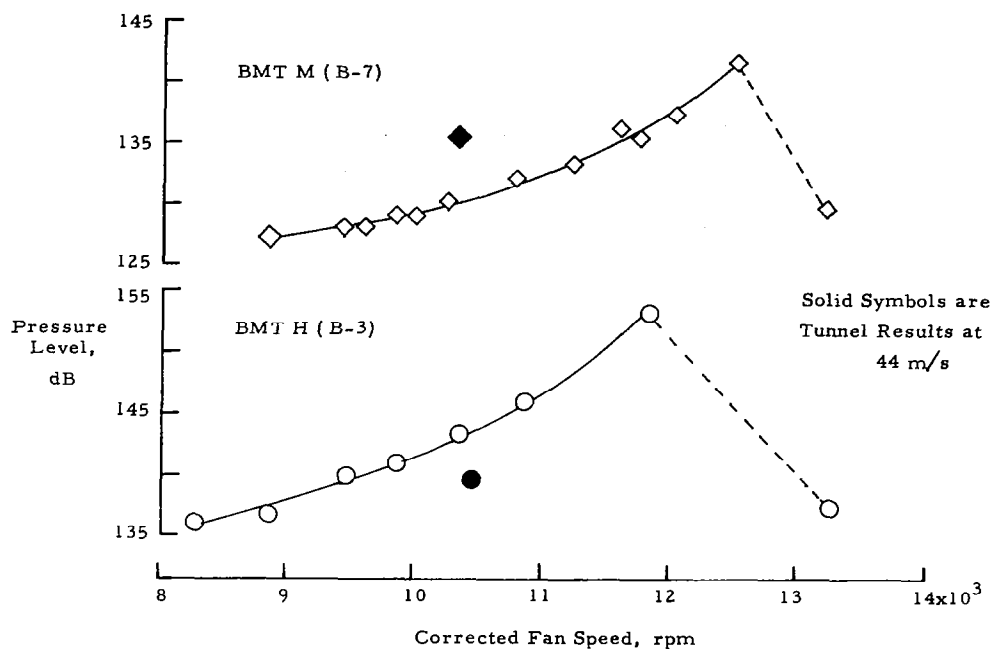


Figure 139.- Amplitude of 6th harmonic of fan speed in flight.

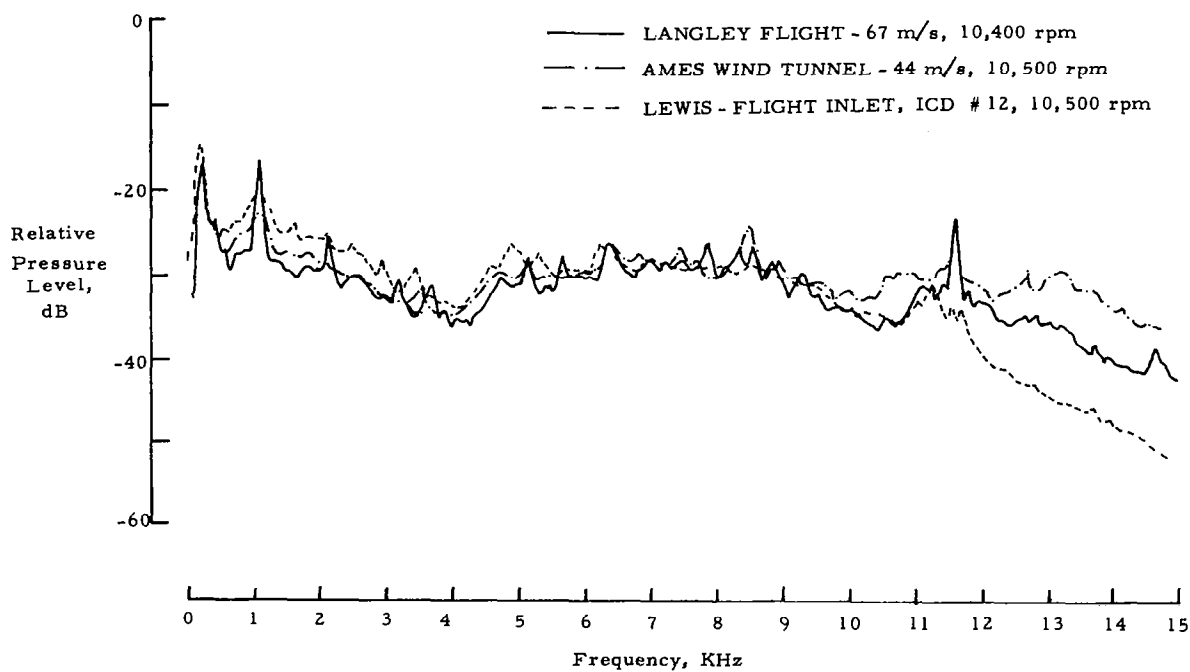


Figure 140.- Overall spectra, BMT H (Lewis B-3), for flight, tunnel, and static.

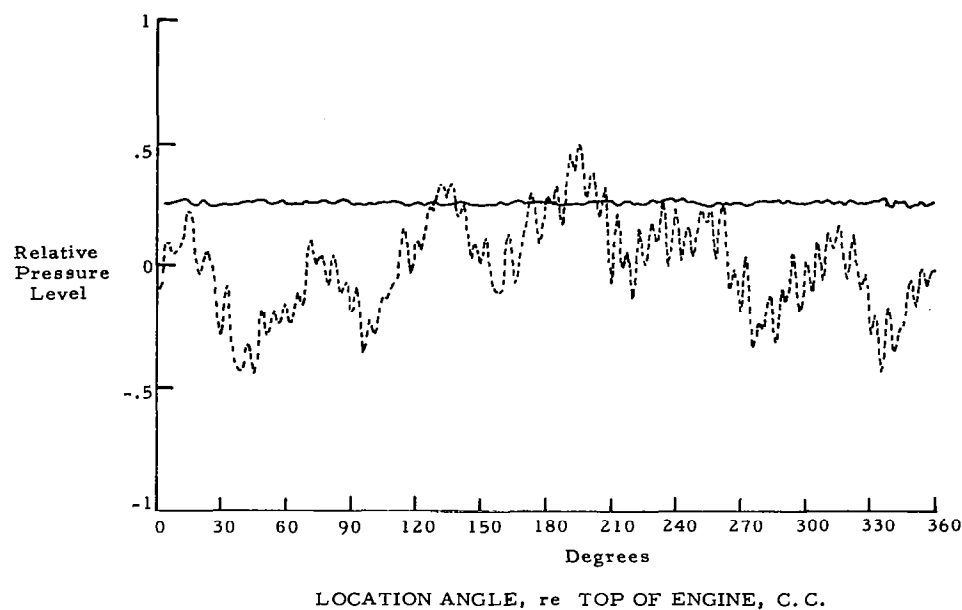


Figure 141.- Mean and standard deviation pressure levels, BMT H (Lewis B-3).  
Langley flight; 67 m/s; 10,400 rpm.

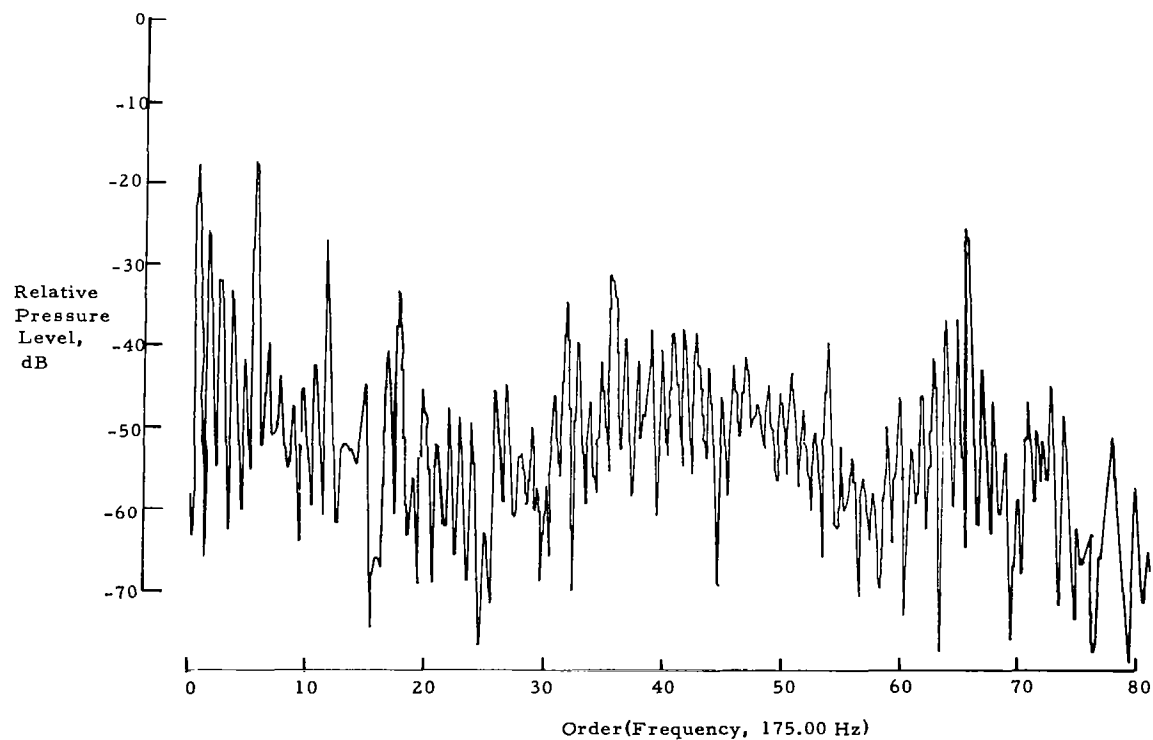


Figure 142.- Enhanced spectra, BMT H. Langley flight; 67 m/s; 10,400 rpm.

#### BELOW SONIC FAN SPEEDS

- BLADE PRESSURES NOT SENSITIVE TO ACOUSTIC CUT-ON MECHANISM
- BLADE PRESSURES ARE SENSITIVE TO PRESSURES CAUSED BY COMPONENTS IN THE BYPASS DUCT
- LARGE SCALE TURBULENCE NOT OBSERVABLE IN FLIGHT, WIND TUNNEL OPERATING OR ICD TESTS
- MAJOR PRESSURE FREQUENCIES SAME IN FLIGHT, WIND TUNNEL, AND ICD TESTS
- DIFFERENCES BETWEEN TEST CONDITIONS APPEAR AS SLIGHT CHANGES IN SPECTRA AT RELATIVELY LOW FREQUENCIES

#### ABOVE SONIC FAN SPEEDS

- IN FLIGHT BLADE PRESSURES ARE DOMINATED BY FIRST FEW FAN SPEED HARMONICS IN ADDITION TO BYPASS COMPONENTS

Figure 143.- Concluding remarks.

	STATIC	TUNNEL	FLIGHT
INSTRUMENTATION CORRECTIONS	✓	✓	✓
INVERSE SQUARE LAW	✓	✓	✓
ATMOSPHERIC ABSORPTION	✓		✓
GROUND IMPEDANCE	✓		✓
CONVECTIVE AMPLIFICATION		✓	✓
DOPPLER FREQUENCY			✓

\*NORMALIZED TO 100' RADIUS,  
LOSSLESS, STATIONARY CONDITIONS

Figure 144.- Data adjustments for comparisons. (Data adjustments normalized to 100-ft-radius, lossless, stationary conditions.)

$N_1^* \approx 10,800$ ; 130 knots;  $\theta_e = 60^\circ$

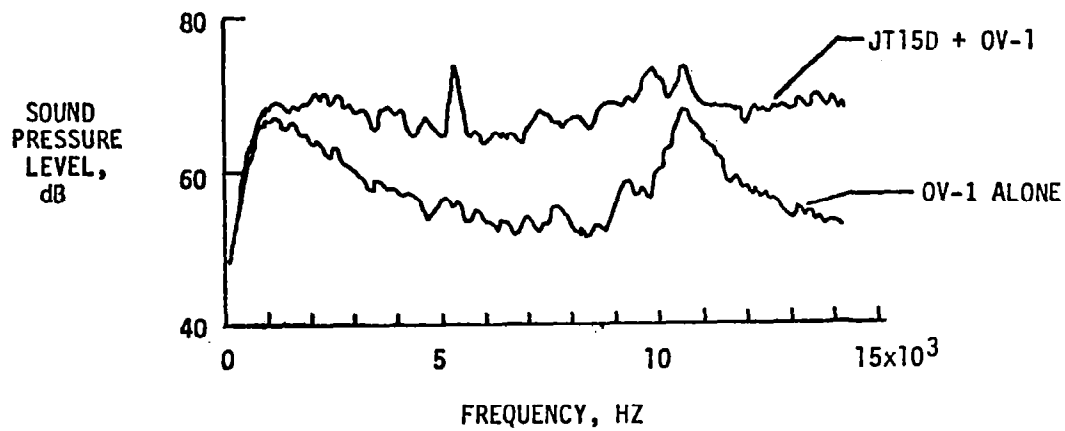


Figure 145.- JT15D/OV-1 signal-to-noise ratio.

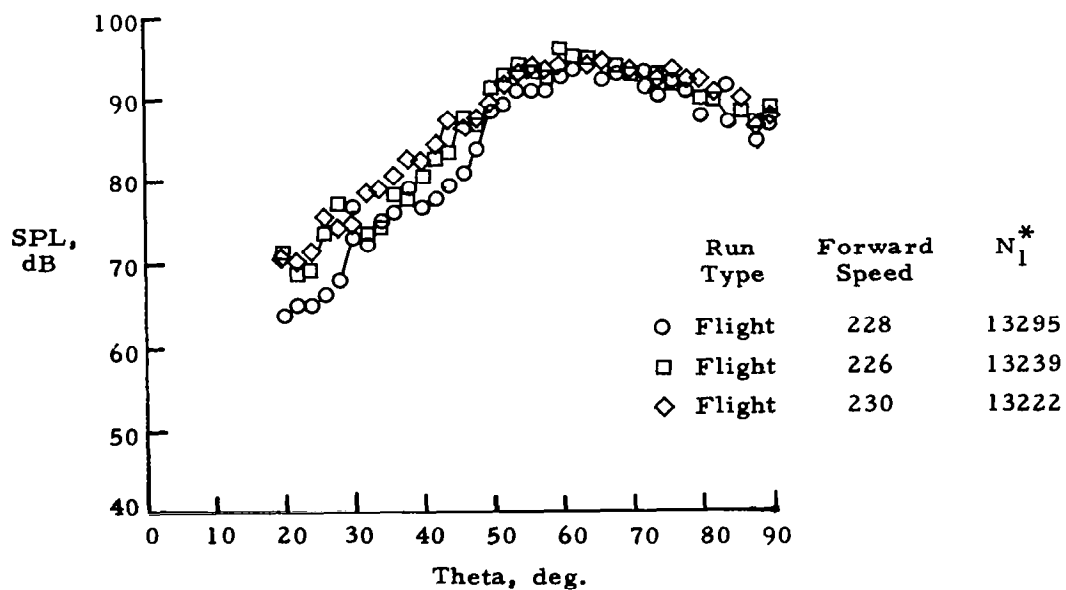


Figure 146.- Repeatability of narrowband BPF flyover noise.

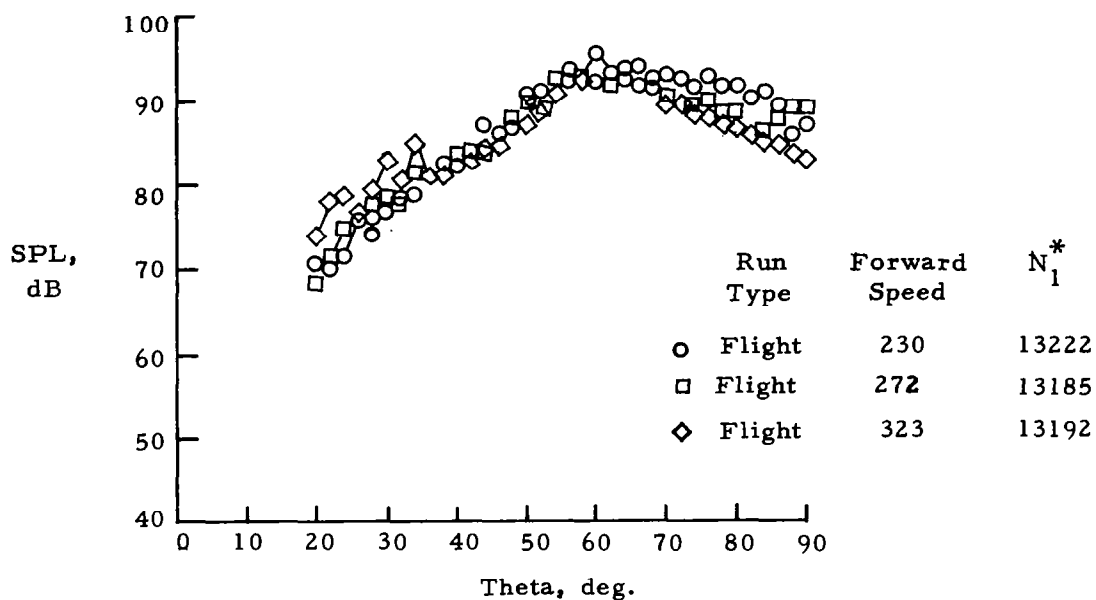


Figure 147.- Forward speed effects on BPF noise.

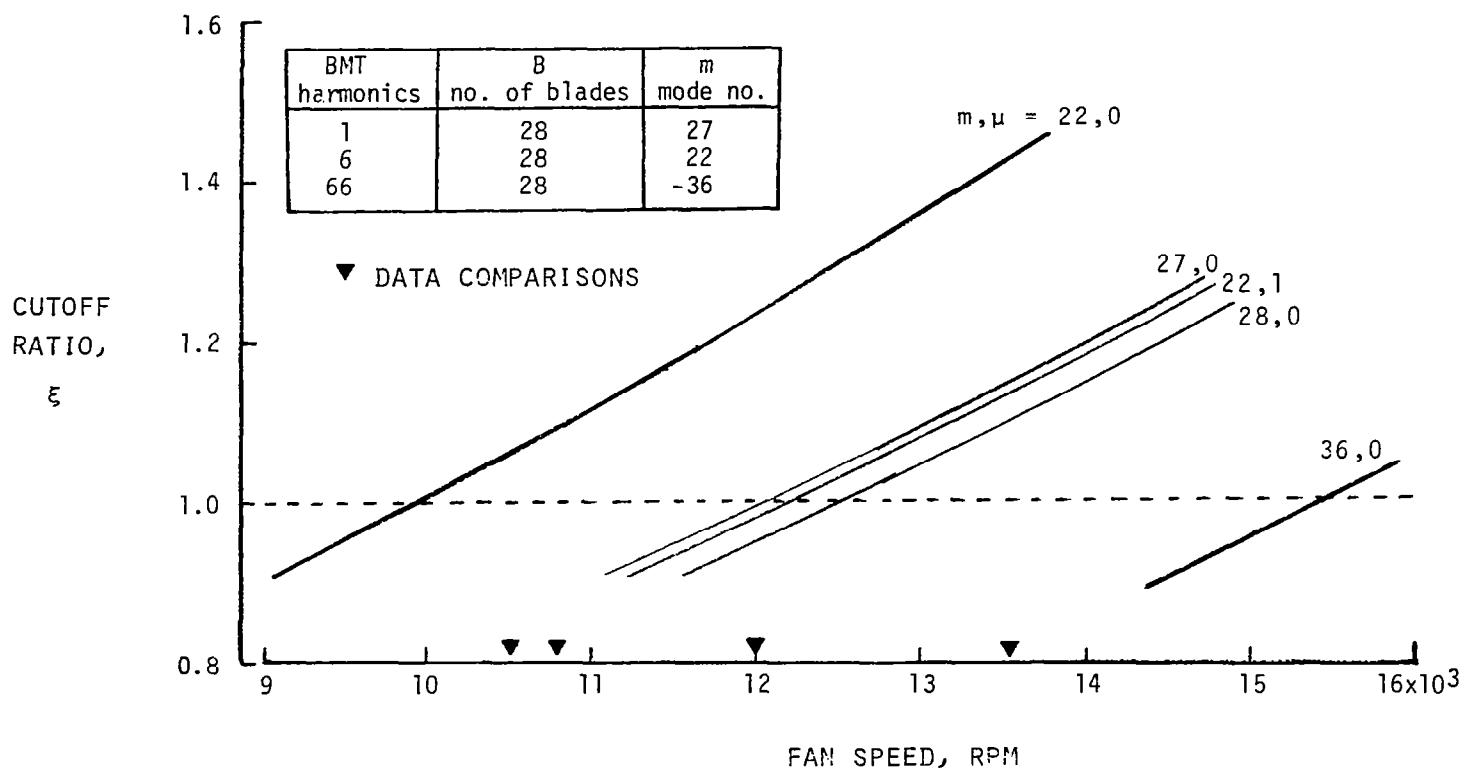


Figure 148.- Cutoff ratios for selected modes.

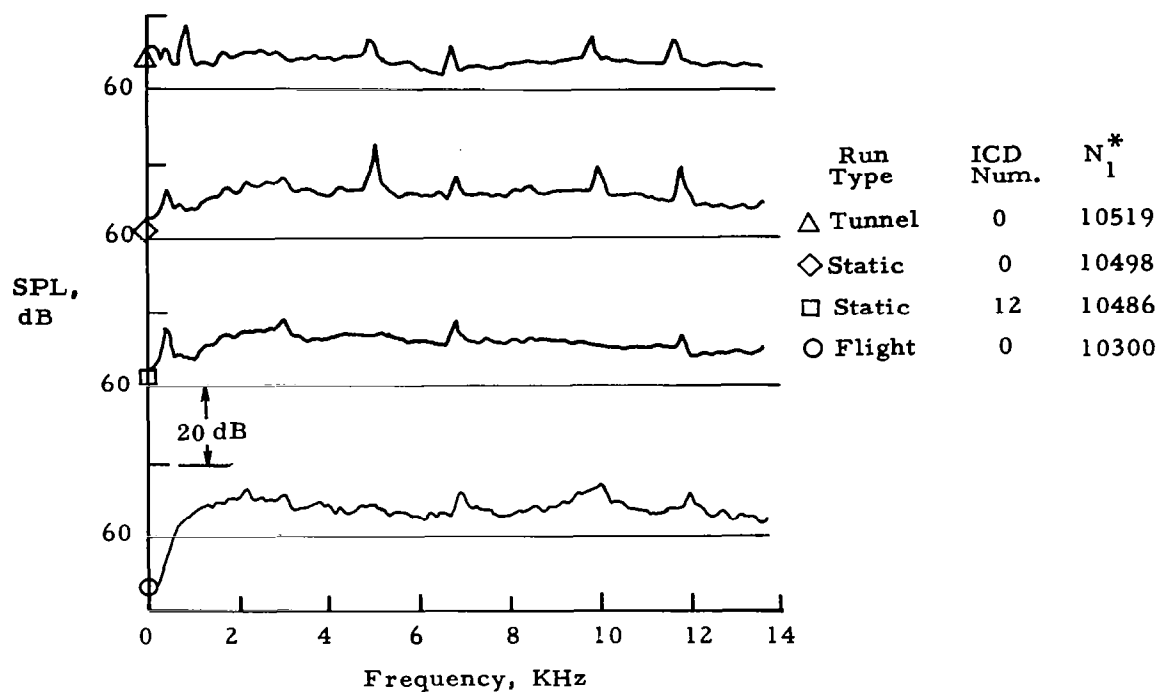


Figure 149.- Comparison of tunnel, static, and flight spectra;  $\theta = 50^\circ$ .

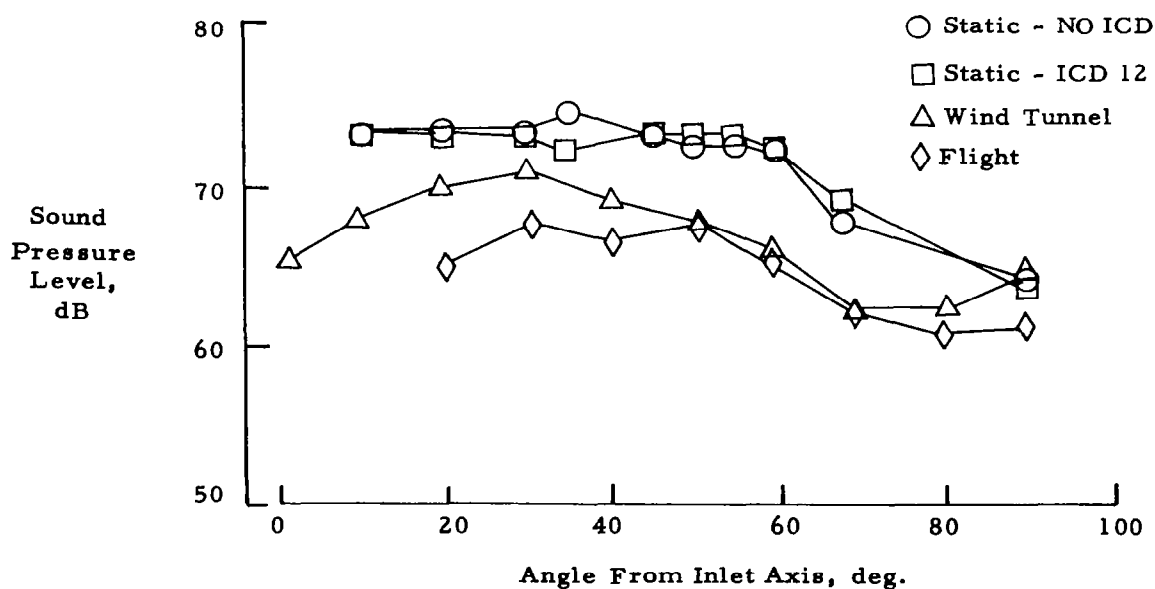


Figure 150.- Broadband far-field noise comparison;  $N_1^* \approx 10,500$ .



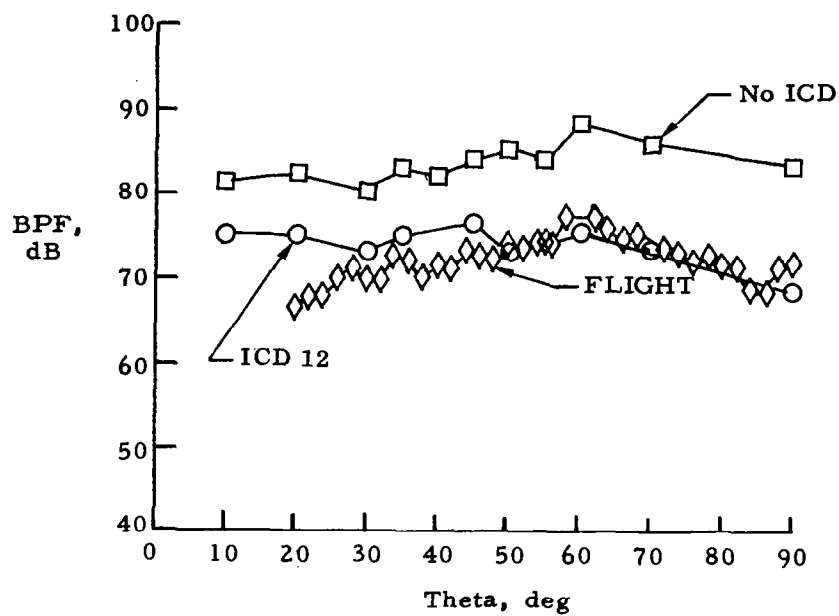


Figure 151.- Comparisons of BPF noise radiation patterns.

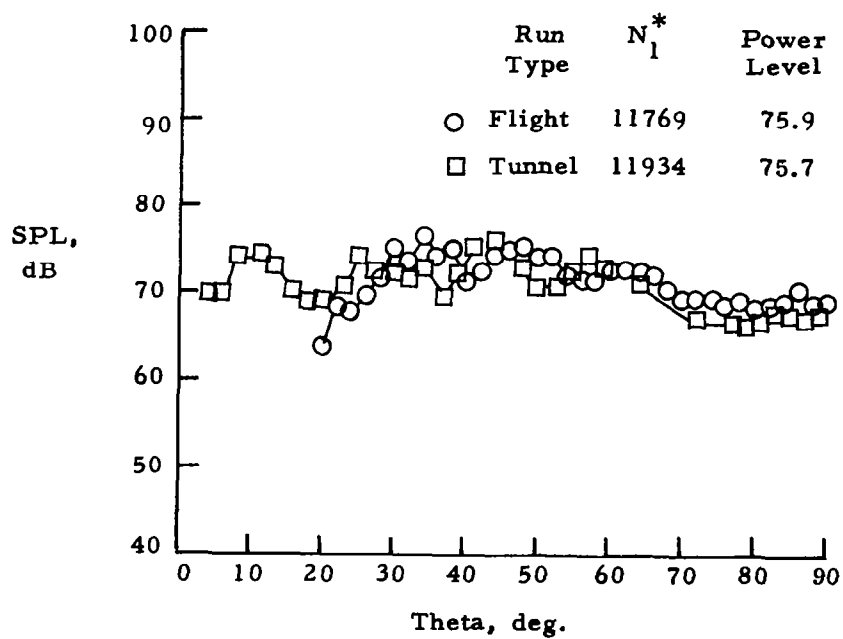


Figure 152.- Comparison between flight and wind tunnel BPF directivity patterns.

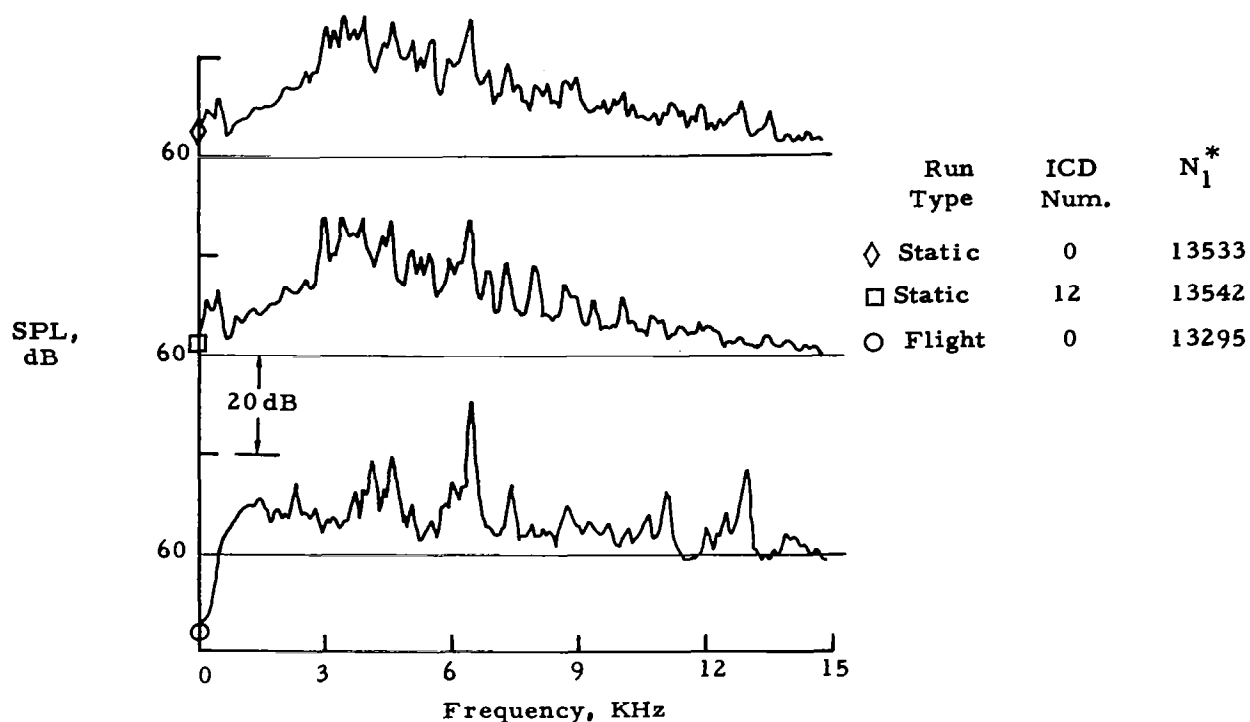


Figure 153.- Supersonic tip speed spectra;  $\theta = 70^\circ$ .

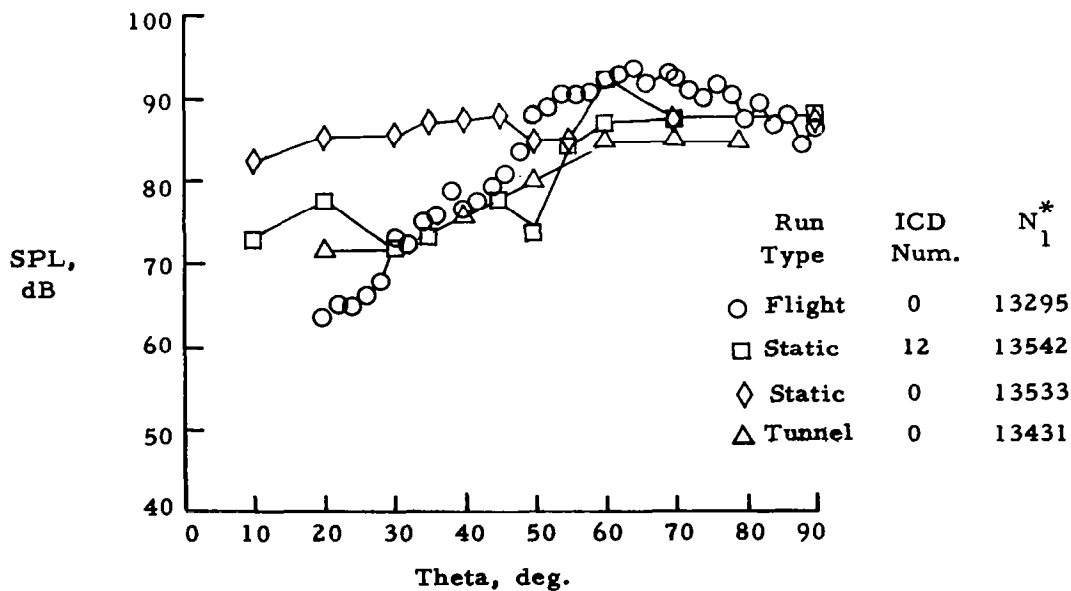


Figure 154.- BPF radiation pattern comparisons - flight, static, and tunnel.

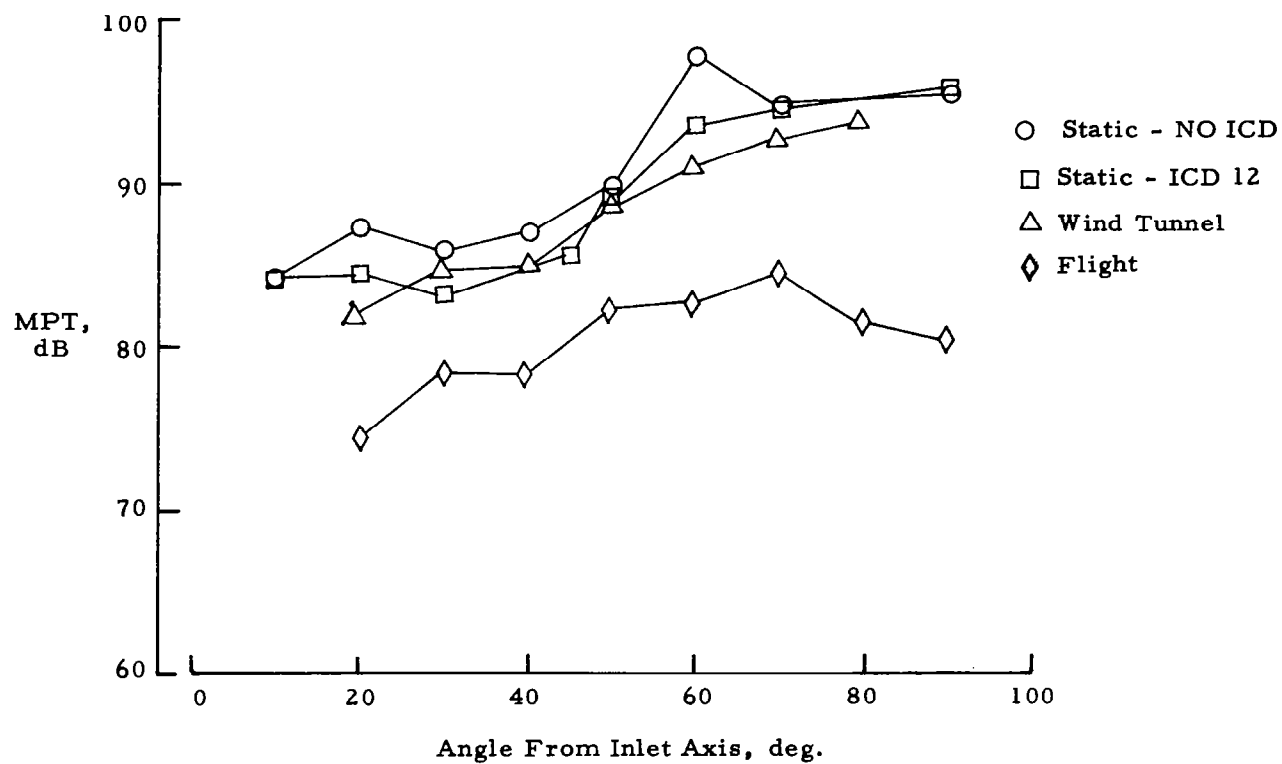


Figure 155.- MPT far-field noise comparison;  $N_1^* \approx 13,500$ .

## REFERENCES

1. Gedge, M. R.: A Design Procedure for Fan Inflow Control Structures. NASA CR-165625, 1980.
2. Perracchio, A. A.; Ganz, U. W.; Gedge, M. R.; and Robbins, K.: Studies on Proper Simulation During Static Testing of Forward Speed Effects on Fan Noise. NASA CR-16526, 1980.
3. Moore, M. T.: Forward Velocity Effects on Fan Noise and the Suppression Characteristics of Advanced Inlets as Measured in the NASA Ames 40 by 80 Foot Wind Tunnel: Acoustic Data Report. NASA CR-152329, 1981.
4. McArdle, J. G.; Homyak, L.; and Chrulski, D. D.: Turbomachinery Noise Studies of the AiResearch QCGAT Engine With Inflow Control. NASA TM-82694, 1981.
5. McArdle, J. G.; Jones, W. L.; Heidelberg, L. J.; and Homyak, L.: Comparison of Several Inflow Control Devices for Flight Simulation of Fan Tone Noise Using a JT15D-1 Engine. AIAA paper no. 80-1025, 1980.
6. Fleeter, S.; Jay, R. L.; and Bennett, W. A.: Rotor Wake Generated Unsteady Aerodynamic Response of a Compressor Stator. ASME paper no. 78-GT-112, 1978.
7. Hanson, D. B.: Study of Noise Sources in a Subsonic Fan Using Measured Blade Pressures and Acoustic Theory. NASA CR-2574, 1975.
8. Savell, C.: Noise Generation by Turbulence Interaction With a Rotor. AIAA paper no. 77-1322, 1977.
9. Preisser, J. S.; Schoenster, J. S.; Golub, R. A.; and Horne, C.: Unsteady Fan Blade Pressure and Acoustic Radiation From a JT15D-1 Turbofan Engine at Simulated Forward Speed. AIAA paper no. 81-0096, 1981.
10. Barber, T. J.; and Weingold, H. D.: Vibratory Forcing Functions Produced by Nonuniform Cascades. ASME J. Eng. for Power, vol. 100, no. 1, Jan. 1978, pp. 82-88.
11. O'Brien, W. F.; and Reimers, S. L.: Measurement of Unsteady Pressures on Fan Blades; Rotor-Downstream Strut Interaction. Report no. VPI-TRG-82-0101, Mechanical Engineering Department, Virginia Polytechnic Institute and State University, Blacksburg, Jan. 1982.
12. Mueller, A. W.; and Preisser, J. S.: Flight Test of a Pure-Tone Acoustic Source. NASA TP-1898, 1981.

## APPENDIX

### BIBLIOGRAPHY

1. Povinelli, F. P., and Dittmar, J. H., "Installation Caused Flow Distortion and its Effects on Noise from a Fan Designed for Turbofan Engines," paper presented at AIAA Seventh Aerodynamics Testing Conference, Palo Alto, CA, September 13-15, 1972. NASA TN D-7076.
2. Goldstein, M. E., Dittmar, J. H., and Gelder, T. F., "Combined Quadrupole-Dipole Model for Inlet Flow Distortion Noise from a Subsonic Fan," NASA TN D-7676, May 1974.
3. Goldstein, M., Rosenbaum, B., and Albers, L., "Noise Generated by Inlet Turbulence," NASA TN D-7667, 1974.
4. Mani, R., "Isolated Rotor Noise Due to Inlet Distortion or Turbulence," NASA CR-2479, October 1974.
5. Feiler, C. E., and Merriman, J. E., "Effects of Forward Velocity and Acoustic Treatment on Inlet Fan Noise," AIAA paper 74-946 presented at AIAA Sixth Aircraft Design Flight Test and Operations Meeting, Los Angeles, CA, August 12-14, 1974. NASA TM X-71591.
6. Heidmann, M. F., "An Observation on Tone Cut-Off in Static Test Data from Jet Engine Fan," NASA TM X-3206, September 1975.
7. Heidmann, M. F. and Dietrich, D. A., "Simulation of Flight-Type Engine Fan Noise in the NASA-Lewis 9 x 15 Anechoic Wind Tunnel," paper presented at Ninety-second Meeting of Acoustical Society of America, San Diego, CA, November 16-17, 1976. NASA TM X-73540.
8. Bekofske, K. L., Sheer, R. E., and Wang, J. C. F., "Basic Noise Research Program-Fan Noise Effect of Inlet Disturbances on Fan Inlet Noise During a Static Test," NASA CR-135177, April 1977.
9. Hanson, D. B., "Study of Noise and Inflow Distortion Sources in the NASA QU-1B Fan Using Measured Blade and Vane Pressures," NASA CR-2899, September 1977.
10. Blankenship, G. L., Low, J. K. C., Watkins, J. A., and Merriman, J. E., "Effect of Forward Motion on Engine Noise," NASA CR-134954, October 1977.
11. Wazyniak, J. A., Shaw, L. M., and Essary, J. D., "Characteristics of an Anechoic Chamber for Fan Noise Testing," ASME Paper 77GT-74 presented at ASME International Gas Turbine Conference, Philadelphia, Pennsylvania, March 25-30, 1977. NASA TM X-73555.

12. Feiler, C. E., and Groeneweg, J. F., "Summary of Forward Velocity Effects On Fan Noise," AIAA Paper 77-1319 presented at AIAA Fourth Aeroacoustics Conference, Atlanta, GA, October 3-5, 1977. NASA TM-73722.
13. Heidmann, M. F., and Dietrich, D. A., "Effects of Simulated Flight on Fan Noise Suppression," AIAA Paper 77-1334 presented at AIAA 4th Aeroacoustics Conference, Atlanta, GA, October 3-5, 1977.
14. Shaw, L. M., Woodward, R. P., Glaser, F. W., and Dastoli, B. J., "Inlet Turbulence and Fan Noise Measured in an Anechoic Wind Tunnel and Statically with an Inlet Flow Control Device," AIAA Paper 77-1345 presented at the AIAA Fourth Aeroacoustic Conference, Atlanta, GA, October 3-5, 1977. NASA TM-73723.
15. Jones, W. L., and Groeneweg, J. F., "State-of-the-Art of Turbofan Engine Noise Control," paper presented at Noise-Con 77, Hampton, VA, October 17-19, 1977. NASA TM-73734.
16. Dietrich, D. A., Heidmann, M. F., and Abbott, J. M., "Fan Acoustic Signatures in an Anechoic Wind Tunnel," Paper 77-59 presented at the AIAA 15th Aerospace Sciences Meeting, Los Angeles, CA, January 24-26, 1977. Journal of Aircraft, Vol. 14, No. 11, November 1977, 1109-1116. NASA TM-73560.
17. Heidmann, F. M., and Clark, B. J., "Flight Effects on Predicted Fan Fly-By Noise," paper presented at the Ninety-fourth Meeting of the Acoustical Society of America, Miami, FL, December 13-16, 1977. NASA TM-73798.
18. Saule, A. V., and Rice, E. J., "Far-Field Multimodal Acoustic Radiation Directivity," paper presented at the Ninety-fourth Meeting of the Acoustical Society of America, Miami, FL, December 13-16, 1977. NASA TM-73839.
19. Woodward, R. P., Wazyniak, J. A., Shaw, L. M., and MacKinnon, M. J., "Effectiveness of an Inlet Flow Turbulence Control Device to Simulate Flight Fan Noise in an Anechoic Chamber," paper presented at the Ninety-fourth Meeting of the Acoustical Society of America, Miami, FL, December 13-16, 1977. NASA TM-73855.
20. Dittmar, J. J., MacKinnon, M. J., and Woodward, R. P., "Reduction of Fan Noise in an Anechoic Chamber by Reducing Chamber Wall Induced Inlet Flow Disturbances," paper presented at the ASA Meeting, Providence, RI, May 16-19, 1978. NASA TM-78854.
21. Kobayashi, H., "Three Dimensional Effects on Pure Tone Fan Noise Due to Inflow Distortion," AIAA Paper 78-1120 presented at the AIAA 11th Fluid and Plasma Dynamics Conference, Seattle, WA, July 10-12, 1978. NASA TM-78885.

22. Balombin, J. R., "Variation of Fan Tone Steadiness for Several Inflow Conditions," AIAA Paper 78-1119 presented at the AIAA Eleventh Fluid and Plasma Dynamics Conference, Seattle, WA, July 10-12, 1978. NASA TM-78886.
23. Kantola, R. A. and Warren R. E., "Basic Research in Fan Source Noise Inlet Distortion and Turbulence Noise," NASA CR-159451, December 1978.
24. Jones, W. L., McArdle, J. G., and Homyak, L., "Evaluation of Two Inflow Control Devices for Flight Simulation of Fan Noise Using a JT15D Engine," AIAA Paper 79-0654 presented at the AIAA 5th Aeroacoustics Conference, Seattle, WA, March 12-14, 1979. NASA TM-79072.
25. Gedge, M. R., "Analytical Models for Use in Fan Inflow Control Structure Design--Inflow Distortion and Acoustic Transmission Models," NASA CR-159189, December 1979.
26. Goldstein, M. E., and Durbin, P. A., "The Effect of Finite Turbulence Spatial Scale on the Amplification of Turbulence by a Contracting Stream, J. Fluid Mech. Vol. 98, Part 3, 1980, pp. 473-508.
27. Balombin, J. R., "Application of Coherence in Fan Noise Studies", NASA TP-1630, February 1980.
28. Rice, E. J., and Saule, A. V., "Far-Field Radiation of Aft Turbofan Noise," paper presented at the Ninety-ninth Meeting of the Acoustical Society of America, Atlanta, GA, April 21-25, 1980. NASA TM-81506.
29. McArdle, J. G., Jones, W. L., Heidelberg, L. J., and Homyak L., "Comparison of Several Inflow Control Devices for Flight Simulation of Fan Tone Noise Using a JT15D-1 Engine," AIAA Paper 80-1025 presented at the AIAA Sixth Aeroacoustics Conference, Hartford, CT, June 4-6, 1980. NASA TM-81505.
30. Heidmann, M. F., Saule, A. V., and McArdle, J. G., "Predicted and Observed Modal Radiation Patterns from JT15D Engine with Inlet Rods," Journal of Aircraft, Volume 17, Number 7, July 1980, 493. NASA TM-79074.
31. Kobayashi, H., and Groeneweg, J. F., "Effects of Inflow Distortion Profiles on Fan Tone Noise," AIAA 79-0577R, AIAA Journal, Volume 18, Number 8, August 1980, 899.
32. Ganz, U. W., "Analytical Investigation of Fan Tone Noise Due to Ingested Atmospheric Turbulence," NASA CR-3302, August 1980.

33. Gedge, M. R., "A Design Procedure for Fan Inflow Control Structures," NASA CR-165625, September 1980.
34. Peracchio, A. A., Ganz, U. W., Gedge, M. R., and Robbins K., "Studies on Proper Simulation During Static Testing of Forward Speed Effects on Fan Noise," NASA CR-165626, September 1980.
35. Tan-atichat, J., Nagib, H. M., and Drubka, R. E., "Effects of Axisymmetric Contractions on Turbulence of Various Scales," NASA CR-165136, September 1980.
36. Mueller, A. W., "A Comparison of the Three Methods Used to Obtain Acoustic Measurements for the NASA Flight Effects Program," NASA TM-81906, October 1980.
37. Preisser, J. S., Schoenster, J. A., Golub, R. A., and Horne, C., "Unsteady Fan Blade Pressure and Acoustic Radiation from a JT15D-1 Turbofan Engine at Simulated Forward Speed," AIAA 81-0096, presented at AIAA 19th Aerospace Sciences Meeting, January 12-15, 1981.
38. Woodward, R. P., and Glaser F. W., "Effect of Inflow Control on Inlet Noise of a Cut-on Fan," AIAA 80-1049R, AIAA Journal, Volume 19, Number 3, March 1981, 387. NASA TM-81487.
39. Knight, V. H. Jr., "In-Flight Jet Engine Noise Measurement System," Presented at the ISA 27th International Instrumentation Symposium, April 27-30, 1981.
40. Rao, K. V., and Preisser, J. S., "Spectral Variance of Aeroacoustic Data," J. Acoust. Soc. Am., Article 69, Section 5, May 1981.
41. Mueller, A. W., and Preisser, J. S., "Flight Test of a Pure Tone Acoustic Source," NASA TP-1898, August 1981.
42. Peracchio, A. A., "Assessment of Inflow Control Structure Effectiveness and Design System Development," AIAA Paper 81-2048, October 1981.
43. Woodward, R. P., and Glaser, F. W., "Effects of Blade-Vane Ratio and Rotor-Stator Spacing on Fan Noise with Forward Velocity," AIAA Paper 81-2032 presented at the AIAA Seventh Aeroacoustics Conference, Palo Alto, CA, October 5-7, 1981. NASA TM-82690.
44. McArdle, J. G., Homyak, L. and Chrulski, D. D., "Turbomachinery Noise Studies of the AiResearch OCGAT Engine with Inflow Control," AIAA Paper 81-2049, prepared for the AIAA Seventh Aeroacoustics Conference, Palo Alto, CA, October 5-7, 1981. NASA TM-82694.



45. Schoenster, J. A., "Fluctuating Pressures on the Fan Blades of a Turbofan Engine," NASA TP-1976, March 1982.
46. Gridley, D., "Program for Narrowband Analysis of Aircraft Flyover Noise Using Ensemble Averaging Techniques," NASA CR-165867, March 1982.

## ATTENDEES

### NASA Langley Research Center

#### Acoustics and Noise Reduction Division:

H. Morgan  
D. Chestnutt  
J. Preisser  
R. Golub  
A. Mueller  
J. Schoenster  
P. Pao  
P. Raney  
R. Silcox  
H. Hubbard  
L. Clark  
L. Watkins

#### Facilities Engineering Division:

V. Knight  
V. Chretien

#### Aeronautical Systems Division:

J. Newbauer

### NASA Lewis Research Center

J. Groeneweg  
J. McArdle  
C. Feiler  
W. Woodward  
L. Heidelberg  
J. Balombin

### Illinois Inst. of Tech.

H. Nagib

### Pratt & Whitney Aircraft Group, United Technologies Corp.

A. Peracchio

### United Technologies Research Corp.

R. Amiet

### George Washington University

M. Myers

### Ames Research Center

D. Hickey

### Boeing Aircraft Company

F. Strout  
A. Andersson

### Integrated Software Services Incorp.

R. Sailey  
C. Shearls

### Kentron International Inc.

D. Gridley  
D. Dennis

### Wyle Laboratories

D. Hilliard

### General Electric Company

R. Holmley  
P. Gliebe

### Douglas Aircraft Company, McDonnell Douglas Corp.

R. Kraft

### Virginia Polytechnic Institute and State University

W. O'Brien  
S. Reimers  
S. Richardson  
C. Hurst

1. Report No. NASA CP-2242		2. Government Accession No.		3. Recipient's Catalog No.	
4. Title and Subtitle  FLIGHT EFFECTS OF FAN NOISE				5. Report Date September 1982	
				6. Performing Organization Code 505-32-03-06	
7. Author(s) David Chestnutt, Editor				8. Performing Organization Report No. L-15493	
				10. Work Unit No.	
9. Performing Organization Name and Address NASA Langley Research Center Hampton, VA 23665				11. Contract or Grant No.	
				13. Type of Report and Period Covered Conference Publication	
12. Sponsoring Agency Name and Address National Aeronautics and Space Administration Washington, DC 20546				14. Sponsoring Agency Code	
15. Supplementary Notes					
16. Abstract  This conference publication contains the highlights of a workshop on research on the simulation of in-flight fan noise and flight effects held at Langley Research Center, Hampton, Virginia, January 26-27, 1982. The workshop was sponsored jointly by the Langley Research Center Noise Control Branch and the Lewis Research Center Propulsion Systems Acoustics Branch. The purposes of the workshop were (1) to review the status of the overall program on the flight effects of fan noise, (2) to display for the first time flight-to-static noise comparisons with the Pratt & Whitney JT15D engine, and (3) to stimulate dialogue between certain industrial, university, and government groups to assess our ability to simulate in-flight fan noise.  The participants agreed that a major plateau had been reached in the static simulation of in-flight fan noise that will allow certain noise control concepts to be evaluated. However, there was a consensus that this plateau should be regarded as an interim step and that the technology should continue to be improved to permit better simulations in the future. Other recommendations concerning these improvements and indications of areas of needed research are detailed in this publication.					
17. Key Words (Suggested by Author(s)) Flight effects Fan noise Turbulence control devices			18. Distribution Statement  Unclassified - Unlimited  Subject Category 71		
19. Security Classif. (of this report) Unclassified	20. Security Classif. (of this page) Unclassified	21. No. of Pages 128	22. Price A07		

National Aeronautics and  
Space Administration

Washington, D.C.  
20546

Official Business

Penalty for Private Use, \$300

THIRD-CLASS BULK RATE

Postage and Fees Paid  
National Aeronautics and  
Space Administration  
NASA-451



3 1 10, H. 820916 500903DS  
DEPT OF THE AIR FORCE  
AF WEAPONS LABORATORY  
ATTN: TECHNICAL LIBRARY (SUL)  
KIRTLAND AFB NM 87117

S

NASA

POSTMASTER:

If Undeliverable (Section 158  
Postal Manual) Do Not Return